TESIS DE LA UNIVERSIDAD DE ZARAGOZA

2025

14

Aleida Lostalé Caparroso

Estudio de la mejora de la eficiencia de rodamientos de rodillos cónicos en base a estrategias de mejora de los materiales y del diseño

Director/es

Clavería Ambroj, Isabel
Castell Muixi, Pere Vicenc

ISSN 2254-7606

Prensas de la Universidad
Universidad Zaragoza

Universidad de Zaragoza
Servicio de Publicaciones

ISSN 2254-7606

Universidad Zaragoza
1542

Tesis Doctoral

ESTUDIO DE LA MEJORA DE LA EFICIENCIA DE RODAMIENTOS DE RODILLOS CÓNICOS EN BASE A ESTRATEGIAS DE MEJORA DE LOS MATERIALES Y DEL DISEÑO

Autor

Aleida Lostalé Caparroso

Director/es

Clavería Ambroj, Isabel
Castell Muixi, Pere Vicenc

UNIVERSIDAD DE ZARAGOZA
Escuela de Doctorado

Programa de Doctorado en Ingeniería Mecánica

2023

Aleida Lostale Caparroso

Estudio de la mejora de la eficiencia de rodamientos de rodillos cónicos en base a estrategias de mejora de los materiales y del diseño

Tesis Doctoral

Estudio de la mejora de la eficiencia de rodamientos de rodillos cónicos en base a estrategias de mejora de los materiales y del diseño

Autor

Aleida Lostale Caparroso

Director/es

Isabel Clavería Ambroj
Pere Vicenc Castell Muixi

Escuela de Ingeniería y Arquitectura
Departamento de Ingeniería Mecánica

2022

TESIS POR COMPENDIO DE PUBLICACIONES

Tesis doctoral presentada como compendio de publicaciones realizadas a lo largo de la fase de desarrollo del presente trabajo de investigación.

En el siguiente listado se incluyen las referencias de las publicaciones mediante orden cronológico de aceptación y los congresos internacionales. Además, en aquellas revistas indexadas JCR se indica el factor de impacto. Se ha asignado también cada una de las publicaciones del compendio los nombres P1, P2, P3 y P4 para referirse de esa forma a ellas a lo largo de la memoria.

- Revistas JCR:

  1. Clavería, I.; Elduque, D.; Lostalé, A.; Fernández, A.; Javierre, C.; Castell, P. Analysis of self-lubrication enhancement via PA66 strategies: Texturing and nano-reinforcement with ZrO and graphene. *Tribology International* **2019**, 131, 332–342. **Q1** (Q1, 15/130, Mechanical Engineering, JCR2021: 5.620) (P1)
  2. Clavería, I.; Lostalé, A.; Fernández, Á.; Castell, P.; Elduque, D.; Mendoza, G.; Zubizarreta, C. Enhancement of Tribological Behavior of Rolling Bearings by Applying a Multilayer ZrN/ZrCN Coating. *Coatings* **2019**, *9*, 434. **Q2** (Q2, 9/19, Materials Science, Coatings & Films JCR2021: 3.236)[1] (P2)
  3. Clavería, I.; Gimeno, S.; Miguel, I.; Mendoza, G.; Lostalé, A.; Fernández, Á.; Castell, P.; Elduque, D. Tribological Performance of Nylon Composites with Nanoadditives for Self-Lubrication Purposes. *Polymers* **2020**, *12*, 2253. **Q1** (Q1, 16/90, Polymer Science, JCR2021: 4.967) (P3)

- Congresos internacionales:

  4. Lostalé, A; Clavería, I; Fernández, A; Muniesa, M; Javierre, C; Elduque, D; Santo Domingo, S; Validation of design solutions and materials for a high performance bearing cage. *The 29th European Modeling & Simulation Symposium* **2017**, *ISBN 978-88-97999-85-0*, 71-76. (P4)

[1] El artículo fue presentado en el congreso "1st Coatings and Interfaces Web Conference, CIWC2019" celebrado del 15 al 29 marzo de 2019.

AGRADECIMIENTOS

En primer lugar, no puedo más que expresar mi más sincero agradecimiento a la Dra. Isabel Clavería, directora y tutora de esta tesis doctoral, por su tiempo y dedicación y por apoyarme y ayudarme en todo momento. Sin este soporte, no hubiera sido capaz de terminar mi doctorado. Tampoco quiero olvidarme de la inestimable ayuda recibida por el Dr. Pere Castell, co-director actual de este trabajo, y por el Dr. Ángel Fernandez. Sus comentarios, sugerencias y experiencia han enriquecido enormemente esta investigación.

Por otro lado, agradecer también la colaboración y gran trabajo de la empresa Fersa Bearings. Sobre todo, me gustaría destacar el trabajo de Sergio Santo Domingo, Pedro Dubón, Alejandro Gasión (y su estupendo equipo), Sofía Gimeno y Nacho Miguel. Ellos me animaron a embarcarme en esta aventura y me han ayudado a dar forma e industrializar la investigación desarrollada.

Por supuesto, no puedo olvidarme de las contribuciones aportadas por el centro tecnológico IK4-Tekniker y por la empresa Brugarolas. Sin duda, su ayuda ha dado un gran valor a la investigación, y sin ella, ésta no habría sido posible.

Además de a los actores más académicos, también me gustaría dar las gracias a mis padres, hermana y novio porque me han apoyado, animado y aguantado durante este largo camino lleno de altibajos y dudas.

Finalmente, me gustaría agradecer a Fundación CIRCE, su soporte y comprensión en la última etapa de esta tesis, dándome facilidades en todo momento para que pudiera concluirla.

¡Muchas gracias a todos!

INTRODUCCIÓN GENERAL

Aproximadamente, el 30% del consumo mundial de energía se pierde en forma de calor debido a la fricción [1]. En particular, en los países industrializados, el coste directo provocado por la fricción y el desgaste se estima en un 7%. Solo en España en 2014, una atención adecuada a estos problemas hubiera supuesto un ahorro de 13.200 millones de euros, o lo que es lo mismo, un 1,4% de su PNB [2]. Aunque no sean más que estimaciones, estas cifras indican claramente la importancia del desarrollo de nuevas tecnologías que permitan un descenso de las pérdidas ocasionadas por la fricción.

Para conseguir esta mejora en el rendimiento final, cada uno de los componentes que conforman los sistemas mecánicos debe, a su vez, trabajar de manera óptima. Por ello, con la mejora en la lubricación y la tribología de los rodamientos, elementos fundamentales en todas las máquinas, se conseguiría una reducción de la fricción entre los componentes rodantes provocando una disminución de las pérdidas y, por consiguiente, un aumento de la eficiencia final del conjunto.

Adicionalmente, el aumento de las prestaciones de funcionamiento de los rodamientos y de su vida útil permitiría la reducción tanto de su tamaño final, ya que serían necesarios elementos con menores dimensiones para conseguir el mismo rendimiento, como en el consumo de recambios lo que derivaría en una disminución del gasto de materias primas y de la generación de residuos, por lo que se obtendrían elementos más respetuosos con el medio ambiente.

Por otro lado, también sería importante la optimización en el uso de lubricantes. Este hito podría conseguirse mejorando la tribología de los rodamientos ya que la cantidad de lubricante a emplear podría ser menor. Por un lado, podría variarse la geometría de los elementos que lo forman, dando lugar a una recirculación del lubricante y, por otro, podrían emplearse materiales con características autolubricantes o con un coeficiente de fricción más bajo.

Esta tesis se centra en el desarrollo de una nueva familia de rodamientos mediante la formulación de nuevos materiales poliméricos autolubricantes, nuevos lubricantes avanzados y nuevos tratamientos superficiales en aceros al carbono. De cara definir un diseño final, cada una de las líneas de trabajo se ha dividido en una fase de desarrollo, una de validación en probeta y, finalmente, una de ensayo sobre rodamiento completo.

A lo largo de la investigación, se han realizado publicaciones científicas que recogen los resultados de las distintas líneas del trabajo. En primer lugar, en el artículo presentado en el congreso internacional *The 29th European Modeling & Simulation Symposium*, celebrado en septiembre de 2017, se muestran los resultados obtenidos a raíz del análisis de la influencia de la variación de la geometría y del uso de diferentes matrices poliméricas en el proceso de inyección del componente plástico de dichos rodamientos (jaula). Posteriormente, y también en el marco del desarrollo de nuevos materiales plásticos, se ha realizado una publicación en la revista *Tribology International* en la que se estudió la influencia de, por un lado, la adición de nanoflakes de grafeno y de dióxido de circonio a los compuestos de poliamida 66 con fibra de vidrio y, por otro, el texturizado de las superficies para mejorar sus propiedades autolubricantes. Finalmente, en septiembre de 2020, se publicaron en la revista *Polymers* las innovaciones obtenidas tras el estudio en que se comparó el comportamiento al desgaste de los composites con matriz de poliamida y diferentes nanoaditivos y aditivos de refuerzo con el fin de conseguir un material autolubricante adecuado para jaulas de rodamientos.

En paralelo al desarrollo de la línea de trabajo polimérica, también se ha progresado en la creación de nuevos recubrimientos en aceros al carbono. Estos avances se centraron en el comportamiento tribológico de un recubrimiento de carbonitruro de circonio aplicado sobre sustratos de acero para rodamientos, se publicaron en la revista *Coatings* y se presentaron en el congreso internacional *1st Coatings and Interfaces Web*

Conference, CIWC2019 celebrado en marzo de 2019.

Por último, en referencia a las innovaciones en nuevos lubricantes, el estudio se ha centrado no solo en la mejora de las prestaciones en términos de resistencia y temperatura sino también en la sostenibilidad de las nuevas formulaciones para reducir su dependencia de los combustibles fósiles y/o de materiales críticos como el litio. Estos resultados no han llegado a plasmarse en una publicación científica todavía, pero en el anexo 1 se presenta el desarrollo de dichos resultados.

Finalmente, cabe destacar la representatividad de la investigación realizada en la presente tesis ya que su desarrollo se ha llevado a cabo en colaboración con la empresa Fersa Bearings y con las contribuciones del centro tecnológico IK4-Tekniker y de la empresa Brugarolas. Esto provoca un alto nivel de madurez tecnológica en los resultados obtenidos lo que hace que puedan ser industrializados en el corto plazo.

LISTADO DE FIGURAS

LISTADO DE TABLAS

ÍNDICE

1. INTRODUCCIÓN

La tesis doctoral "Estudio de la mejora de la eficiencia de rodamientos de rodillos cónicos en base a estrategias de mejora de los materiales y del diseño" ha sido desarrollada dentro del grupo de investigación i+ de la Universidad de Zaragoza, en el Área de Ingeniería Mecánica dentro del Departamento de Ingeniería Mecánica de la Escuela de Ingeniería y Arquitectura en colaboración con la empresa Fersa Bearings, S.A. Ha sido dirigida conjuntamente por la Dra. Isabel Clavería Ambroj y el Dr. Pere Vicenc Castell Muixi y se presenta como compendio de publicaciones, las cuales se muestran íntegramente en la sección 6 del presente documento.

Esta memoria pretende sintetizar todo el trabajo realizado a lo largo de los 7 años de investigación; se incluye y presenta información desde objetivos y metodología de la tesis, hasta la aplicación de la metodología, conclusiones y futuras líneas de investigación.

Mediante el desarrollo de 3 líneas de trabajo basadas en sus variables más influyentes se podrá definir un diseño más eficiente de rodamientos de rodillos cónicos que derivará en una nueva gama de producto de la empresa Fersa Bearings.

El hecho de que el 30% del consumo mundial de energía se pierda en forma de calor debido a la fricción [1] hace patente la necesidad del desarrollo de nuevas tecnologías que permitan un descenso de las pérdidas ocasionadas por la fricción. Para conseguir esta reducción, el comportamiento individual de los componentes mecánicos que forman los equipos que nos rodean debe de ser más eficiente. En este sentido, los rodamientos juegan un papel fundamental por lo que la mejora de su lubricación y tribología resulta clave en el incremento de la eficiencia final del conjunto.

De igual modo, también resulta fundamental aumentar la sostenibilidad de los sistemas mecánicos. A este respecto, el aumento de las prestaciones de funcionamiento de los rodamientos y de su vida útil daría lugar, por un lado, a poder reducir sus dimensiones y, por otro, a la necesidad de un menor consumo de recambios con lo que se reduciría el consumo de materias primas y los residuos generados.

Además, la presente tesis se centra en mejorar el impacto ambiental de los rodamientos gracias al avance en el uso de lubricantes. Para ello, de una parte, se mejorará la tribología de los rodamientos (por lo que la cantidad de lubricante necesaria sería menor) mediante la variación de su geometría o el uso de nuevos materiales autolubricantes o con un coeficiente de fricción más bajo y, de otra parte, se desarrollarán formulaciones que eviten el uso de hidrocarburos o materiales críticos como el litio.

El principal objetivo consiste, por tanto, en incrementar la eficiencia de los rodamientos de rodillos cónicos mediante la mejora de su respuesta a fricción y fatiga, con el fin de incrementar sus prestaciones de temperatura, resistencia mecánica y medioambientales.

1.1. JUSTIFICACIÓN DE LA TESIS DOCTORAL

En los últimos años, el sector de la automoción se está teniendo que enfrentar a la necesidad de reducir su impacto ambiental, especialmente debido a la influencia del cambio climático y a la mayor concienciación de la sociedad. Este hecho, las nuevas directivas publicadas y el aumento del coste de la energía, está provocando que las compañías lleven a cabo acciones que deriven en una mayor sostenibilidad de sus productos.

Por ello, el presente doctorado surge con la motivación de desarrollar nuevos rodamientos avanzados para aplicaciones que requieran una gran eficiencia fruto de una menor fricción y desgaste. Para conseguir este fin, se van a desarrollar nuevos materiales poliméricos (tanto matrices como aditivos), se van a llevar a cabo tratamientos superficiales para fabricar componentes mejorados que aumenten las prestaciones de los rodamientos y los capaciten para trabajar en condiciones extremas y, finalmente, se formularán nuevos lubricantes (grasas) que mejoren las características de fricción y desgaste, obteniéndose rodamientos con una durabilidad mayor. Esto permitirá obtener nuevos productos para aplicaciones más eficientes que darán lugar a una nueva gama de producto “High Efficiency Bearings” en la empresa Fersa Bearing, S.A.

Con relación a esta nueva familia, cabe destacar que, a la hora de seleccionar la referencia de rodamiento a estudiar dentro de esta tesis doctoral, se consideró la opinión y experiencia de la propia empresa. El rodamiento elegido fue la referencia F 15100 con un diámetro exterior de 140mm, un diámetro interior de 82 mm y una masa de 6,45 kg (ver Figura 1). Este rodamiento se ensambla en ejes delanteros de vehículos pesados (ver Figura 2).

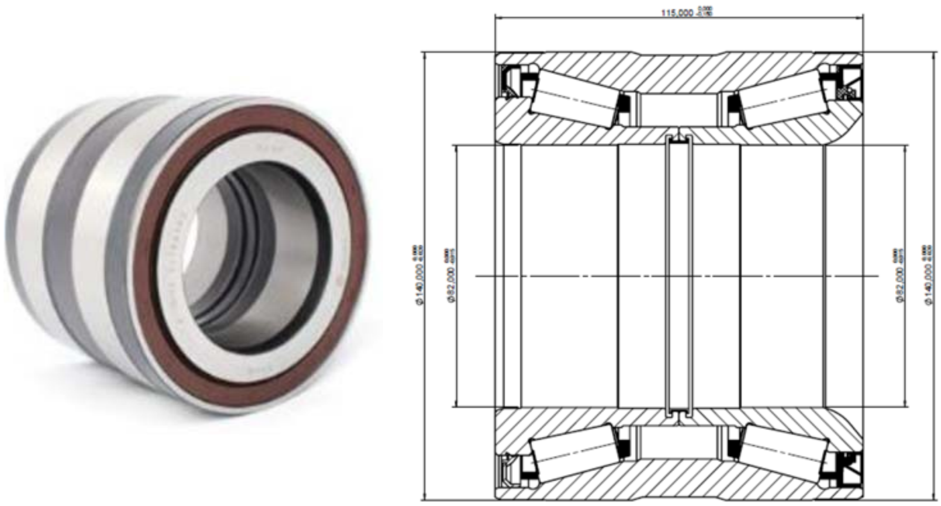

(a) (b)

Figura 1. Rodamiento referencia F15100: (a) imagen real, (b) sección rodamiento

Figura 2. Aplicación rodamiento referencia F15100

Los motivos de seleccionar esta referencia fueron, por un lado, la existencia de una caracterización detallada de la misma, desde varios puntos de vista (ensayos de fricción, vida, costes, etc.), pero siempre enfocada al comportamiento del acero de los elementos principales (aro exterior, aros interiores y elementos rodantes). Sin embargo, otros componentes como la jaula (de material polimérico) o la lubricación no habían sido estudiados hasta el momento. Este hecho, junto con la asignación de Fersa Bearings como nuevo proveedor de esta referencia para un importante fabricante de vehículos pesados, hacían que la referencia F15100 fuera la más adecuada para ser estudiada en profundidad en la presente tesis doctoral.

1.2. Objetivos y Metodología

1.2.1. Objetivos

El objetivo general de la presente tesis doctoral es mejorar el comportamiento, frente fricción y fatiga, de los rodamientos de rodillos cónicos con el fin de incrementar sus prestaciones de temperatura, resistencia mecánica y medioambientales.

En base al objetivo principal, se desarrollan los siguientes objetivos específicos:

- Incrementar el conocimiento en nuevos materiales poliméricos para la fabricación de jaulas de altas prestaciones.
- Potenciar la línea de trabajo de procesamiento de materiales poliméricos. Procesamiento selectivo de variables.
- Potenciar la línea de trabajo de aditivación de materiales. Caracterización de nuevas mezclas.
- Potenciar la línea de trabajo de desarrollo de nuevos recubrimientos mediante la tecnología *Physical Vapour Deposition* (PVD).
- Formular nuevas grasas de altas prestaciones que tengan mejores prestaciones medioambientales.
- Incrementar el *roadmap* de producto de Fersa Bearings, ofreciendo rodamientos adaptados a trabajar en condiciones extremas.
- Generar procesos más flexibles y adaptables a las cambiantes tendencias del mercado.

1.2.2. Metodología

Partiendo de estos objetivos, se comenzó la tesis doctoral realizando una investigación preliminar del diseño de los rodamientos de rodillos cónicos, identificando sus principales componentes y, mediante una revisión del estado del arte, analizando las variables de diseño que influían en su comportamiento a fricción y fatiga.

Tras este estudio inicial, se concluyó que la tesis doctoral debía de estar sustentada en 3 líneas de investigación:

- Nuevos materiales poliméricos autolubricantes.
- Nuevos lubricantes avanzados adaptados a los nuevos rodamientos.
- Nuevos tratamientos superficiales en aceros al carbono.

Dentro de cada línea de investigación, se realizó una fase de desarrollo a la que siguió una fase de validación, a nivel de probeta, en la que se ejecutaron los ensayos más representativos que caracterizaron los nuevos compuestos. Posteriormente, se ensayó el comportamiento, a fricción y a fatiga, del rodamiento completo, estudiando, en cada caso, combinaciones de las innovaciones con las que se obtuvieron los mejores resultados. Como consecuencia de estos ensayos, se definió un diseño óptimo y final.

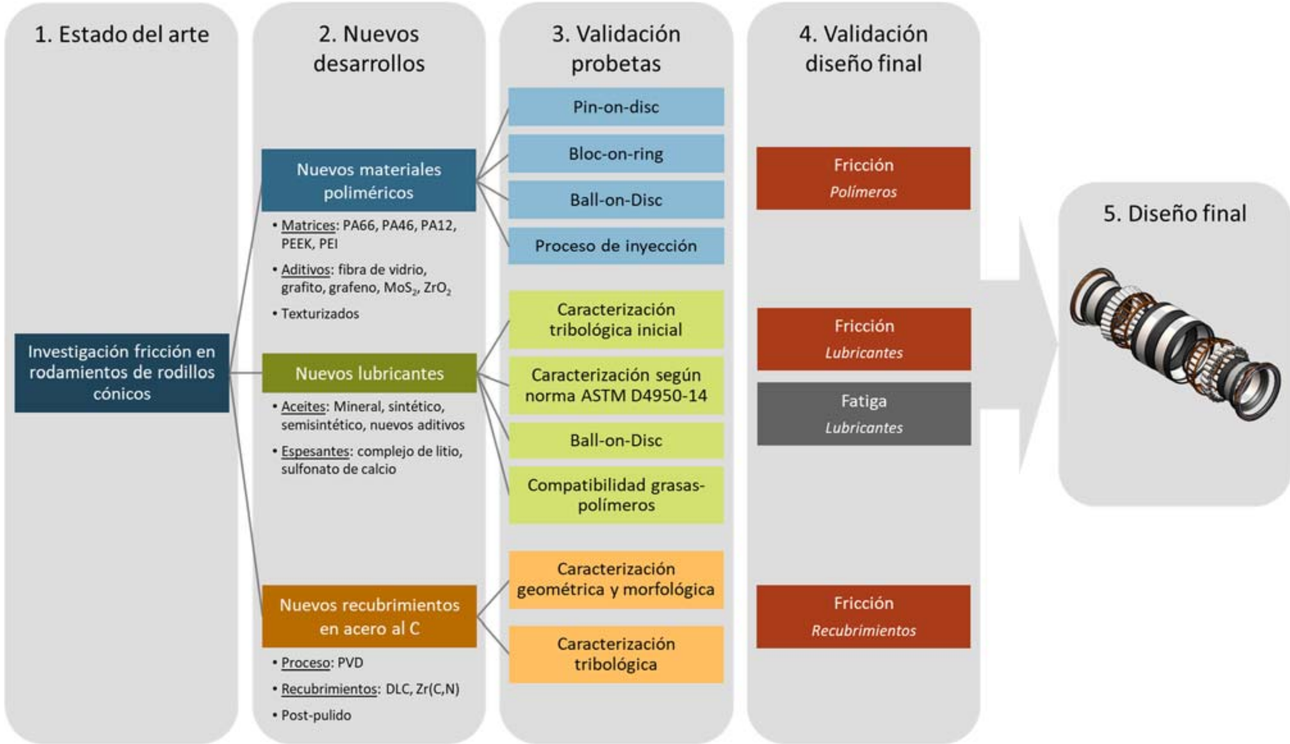

Figura 3. Metodología seguida para el desarrollo de la tesis doctoral

2. ESTADO DEL ARTE

2.1. GENERAL

Los rodamientos son los elementos de máquinas más empleados en la industria para facilitar el par cinemático que permite la rotación relativa entre elementos móviles. De los diversos tipos de rodamiento destaca el rodamiento de rodillos cónicos como el más empleado en todo tipo de transmisiones donde los requerimientos de rigidez, capacidad de carga, velocidad de giro y combinación de cargas axiales y radiales deban de tener un equilibrio ponderado entre sí.

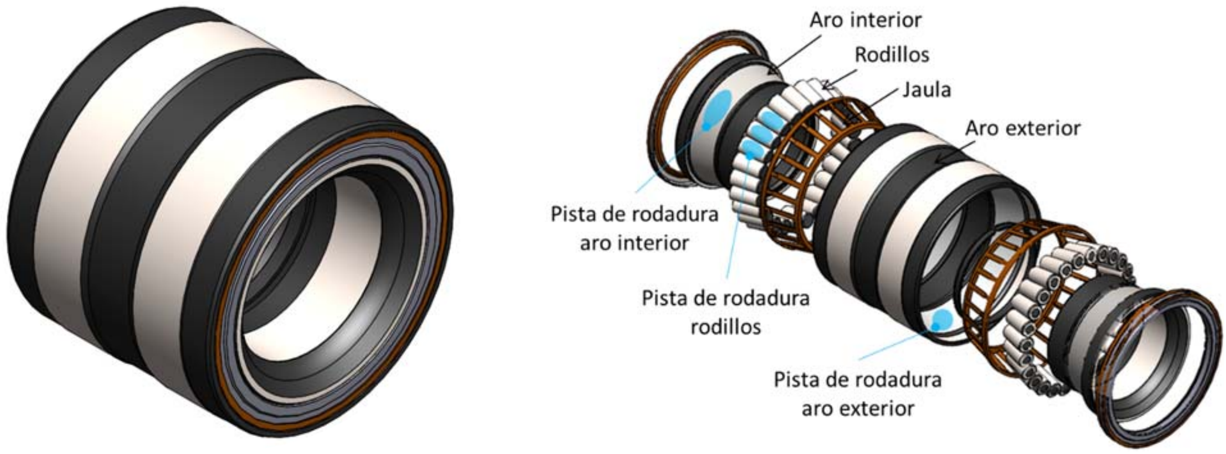

(a) *(b)*

Figura 4. Ejemplo de un rodamiento: (a) conjunto ensamblado, (b) vista explotada de los componentes y pistas de rodadura

Los componentes principales de un rodamiento son jaulas, elementos metálicos y lubricante. Entre estos componentes, las jaulas tienen una influencia importante en la adecuación de un rodamiento a cada aplicación particular. Sus principales funciones son:

- Mantener los elementos de rodadura (en este caso rodillos cónicos) separados entre sí para evitar el contacto directo entre rodillos con velocidades tangenciales opuestas, y por tanto prevenir el desgaste prematuro de estos, manteniendo la fricción y la generación de calor por rozamiento al mínimo posible.
- Mantener una distribución uniforme de los elementos de rodadura a lo largo de toda la circunferencia media del rodamiento y así proporcionar no sólo una distribución uniforme de las cargas mecánicas, sino favorecer la rotación y velocidad de giro constante y por tanto un funcionamiento silencioso.
- Guiar los elementos de rodadura desde zonas de baja carga, mejorando así las condiciones de rodadura en el rodamiento y al mismo tiempo evitando deslizamientos indeseados que desgasten prematuramente los componentes.
- En el caso particular de rodamientos cónicos, actuar como retén de los numerosos rodillos que lo componen para facilitar las operaciones de montaje y desmontaje.

Las jaulas de rodamiento cumplen, por tanto, una función pasiva respecto al funcionamiento del rodamiento y **es objeto de este doctorado mejorar su comportamiento ante estas funciones descritas introduciendo nuevos materiales y convirtiéndola en un elemento activo respecto a la lubricación del rodamiento modificando su geometría y estructura superficial.**

En servicio, las jaulas de rodamiento por lo general sufren distintos tipos de esfuerzos derivados de fuerzas de fricción y de inercia, así como deformación bajo presión. Además, el uso de lubricantes, grasas y aceites, solventes orgánicos o refrigerantes pueden afectarles químicamente envejeciendo el material y mermando sus propiedades. Es por esta razón que tanto la selección adecuada de las matrices termoplásticas como sus aditivos y refuerzos son de especial importancia para asegurar que se pueden cumplir todos los requisitos planteados, mejorando no sólo las prestaciones de las jaulas sino también las del propio rodamiento.

Las jaulas tienen distintas geometrías en función del tipo de rodamiento en el que instalan, siendo las denominadas “jaulas sólidas” las que se emplean en los rodamientos cónicos con más frecuencia y para las que la innovación en nuevos materiales y funcionalidades es más prolífica. Este tipo de jaulas se caracteriza por combinar de manera ventajosa tanto la resistencia como la elasticidad. Mediante el uso de materiales termoplásticos se aúnan las ventajas de implementar un proceso de fabricación seriada como es la inyección con las buenas propiedades finales de deslizamiento de la jaula polimérica respecto a las superficies de acero de los rodillos ya lubricadas. Así mismo, la buena calidad superficial obtenible por inyección permite un contacto suave con las superficies de extrema calidad de los rodillos minimizando la fricción y reduciendo tanto la generación de calor como el desgaste. Si se emplean materiales termoplásticos, su menor densidad respecto a los metales o composites permite reducir los efectos de inercia siendo óptimos para su utilización en rodamientos que giren a altas velocidades o que tengan un uso continuo.

Las limitaciones más importantes que tienen las jaulas termoplásticas son la elevación de temperatura que sufre dada su limitada conductividad térmica que hace que, en condiciones de uso continuo o severo-intermitente, puedan alcanzar los límites de uso de la matriz plástica. También limita el uso de determinados lubricantes, especialmente aceites, que pueden reducir exponencialmente su vida ante determinadas condiciones de carga por envejecimiento del material termoplástico.

Por su parte, **los elementos metálicos de los rodamientos** objeto del presente doctorado están fabricados con acero de alto contenido en carbono (100Cr6, según ISO 683-17 [3]). La composición química de este acero es: Carbono (0.93–1.05%), Manganeso (0.25–1.20%), Cromo (0.90–1.60%), Molibdeno (0–0.10%), Níquel (0–0.25%) and Hierro (95.75–97.92%) y otros componentes como: Oxígeno (max. 10–15 ppm), Aluminio (max. 0.050%), Titanio (max. 30–50 ppm) and Calcio (max. 10 ppm) [4]. Así mismo, como consecuencia del requerimiento de resistencia a fatiga de los rodamientos, el acero debe someterse a una transformación martensítica mediante un tratamiento de endurecimiento, ajustando la dureza de la superficie a 59-63 HRC (escala de dureza Rockwell C) a una temperatura de 180-200ºC.

Una parte fundamental de estos elementos metálicos son sus pistas de rodadura las cuales sufren distintos procesos de mecanizado hasta alcanzar la calidad superficial necesaria para asegurar un correcto contacto entre superficies. Cabe destacar que el contacto producido entre las pistas de rodadura de los aros exteriores, interiores y rodillos es una rodadura sin deslizamiento. Este hecho provoca que se generen las principales zonas de fricción dentro del rodamiento como consecuencia de las elevadísimas presiones originadas por los distintos elementos de la transmisión (engranajes, ejes, etc…). Así mismo, mencionar también el fenómeno de pitting o micropitting producido en el contacto y generado por un proceso de fatiga sub-superficial. Además, si las superficies no están suficientemente lubricadas, pueden generarse puntos de corrosión.

Uno de los factores clave que afectan de una manera muy significativa el funcionamiento de un rodamiento, es el lubricante empleado. La lubricación en los rodamientos tiene la función de evitar o de reducir el contacto metálico entre las superficies de rodadura y de deslizamiento, es decir, mantener bajos el rozamiento y el desgaste.

2.2. MATERIALES POLIMÉRICOS

En los últimos años, el desarrollo en la ingeniería de plásticos ha permitido el uso de resinas termoplásticas en partes de elementos de máquinas en sustitución de metales. Los rodamientos son uno de los componentes mecánicos más utilizados en la industria y sobre los que se puede aplicar la sustitución por materiales poliméricos en algunos de sus componentes como las jaulas. Las nuevas tendencias en rodamientos se centran en obtener rodamientos de alto rendimiento capaces de trabajar a alta velocidad y temperatura [1][5] para lo cual es necesario mejorar las propiedades tribológicas de los rodamientos y de sus elementos.

Para su uso como triboelementos, las matrices de resinas termoplásticas a menudo se han combinado con diversos rellenos [7]-[12]. Los rellenos con morfología de fibra, como el carbono (FC) y las fibras de vidrio (FV), pueden mejorar las propiedades mecánicas y la resistencia al desgaste de la matriz como resultado de sus efectos de soporte de carga y la alta resistencia al desgaste. Así mismo, las cargas de partículas poliméricos o nanotubos de carbono también pueden ser útiles para mejorar las propiedades mecánicas y tribológicas [13].

2.2.1. Matriz polimérica

Actualmente, las jaulas para rodamientos de vehículos están fabricadas en distintos materiales como acero, latón, polímeros termoestables reforzados o polímeros termoplásticos. La poliamida (PA) se considera uno de los sustitutos de los metales más prometedores debido a sus buenos rendimientos tribológicos, propiedades mecánicas y termoestabilidad [14]. Los buenos resultados tribológicos y las propiedades mecánicas de PA se atribuyen a sus abundantes grupos amida en la columna vertebral, que pueden formar enlaces de hidrógeno intermoleculares y conducir a una fuerte fuerza intermolecular [15]. Como contrapunto, sus grupos amida causan una severa higroscopicidad de PA, lo que conduce al deterioro de las propiedades mecánicas, resistencia al desgaste y estabilidad dimensional de los productos de PA en ambientes húmedos [17]. La opción más extendida en cuanto a la utilización de poliamidas es la inyección de PA66 con mayor o menor refuerzo con fibra de vidrio (entre un 10 y un 30%). De hecho, actualmente la empresa Fersa Bearings emplea PA66+25%fibra de vidrio como material para el desarrollo de algunos modelos de jaulas.

Uno de los factores más limitantes a la hora de utilizar matrices poliméricas en las jaulas de rodamientos son las altas temperaturas a las que puede llegar a estar sometido este componente a causa de la fricción. En la Figura 5 se puede ver una clasificación de los plásticos en función de su temperatura de trabajo [16].

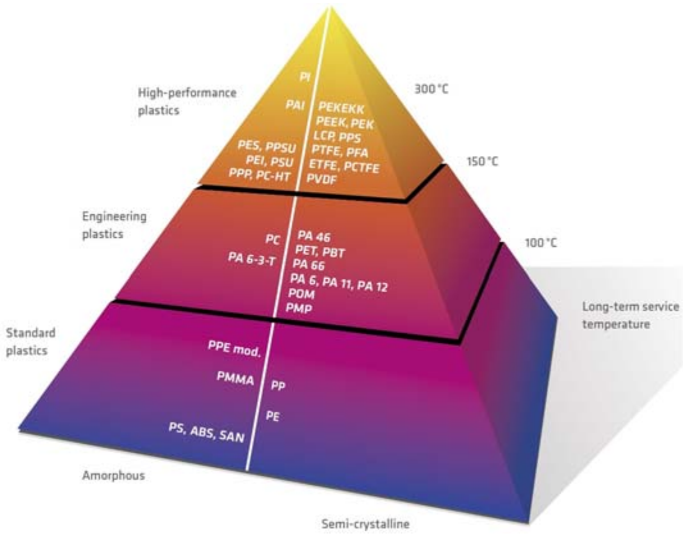

Figura 5. Clasificación de los plásticos en función de su temperatura de trabajo

- **Poliamida 66 (PA66)**: termoplástico semicristalino, también conocido como Nylon 66, en el que cada unidad de base contiene 6 átomos de carbono. Sus principales características son [28]: una resistencia mecánica, dureza, rigidez y tenacidad medias-altas, una elevada capacidad de amortiguación mecánica, buena resistencia a la fatiga, excelente resistencia al desgaste, en la mayoría de los casos, buenas propiedades de deslizamiento y absorción de humedad y reducida estabilidad dimensional. Se trata de un material que se ha usado ampliamente para aplicaciones de engranajes y rodamientos, pero, a pesar de que sus propiedades tribológicas han sido estudiadas por en algunas ocasiones [18][19], sus mecanismos de desgaste en componentes mecánicos no se comprenden completamente. Recientemente, se ha resaltado la importancia de la cristalinidad general para las propiedades tribológicas de la poliamida 66. Sin embargo, el grado de cristalinidad no es el mismo que el de la microestructura, ya que diferentes microestructuras pueden tener la misma cristalinidad. En investigaciones anteriores, una amplia variedad de polímeros y sus compuestos fueron analizados, como es el caso de PA66 [20]-[22] o de la PA66 reforzada con fibra de vidrio [23]-[27]. Como conclusiones, se encontró que la PA66 sin reforzar tenía una alta tasa de desgaste a bajas temperaturas. Sin embargo, con el aumento de la entrada de calor, propia del rozamiento en régimen operativo, se descubrió que se producía una capa superficial blanda que se comportaba como una capa autolubricante y que reducía la fricción y el desgaste. Por su parte, de los ensayos con PA66 reforzada con un 30% de fibra de vidrio se concluyó que, a pesar de la naturaleza abrasiva de la carga, estos compuestos tenían mejor comportamiento a desgaste y podrían usarse como engranajes si la cristalinidad del material de la matriz era baja y la temperatura máxima de la superficie era limitada (150°C).

Otros materiales que también pueden resultar apropiados para ser sustitutos de materiales metálicos son:

- **Acrilonitrilo Butadieno Estireno (ABS)**: termoplástico amorfo muy resistente a los golpes, muy utilizado en automoción y otros usos industriales y domésticos. Posee elevada resistencia química y a la fatiga, alta dureza y rigidez, resistencia a la abrasión y a las manchas.

- **Polioximetileno (POM)**: termoplástico semicristalino que ofrece una alta resistencia mecánica y rigidez. Tiene muy buenas propiedades de deslizamiento y resistencia a la abrasión, así como una baja absorción de la humedad y una buena estabilidad dimensional. Su particular resistencia a la fatiga y sus buenas propiedades de mecanizado hacen que el POM sea un material muy versátil para piezas complejas.

- **Poliamida 46 (PA46)**: termoplástico semicristalino, también conocido como Nylon 46. Tiene una elevada estabilidad dimensional térmica y, a altas temperaturas, ofrece considerables ventajas respecto a otras poliamidas en lo referente a propiedades mecánicas, resistencia a fisuras y a fatiga. En consecuencia, es un material muy indicado para aplicaciones en que se exija fricción y desgaste a altas temperaturas. En los últimos tiempos ha habido un creciente interés en el desgaste y las propiedades de fricción de la PA46 y sus compuestos de fibra [28]-[32]. Kurokawa y col. [29], por ejemplo, comparó varias poliamidas reforzadas con carbono para aplicaciones de engranajes. En estos estudios encontraron que los compuestos PA66 y PA46 fallaron por el desgaste de los dientes en contraste con los compuestos PA12 y PA6 que fallaron por fatiga con poco desgaste. El mayor desgaste de los compuestos PA46 se atribuyó a su alta cristalinidad. Por otro lado, la PA46 con refuerzo de fibra de vidrio fue investigado por Unal et al. [33] quien nuevamente encontró altos coeficientes de fricción y una alta tasa de desgaste en comparación con los compuestos PA66.

- **Poliamida 12 (PA12)**: termoplástico cristalino, también conocido como Nylon 12 y derivado por modificación de las estructuras químicas (longitud de las cadenas y organización química) de una poliamida 66. Posee una excelente resistencia química y térmica, una alta estabilidad dimensional y baja densidad, resistente al desgaste, dureza extrema. Para mejorar las propiedades mecánicas de PA12 para aplicaciones de ingeniería, se han incorporado nanomateriales como nanotubos y nanofibras de carbono, nanotubos y nanofibras de halloysita y nanoplaquetas de grafeno, produciendo materiales compuestos y nanocompuestos [34]-[36]. Se trata de una poliamida con menor absorción de agua que PA66 y PA46. El estudio de esta poliamida se decidió incluir en la presente tesis debido a su alta estabilidad dimensional y baja densidad, resistente al desgaste, dureza extrema. Como ha quedado demostrado, la poliamida es un importante material de ingeniería y podría usarse en aplicaciones de fricción y desgaste. Sin embargo, normalmente tiene un alto coeficiente de fricción en condiciones secas contra otros materiales. En comparación con PA66 y PA46, PA12 absorbe muy poca humedad, lo que permite que los componentes fabricados con ella conserven un alto grado de estabilidad dimensional, incluso en entornos con niveles fluctuantes de humedad. Además, presenta una excelente resistencia a los productos químicos, incluidos fluidos hidráulicos, aceite, combustibles, grasas (positivo para el caso de rodamientos), agua salada y solventes. Cuando se enfrenta en seco en aplicaciones contra acero, poliacetal, tereftalato de polibutileno (PBT) y otros materiales, la PA12 tiene un coeficiente de fricción muy bajo. Incluso cuando se coloca bajo una carga cíclica de alta frecuencia, la PA12 sigue siendo resistente a la fatiga.

- **Polieteretercetona (PEEK)**: las poliariletercetonas son termoplásticos resistentes a muy altas temperaturas (apto para uso continuo en temperaturas de hasta 260°C [35]). La alta resistencia mecánica de estos polímeros aromáticos semicristalinos se mantiene incluso a altas temperaturas. Algunos de estos polímeros presentan muy buena tenacidad a bajas temperaturas, alta resistencia a la fatiga, muy poca tendencia a la deformación a alta temperatura (creep) así como buenas propiedades de deslizamiento y desgaste (coeficiente de fricción bajo). Su resistencia química es también muy favorable. Su columna vertebral relativamente rígida brinda una excelente estabilidad a altas temperaturas. Tiene una alta temperatura de transición vítrea, un alto punto de fusión y una alta temperatura de servicio continuo junto con una fácil procesabilidad por moldeo por inyección y otras técnicas usadas en los polímeros termoplásticos [38]-[40]. Se han llevado a cabo muchas investigaciones sobre las propiedades de fricción y desgaste de PEEK y sus compuestos. Friedrich et al. [42] examinaron los efectos de la rugosidad y la temperatura de la contra cara en la fricción y el desgaste. También se revisaron las propiedades tribológicas de los materiales PEEK para aplicaciones deslizantes [43]. Schelling y Kausch [44] discutieron el efecto de la cristalinidad de PEEK en la fricción y el desgaste en las pruebas de fricción seca tanto recíprocas como deslizantes.

- **Polisulfuro de fenileno (PPS)**: termoplástico amorfo con elevada resistencia mecánica y rigidez, temperatura de servicio elevada (>200°C), resistencia a la abrasión y al desgaste, resistencia a la deformación a alta temperatura (creep), estabilidad dimensional, resistencia química, baja absorción de humedad y excelentes propiedades eléctricas.

- **Polieteramida (PEI)**: termoplástico amorfo que ofrece una increíble termorresistencia (excelente estabilidad de las propiedades físicas y mecánicas a temperaturas elevadas gracias a una temperatura de transición vítrea de más de 180°C), una gran resistencia y rigidez y una amplia resistencia química [38]. PEI destaca por su estabilidad en un amplio rango de temperaturas. Es amorfo y cuando no se modifica es transparente y exhibe resistencia inherente a la llama y baja evolución de humo. También exhibe relajaciones fuertes en la región de transición vítrea, lo cual es importante para comparar el comportamiento dinámico mecánico y dieléctrico [45]. El PEI generalmente es menos costoso que el PEEK, más versátil y se usa ampliamente como termoplástico amorfo.

Las propiedades más significativas de los materiales analizados se resumen en la Tabla 1.

	Densidad [g/cm3]	Módulo elástico medio [MPa]	Resistencia tracción [MPa]	Coeficiente de fricción medio	Absorción de agua a 100% humedad [%]	T procesado [ºC]	Tg [ºC]	Tm [ºC]	Coste [€/kg]
PA66	1,14	2850	78	0,3	9	230-260	50	220	2,5
POM	1,41	2900	65	0,1-0,3	8	190-210	-30	183	1,7
ABS	1,05	2300	43	0,5	0,5	210-240	105	190	1,5
PA46	1,18	3300	100	0,4	4	300-310	43	295	8,0
PA12	1,01	1800	45	0,35	1,5	210-230	40-43	190	6,0
PEEK	1,31	3500	93	0,3-0,38	0,12	260-300	150	341	79,2
PPS	1,43	3400	55	0,04	0,04	290-320	85	280	26,8
PEI	1,27	3447	120	0,386	1,25	240-250	210	-	13,6
PTFE	2,19	2200	36	0,02-0,28	<0,01	240-360	-20	327	5,2

Tabla 1. Propiedades matrices poliméricas analizadas

2.2.2. Aditivos

Las poliamidas 6, utilizadas como sustitutas de los metales, son termopláticos de ingeniería de alto rendimiento que se utiliza en aplicaciones eléctricas/electrónicas, de automóviles, de embalaje, textiles y de consumo debido a sus excelentes propiedades mecánicas. Sin embargo, las limitaciones en el nivel de propiedades mecánicas, la baja temperatura de deflexión térmica, la alta absorción de agua y la inestabilidad dimensional han impedido su amplia gama de aplicaciones. A pesar de ello la familia de la PA6 aditivado con grafito, carbono y cera ha encontrado su aplicación en aplicaciones de campo de alta velocidad, sin la necesidad de lubricación exterior [46][47].

Por otra parte, algunos científicos [48]-[51] informaron que el coeficiente de fricción puede, en general, reducirse y la resistencia al desgaste mejora cuando los polímeros se refuerzan con fibra de vidrio, carbono y aramida. De hecho, el comportamiento tribológico de los polímeros se ve afectado por las condiciones ambientales, de funcionamiento y por el tipo, tamaño, cantidad, forma y orientación de las fibras [42].

Se han realizado numerosas investigaciones que exploran la influencia del contenido de relleno, las condiciones de prueba, la geometría de contacto y el entorno en el comportamiento de fricción y desgaste de los polímeros. Franke et al.[53] y Hooke et al.[54] informan que el coeficiente de fricción puede, en general, reducirse y aumentar la resistencia al desgaste seleccionando las combinaciones de materiales correctas.

Algunos de los aditivos más prometedores de cara a la mejora de las propiedades tribomecánicas de las matrices poliméricas son:

- **Grafito y micrografito**: forma cristalina del carbono (junto con el diamante). La adición de fibras cortas a polímeros resistentes al desgaste y a altas temperaturas está destinada principalmente a mejorar otras propiedades como rigidez, resistencia al impacto, conductividad térmica y resistencia a la fluencia a temperaturas elevadas [55].

- **Microfibras de vidrio**: el uso de termoplásticos reforzados con fibra corta de vidrio (RTFV) está siendo progresivamente una opción muy elegida en la industria, especialmente para aplicaciones técnicas, debido a sus propiedades mecánicas interesantes, como, por ejemplo, la relación densidad/alta rigidez [56]-[58].

- **Micro y nano fibras de carbono:** la fibra de carbono es una fibra que se utiliza normalmente como material de refuerzo en materiales de alto rendimiento (ligeros, alta resistencia, flexibles, etc.). Presentan grandes áreas superficiales y capacidad y velocidad de adsorción superiores en comparación con otros materiales como los polvos o gránulos de carbón activado. A partir de estudios recientes realizados con diferentes tipos de fibras de carbono (PAN-based vs Idemitsu HT pitch-based), se puede concluir que la resistencia al desgaste del compuesto será mejor cuanto menos sensibles reaccionen las fibras contra la fricción fibra-fibra y la rotura temprana [59][60].

- **Sulfuro de molibdeno (MoS_2):** existen muchos informes de investigación sobre la mejora en la resistencia al desgaste de diversas poliamidas tales como PA6, PA66, PA11, PA46, etc., con lubricantes sólidos, tales como sulfuro de molibdeno (MoS_2), grafito (Gr) y politetrafluoroetileno (PTFE). Como variante de aditivo en base a molibdeno, el MoS_2 es un sulfuro cristalino negro de molibdeno con una estructura en capas y, en su aspecto y tacto es similar al grafito. Este compuesto ya ha sido analizado como aditivo a especies poliméricas como la poliamida por algunos investigadores [61][62].

- **Materiales de cambio de fase:** los materiales con cambio de fase (en inglés, Phase Change Material, PCM) son materiales con un alto calor latente que, a la temperatura de cambio de fase (sólido ↔ líquido), son capaces de almacenar o liberar grandes cantidades de energía (hasta 100 veces más que si emplea el calor sensible). El interés de este tipo de materiales radica en que, durante el cambio de fase, la temperatura se mantiene constante mientras que el material va absorbiendo o liberando energía [63].

- **Nanoplatelets de grafeno:** es una forma alótropo del carbono consistente en láminas formadas por carbono de espesor atómico. Estos materiales se obtienen a partir del grafito exfoliando las láminas que lo forman. Los nanoplatelets de grafeno están formados por varias capas de grafeno apiladas (entre 1 y 10 capas) con un espaciado entre capas superior a la del grafito. Esta estructura presenta unas propiedades excelentes: material flexible, elevada transparencia, buena conductividad eléctrica y térmica, alta dureza (200 veces superior al acero) y excelentes propiedades mecánicas (tracción e impacto) entre otras propiedades. Este aditivo tiene un precio aproximado de 60€/Kg (para nanoplatelets de entre 10-20 capas) [64].

- **Nanografeno:** el nanografeno es una lámina simple de grafeno, un millón de veces más delgada que el milímetro. El nanografeno tiene un bajo coste respecto al nanotubo o nanofibra de carbono. Esta gama de morfología laminar se puede utilizar como material lubricante para la preparación de mezclas con termoplásticos y materiales conductores. La adición de este aditivo supone incrementar espectacularmente la conductividad térmica de la mezcla con polímero, el módulo de Young, la resistencia, la conductividad, la resistencia a la permeación de gases, etc. El precio aproximado del nanografeno es de 72€/cm2. En el caso del nanografeno su procesamiento para ser extruido con plásticos resulta muy complejo ya que no se vende en polvo si no en formato de plaquetas [65][66].

- **Nanopartículas de zirconia:** el dióxido de zirconio (ZrO_2), también conocido como zirconia, es un material cerámico con propiedades mecánicas adecuadas para uso en determinadas estructuras. Las propiedades de la zirconia son similares a las del acero inoxidable, presenta una resistencia a la tracción que puede ser de 900 a 1200 MPa y resistencia a la compresión alrededor de los 2000 MPa. La resistencia a la fractura del óxido de zirconia se debe a que, en el momento de una fisura, ésta produce un aumento de energía provocando presiones tangenciales y un cambio de estructura, pasando de su forma tetragonal a la monoclínica (que tiene un 4,7% más volumen) y por consiguiente se detiene el progreso de la grieta por las fuerzas de compresión [52]. Se trata de un biomaterial con una excelente resistencia y dureza [68]-[71]. Las nanopartículas de zircona se caracterizan por su elevada dureza y pueden ser utilizadas en materiales plásticos para mejorar su resistencia al rayado. Se sabe que el desarrollo de compounding en base poliamidas con la inserción de $ZrO2$ implica incrementos de la resistencia a la temperatura, así como la mejora de las propiedades ignífugas.

2.2.3. Texturizado

En la última década, el desarrollo de nuevas técnicas de modificación superficial ha repercutido en el desarrollo de métodos de tratamiento superficial innovadores que pretenden sustituir a los empleados actualmente a fin de mejorar las propiedades tribológicas de sistemas sometidos a fricción. De esta manera, diferentes técnicas mecánicas, litográficas o de haz energético vienen siendo empleadas con el fin de estudiar el efecto de la modificación topográfica en la mejora de la fricción y reducción del desgaste en este tipo de sistemas [72]-[74]. La actividad fundamental es el micro-mecanizado de precisión (texturizado) de formas geométricas en superficies lubricadas que actúen como pequeños depósitos de lubricante mejorando las propiedades citadas anteriormente. Mediante estas técnicas se han realizado grandes avances en el texturizado de varias superficies tribológicas como motores, sellos, o rodamientos [75], siendo la técnica de texturizado láser la más avanzada para la modificación superficial de materiales con aplicaciones tribológicas. Esta técnica constituye además un proceso rápido, limpio y con una gran precisión en el control de las dimensiones topográficas. La aplicación del texturizado láser ha demostrado su competencia en componentes utilizados en automoción y aeronáutica, como son, los pistones [76]-[78], camisas y cilindros de motor [79], así como componentes de forja [80].

Varios estudios han confirmado la reducción del coeficiente de fricción y del desgaste como consecuencia del texturizado de una superficie en los denominados “conformal contacts” [81]-[83], en los que la fricción se da entre dos superficies que encajan de tal forma que la carga recae sobre un área superficial relativamente grande. Este tipo de sistemas es el que se encuentra en los cojinetes de deslizamiento de cualquier tipo de máquina, desde motores pequeños hasta turbinas. Los resultados demuestran que las mejoras tribológicas obtenidas del micro-mecanizado dependen de los principales parámetros de texturizado: geometría, dimensiones y densidad de los motivos texturizados. Además, los parámetros de texturizado óptimos para cada aplicación dependen directamente también de las condiciones de funcionamiento de cada componente en particular. Es decir, parámetros como la presión de contacto entre superficies, velocidad de deslizamiento, y el tipo y cantidad de lubricante utilizado, entre otros, determinarán la magnitud de las mejoras obtenidas.

La geometría típica de texturizado, aplicada para mejorar las propiedades tribológicas de un sistema, consiste en cráteres o “dimples”. En sistemas sometidos a fricción bajo lubricación líquida, este tipo de topografía actúa como reservorios de lubricante. Estos reservorios constituyen celdas de presión hidrodinámica que aseguran la disipación de calor de una forma más eficiente. En aquellos sistemas sin lubricación o con lubricación sólida, los dimples actúan como trampas para los residuos resultantes del desgaste de los materiales, evitando la acumulación de los mismos en la zona de contacto [82]-[84]. En varios estudios [85], las superficies de los dimples aparecen suavizadas tras el proceso de fricción, confirmando esta hipótesis. Estos dimples permiten, además, modificar la anchura y altura de la etapa de régimen de lubricación límite (en la que la fricción y el desgaste presentan su valor máximo) y alcanzar fricciones y desgastes más bajos, propios del régimen de lubricación hidrodinámica) [86]. La reducción del desgaste y la mejora en la capacidad de carga son especialmente notables en las zonas de lubricación límite y mixta. Otra ventaja adicional de este tipo de topografía es que no interfiere con la macro-geometría de la superficie de contacto producida por la ondulación y la rugosidad del material [87].

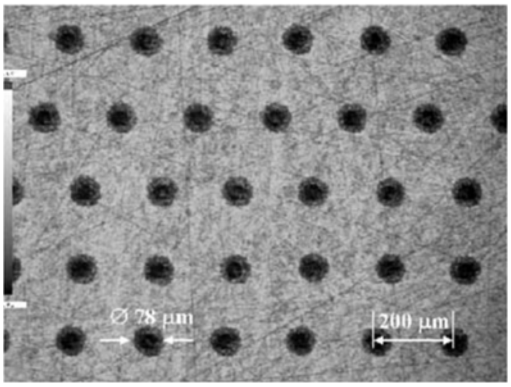

Figura 6. Texturizado mediante dimples circulares [84].

Según el estudio teórico de Cupillard et al. [88]sobre la dinámica de fluidos durante el funcionamiento de un cojinete de deslizamiento con la superficie texturizada, la reducción de la fricción y el aumento en la capacidad de carga del sistema son consecuencia del flujo de lubricante en el interior de los dimples. Dentro de estas cavidades, el lubricante puede recircular o quedarse estancado retardando su movimiento, produciéndose, en ambos casos, una disminución de la fricción. La circulación del lubricante dependerá, por tanto, de la geometría de los dimples (diámetro y profundidad) existiendo una combinación óptima que permite obtener una mejora hidrodinámica.

Schubert et al. [89], en su estudio de simulación sobre el efecto de los parámetros de dimple en la modificación de la curva de Stribeck, concluyen que el parámetro más influyente sobre la presión hidrodinámica resultante de la circulación de fluido es el diámetro. La profundidad, sin embargo, ejerce un efecto menor en la tribología del sistema.

Además de las dimensiones de los dimples, la densidad de los mismos sobre la superficie es un parámetro determinante para la reducción de la fricción entre los materiales. Su influencia en el coeficiente de fricción es, además, independiente del efecto que puedan tener el diámetro y la profundidad [90][91].

La distribución del área de superficie texturizada también influye en las propiedades tribológicas de un sistema. Marian et al. [92] han obtenido que la distribución de dimples (en este caso de forma cuadrada) para obtener un valor óptimo de la capacidad de carga de un cojinete de deslizamiento, es aquella en la que se texturiza la mitad de la superficie en la dirección circunferencial del cojinete, y el 90-100% en la dirección radial (ver Figura 7).

(a) *(b)*

Figura 7. Cojinetes texturizados con dimples: (a) circulares [86], (b) cuadrados [89]

El desarrollo de la tecnología de micro-mecanizado por láser se ha focalizado en el empleo de láseres de Nd-YAG con sistema de automatización que permita la manipulación de las trayectorias del haz láser, consiguiendo un mecanizado de cualquier geometría prefijada. [93].

El mecanizado láser es fundamental en la eliminación de material en el intervalo de tiempo que dura el pulso. Dependiendo de la duración de éste, los procesos físicos que se generan en el material son de distinta naturaleza. Pulsos muy largos pueden provocar la acumulación de material entorno a la cavidad generada por el láser ("recast layer") [94] o la aparición de zona afectada térmicamente ("Heat Affected Zone" (HAZ)), micro-grietas y ondas de choque.

Es importante remarcar que no existe una gran cantidad de documentación científico-tecnológica referente al estudio del micro-mecanizado láser en comparación con otras técnicas de mecanizado de precisión, como es la electroerosión por penetración (Electro-Discharge Machining (EDM)). Entre los estudios más recientes, cabe destacar el trabajo llevado a cabo por J. Giboz et al [95], en el que se comparan las precisiones alcanzadas en la fabricación de moldes para microinyección de termoplásticos. En este estudio, se muestran las ventajas y desventajas del micro-mecanizado láser frente a otras técnicas como el EDM o litografía. Es evidente que el desarrollo de la tecnología láser necesita de la mejora del conocimiento asociado al proceso con el fin de alcanzar un acabado superficial en el mecanizado comparable al obtenido mediante EDM. De esta manera, se conseguirá sustituir esta última técnica (lenta y costosa) por el micro-mecanizado láser, proceso limpio medioambientalmente y efectivo desde un punto de vista productivo. Otros trabajos donde se ha llevado a cabo un estudio del micro-mecanizado de moldes mediante EDM y láser es el realizado por J. Fleischer et al. [96], mostrando la necesidad de una combinación de los dos procesos para alcanzar precisiones requeridas por la industria en un tiempo relativamente rápido.

2.3. Lubricantes

La fricción en los elementos mecánicos es un factor principal para la pérdida de energía y la lubricación es una de las formas más efectivas de reducir la fricción y disminuir el calor adicional, que se produce en los sistemas mecánicos. Por lo tanto, mejorar las propiedades de los lubricantes es uno de los factores más importantes para mejorar la eficiencia energética de un sistema mecánico, disminuir el consumo de fuel y minimizar la huella del carbono [97].

El comportamiento respecto al rozamiento y al desgaste del rodamiento, así como la duración que pueda alcanzar dependen del régimen de lubricación. En los rodamientos aparecen principalmente los siguientes regímenes de lubricación [98]:

- Lubricación total o hidrodinámica: Las superficies de los cuerpos en movimiento relativo están separadas totalmente o casi totalmente por una película lubricante. Existe pues rozamiento líquido prácticamente puro. Este régimen de lubricación, denominado también lubricación líquida, es el que se debe pretender alcanzar.
- Lubricación parcial o mixta: Debido a un espesor insuficiente de la película lubricante aparecen contactos metálicos en algunas zonas. Se origina rozamiento mixto.
- Lubricación límite: Durante la lubricación parcial aparecen presiones y temperaturas muy elevadas en los puntos de contacto metálico. Si el lubricante contiene aditivos apropiados, se originan reacciones entre los aditivos y las superficies metálicas. Así se forman productos de reacción con capacidad lubricante que originan la formación de una capa límite.

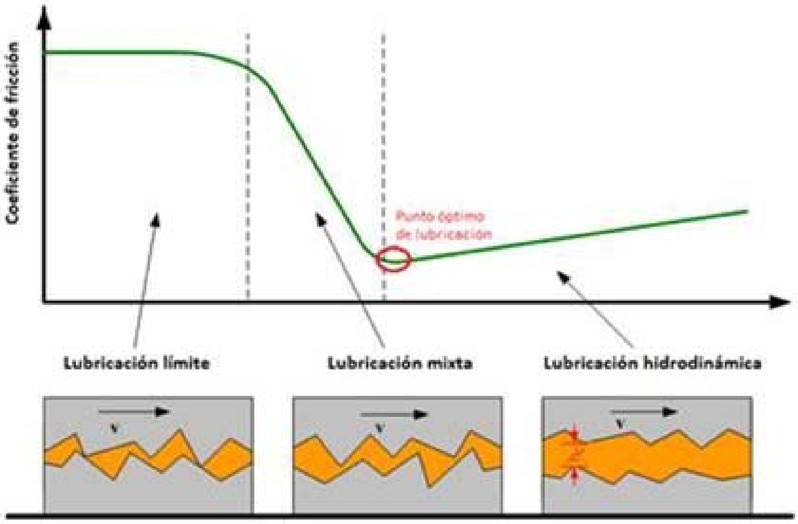

Figura 8. Coeficiente de fricción en función del régimen de lubricación y el espesor mínimo de película del lubricante.

Los regímenes de lubricación anteriormente mencionados pueden aparecer tanto con una lubricación por aceite como con una por grasa. La película lubricante formada en el caso de lubricación con grasa, donde también aplican las leyes básicas de la teoría elastohidrodinámica (EHD), dependerá principalmente de la viscosidad del aceite básico, aunque también tenga un efecto lubricante adicional el espesante de dicha grasa.

Al emplear grasas, formadas básicamente por aceite y espesante, la lubricación de los rodamientos se efectúa principalmente por el aceite básico que el espesante va cediendo poco a poco al cabo del tiempo. Para determinar la razón de viscosidades se toma la viscosidad de servicio del aceite básico y, en el caso de valores bajos, el espesante y los aditivos contribuyen a una lubricación eficaz.

En la lubricación con grasa sólo una pequeña parte del lubricante toma parte activamente en el proceso de lubricación ya que, tras el montaje y puesta en marcha, las grasas de consistencia normal son desplazadas en gran parte del rodamiento y se deposita a los lados. La grasa que queda en las superficies de rodadura y dentro o inmediatamente al lado del rodamiento va cediendo constantemente la cantidad mínima necesaria de aceite para lubricar las superficies funcionales. La cantidad de lubricante eficaz entre las superficies de rodadura es pues suficiente, bajo solicitaciones a carga moderadas, durante un tiempo relativamente largo. La cesión de aceite depende del tipo de grasa, de la viscosidad del aceite básico, de la magnitud de la superficie que lo cede, de la temperatura y de la solicitación mecánica de la grasa.

La eficacia del espesante de la grasa se reconoce al medir el espesor de la película lubricante en función del tiempo de funcionamiento. Al arrancar el rodamiento se origina en dependencia del tipo de espesante, un espesor de la película en la zona de contacto, considerablemente mayor que el correspondiente al aceite básico. La variación de la grasa y el desplazamiento de la misma dan lugar a una rápida disminución del espesor de la película lubricante (ver Figura 9. [99]). Por lo tanto, la eficacia lubricante del espesante en el servicio de los rodamientos se demuestra principalmente en la zona de rozamiento mixto.

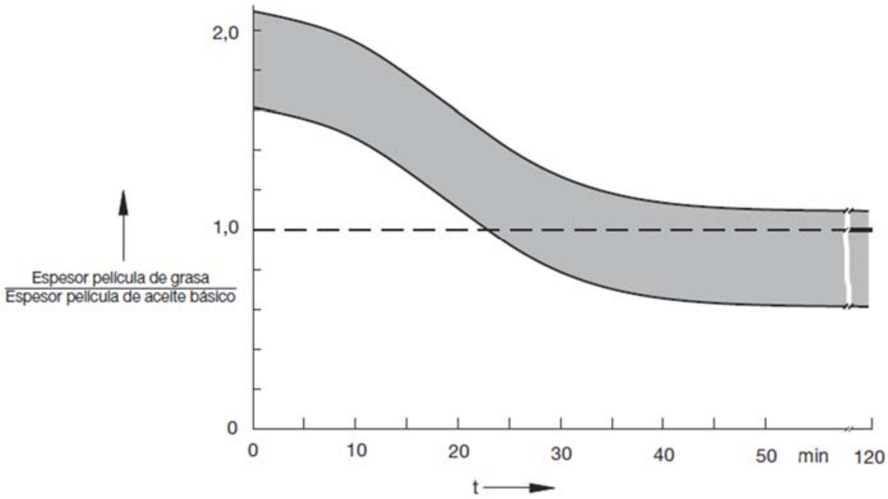

Figura 9. Razón de espesores de la película de grasa y la película del aceite básico en función del tiempo de funcionamiento.

Las grasas más habituales para la lubricación de rodamientos tradicionalmente han sido aquellas basadas en jabones de litio como espesantes. El aumento de las exigencias en las condiciones de trabajo llevó al desarrollo de grasas basadas en espesantes con puntos de fusión más elevados; primero fueron los jabones complejos de litio, posteriormente los jabones complejos de aluminio, después los espesantes inorgánicos como las bentonas o el óxido de silicio pirogénico; y más recientemente los espesantes basados en compuestos de urea o los modernos espesantes a base de sulfonatos de calcio complejos. La mayoría de grasas empleadas en rodamientos emplean aceites minerales como aceite base; pero cuando se trata de lubricar en condiciones extremas, se impone el uso de aceites base sintéticos como poli-alfa-olefinas (PAO's), poli-alquilen-glicoles (PAG's), poli-iso-butileno (PIB), ésteres sintéticos, silicones, poli-éteres fluorados (PFPE's), etc [100][101]. La dificultad en la formulación moderna de grasas estriba en saber "espesar" estos aceites sintéticos para conseguir grasas de altas prestaciones. Además, cuando se busca compatibilidad con materiales plásticos, el empleo de algunos tipos de aceites base sintéticos puede incrementar considerablemente dicha compatibilidad.

Los sistemas mecánicos modernos usados tanto en los procesos industriales como en los sistemas automotrices están diseñados para operar bajo un extenso intervalo de temperaturas y sometidos a grandes esfuerzos. Como consecuencia muchas de las maquinarias nuevas están diseñadas para trabajar a velocidades y presiones extremas, requiriendo de ciertas propiedades de lubricación específicas que las grasas convencionales no son capaces de satisfacer. Por ello ha sido necesaria la creación de una nueva generación de lubricantes capaces de satisfacer estos requerimientos.

Las grasas de poliurea [102][103] y las de sulfonatos de calcio complejos [104][105], se encuentran entre los avances más importantes en la tecnología de grasas. Estas grasas presentan importantes ventajas con respecto a las grasas jabonosas convencionales:

- Pueden ser sometidas a presiones y temperaturas altas sin que se vea afectada su constitución
- Presentan una resistencia alta a la oxidación
- Son buenos protectores frente a la corrosión
- Poseen estabilidad estructural alta
- Sus propiedades no se ven afectadas a temperaturas altas

Sin embargo, su fabricación es más complicada que la de una grasa simple de jabón y su coste relativamente más alto.

Los nano-lubricantes son un nuevo tipo de lubricantes fabricados con nanoestructuras, dispersantes y aceite base que han mejorado las propiedades de lubricación. Las propiedades anti-desgaste, anti-fricción y extrema presión de nano-lubricantes que contienen diferentes nanopartículas (NP) como fullerenos, dióxido de titanio (TiO2), oxidos de cobre (CuxO), nano-diamantes (ND), grafeno… ha sido analizada por varios investigadores [106]-[112]. En la Figura 10, por ejemplo, se muestra el incremento del 60% de la resistencia a la carga para un lubricante aditivado con nanoesferas de fullerenos basados en WS2, obtenidos en el marco del proyecto europeo FOREMOST (FP6-NMP3-CT-2005-515840) coordinado por IK4-TEKNIKER [113].

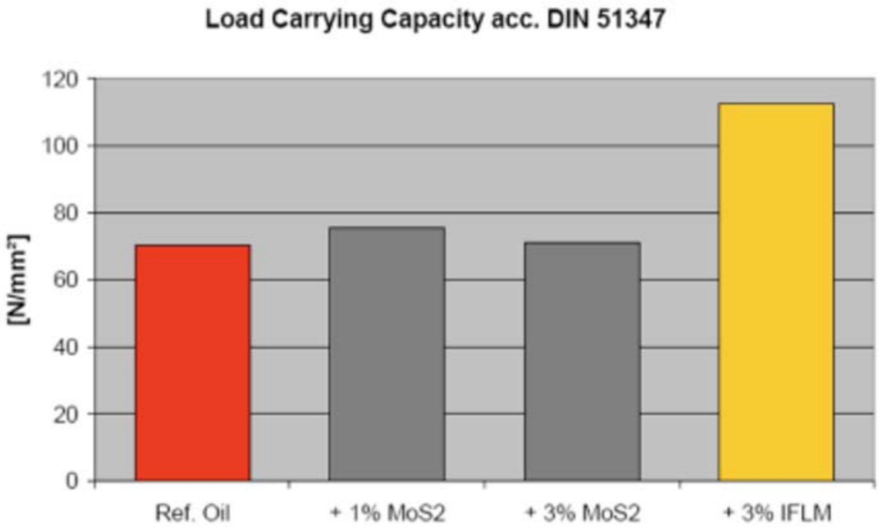

Figura 10. Test de Brugger sobre diferentes aceites convencionales con escamas de MoS2 o nanoesferas de fullereno basadas en WS2

2.4. RECUBRIMIENTOS EN ACERO AL C

En los rodamientos, al igual que en otros elementos mecánicos, se produce un contacto metal-metal, produciéndose adherencia, abrasión y fatiga, en definitiva, desgaste. El mecanismo de desgaste predominante, y responsable del fallo de un rodamiento, es la Fatiga de Contacto por Rodadura (FCR). Existen diversos parámetros que determinan la resistencia de un componente a este mecanismo de desgaste como pueden ser las propiedades del material, la geometría de contacto, la cinemática, las cargas, las propiedades de lubricación, la temperatura, la deformación cíclica o la topografía de la superficie. En una primera etapa del fallo, se producen microgrietas debido a la acumulación local de dislocaciones entre los cuerpos en contacto. En este estadio las tensiones se originan debido a las altas tensiones locales y la deformación plástica asociada en torno a las inhomogeneidades en la sub-superficie o los defectos superficiales. La segunda etapa consiste en el lento crecimiento de microgrietas hasta que se alcanza la resistencia a la fractura, conocida como micropitting.

Estos fenómenos y, por lo tanto, la fricción y el desgaste en los rodamientos, pueden ser reducidos mediante la aplicación de recubrimientos, alargando así su vida útil. Los 2 parámetros principales de los recubrimientos son:

- Material de la capa funcional
- Técnica de deposición

Con relación al **material de la capa funcional**, se pueden encontrar estudios en los que, mediante la realización de ensayos de fatiga por contacto de rodadura sobre recubrimientos aplicados mediante la técnica PVD empleando distintos materiales depositados como capa funcional, se ha demostrado una mejora en la vida de los componentes [118]-[120].

Por otro lado, por ejemplo, Mchalczewski et al. [121] evaluaron el comportamiento tribológico (resistencia adhesiva y vida a fatiga) de recubrimientos standard (TiN, CrN) y de recubrimientos de baja fricción (WC/C (tipo de DLC perteneciente al grupo a-C:H:Me) y MoS2/Ti) aplicados en acero 20MnCr5 endurecido. Los ensayos tribológicos determinaron que los recubrimientos PVD mejoran la resistencia al desgaste adhesivo (scuffing) pero, a fatiga, el único recubrimiento que mostró un comportamiento satisfactorio fue el WC/C.

Como constatan los trabajos descritos, dado su buen comportamiento, la mayoría de los trabajos científicos, dedicados a la mejora de desgaste y fricción en rodamientos mediante la aplicación de recubrimientos PVD, se ha centrado en la familia de recubrimientos DLC.

El DLC es una capa de carbono amorfo (a-C) o carbono amorfo hidrogenado (a-C:H) con un alto porcentaje de enlaces C sp3 meta-estables. Los recubrimientos que contienen carbono muestran un efecto positivo en las propiedades a fricción con coeficientes de fricción más bajos. En consecuencia, los recubrimientos con carbono amorfo son inertes, produciéndose muy pocas reacciones adhesivas entre el par de fricción. Además, las altas presiones de contacto pueden transformar el carbono amorfo en grafito, capaz de trabajar como lubricante sólido.

Entre las distintas categorías, los DLCs dopados o aleados tienen la capacidad de cumplir con los requisitos, cada vez más estrictos, de las aplicaciones de sistemas mecánicos avanzados. Aunque lo que se busca en principio es un aumento de dureza, la generación de tensiones internas compresivas, particularmente en recubrimientos con una alta relación sp3/sp2, favorece la delaminación de la capa. La acumulación de estas tensiones se ha superado mediante (i) el dopaje con elementos metálicos o (ii) el uso de un gradiente de subcapas funcionales. Los nuevos elementos incorporados pueden estar diluidos en la matriz, produciéndose una nueva fase en el recubrimiento, o pueden estar presentes como una fase separada modulada a escala nanométrica para formar multicapas o nanocomposites. Esta nueva generación de recubrimientos nanocomposite multicomponente abre nuevas posibilidades a la mejora de propiedades mediante un apropiado control de su composición y estructura a nanoescala [123].

Otro punto a favor de este tipo de recubrimiento es que los DLC tienen un papel destacado como parte de la ECO-Tribología [124], que, mediante avances en modificación superficial partiendo de tecnologías convencionales, busca contribuir al cumplimiento de las regulaciones medioambientales para conseguir una sociedad más sostenible. En este sentido, la tecnología de recubrimientos DLC ha avanzado de manera importante en los últimos años. Hace ya más de un lustro que automóviles y partes de máquinas industriales cuentan con estos tribo-recubrimientos de baja fricción. El DLC aporta alta dureza, baja rugosidad superficial y estabilidad química. Nissan Motor Co. Ltd. desarrolló un DLC libre de hidrógeno que, aplicado en el empujador de válvula, mejoró de manera importante el uso de combustible del motor V6 [125]. El carácter químicamente inerte de estas capas se utiliza en el control de la descomposición de lubricante en la superficie de deslizamiento [126].

Si bien los DLCs parecen ser los recubrimientos más prometedores en este campo, hay trabajos que ponen de manifiesto ciertos aspectos a mejorar. Así, por ejemplo, se ha encontrado dispersión en su comportamiento y respuesta tribológica en condiciones de rodadura, incluso entre capas generadas en un mismo proceso de recubrimiento [118], lo que requiere por tanto de una optimización de los procesos y las capas.

Es importante también considerar no únicamente el recubrimiento sino el conjunto DLC-lubricante. Podgornik et al. en un trabajo en el que evaluaron el comportamiento de recubrimientos DLC en condiciones de lubricación límite, usando aceites con aditivos extrema presión (EP) y antidesgaste (AW) [127], revisan la importancia de la lubricación en el comportamiento de estos recubrimientos. Aunque los recubrimientos DLC muestran baja fricción y desgaste en condiciones de deslizamiento en seco [128][129], en la mayoría de los casos se emplea lubricación. Algunos estudios tribológicos sugieren que la lubricación de los DLCs no es buena, pudiendo, bajo ciertas condiciones, empeorar el comportamiento tribológico incluso respecto al sistema no lubricado [130][131]. En otros casos, sin embargo, los DLCs lubricados pueden mejorar el comportamiento tribológico [132][133], especialmente en casos de combinaciones recubierto/no recubierto [134], poniendo de manifiesto también, que recubrir los dos materiales no siempre tiene porqué ser la mejor opción.

Por último, un aspecto a tener muy en cuenta, tanto por las especificaciones que tiene que cumplir el rodamiento para su correcto funcionamiento como por la efectividad del recubrimiento aplicado, es la rugosidad. Salvadori et al.. estudiaron la evolución de la rugosidad de las superficies recubiertas con DLC, en función del espesor de la capa de DLC, partiendo de rugosidades iniciales entre 4 y 400 nm. Comprobando que, para rugosidades iniciales altas, la rugosidad de la capa aumenta con el espesor DLC hasta un máximo y luego disminuye, mientras que, para rugosidades iniciales bajas, la rugosidad de recubrimiento no muestra una tendencia sistemática [135].

Una vez analizado el estado del arte de los recubrimientos DLC en rodamientos, cabe fijarse en otra familia de recubrimientos que en los últimos años ha demostrado ser un buen candidato para su empleo en rodamientos ya que proporcionan baja fricción y alta resistencia al desgaste. Se trata de los recubrimientos en base carbono-nitrógeno (CNx) [114]. El carbonitruro de circonio, Zr(C,N) es uno de estos recubrimientos para el que, por ejemplo, el centro tecnológico IK4-TEKNIKER ha desarrollado y patentado una formulación que ha reportado unos resultados más que prometedores en cuanto a fricción y desgaste en condiciones de rodadura-deslizamiento [136]. Este recubrimiento presenta las siguientes ventajas respecto a los DLCs:

- Mayor alargamiento de la vida del componente.
- Capacidad de soportar presiones mucho más altas.
- Posibilidad de trabajar a temperaturas más altas.
- No precisa de formulaciones especiales de aditivos en los aceites de lubricación.

La adaptación de este recubrimiento para su aplicación en rodamientos puede dar lugar a una mejora más que apreciable en el comportamiento de dicho componente.

En referencia a las **tecnologías de deposición**, pueden mencionarse la proyección térmica, el CVD (Chemical Vapour Deposition) o el PVD (Physical Vapour Deposition), siendo esta última tecnología la que ha dado lugar a sistemas con mejor comportamiento frente a la Fatiga por contacto de Rodadura (FCR) [114].

En este sentido, se ha demostrado que capas depositadas por PVD soportan niveles más altos de esfuerzo por cizalla durante la rodadura que recubrimientos producidos por CVD o proyección térmica [114][116].

Las técnicas modernas de PVD permiten obtener recubrimientos con la estructura y las propiedades requeridas. En estos métodos, el material a partir del cual se forman los recubrimientos suele evaporarse térmicamente o ser bombardeado con iones. El Cathodic Arc (CA) y el Magnetron Sputtering (MS) son las técnicas de deposición de recubrimientos PVD más utilizadas. La técnica CA tiene una alta ionización del plasma y una alta energía de iones de hasta 100 eV, lo que permite altas tasas de deposición, y una gran distancia entre la fuente y el sustrato permitiendo el recubrimiento de elementos de grandes dimensiones. Los recubrimientos obtenidos por el método CA se caracterizan por una alta dureza, buena adherencia al sustrato, alta densidad y homogeneidad. Sin embargo, la desventaja de este método es la elevada rugosidad del recubrimiento resultante debido al gran número de macropartículas en su superficie, que se ve limitada por las construcciones adecuadas del cátodo, el filtrado del plasma y el control del movimiento del punto del cátodo.

Por su parte, la técnica de MS se utiliza ampliamente tanto en condiciones de laboratorio como industriales. Este método de pulsos tiene muchas ventajas como, por ejemplo, la estabilidad del proceso y el control preciso del mismo. Estudios recientes describen como, aplicando recubrimientos CNx en rodamientos mediante la técnica de Magnetron Sputtering de alta potencia (High Power Impulse Magnetron Sputtering, HiPIMS), se obtienen recubrimientos con una alta elasticidad y dureza [114].

A este respecto, el acero empleado en la presente tesis doctoral, denominado 100Cr6 (según ISO 683-17 [3]), es un sustrato muy exigente a la hora de aplicar un recubrimiento sobre él, ya que exige temperaturas de deposición no superiores a los 180ºC (temperatura de revenido de dicho acero) con el fin de mantener su estructura intrínseca y sus propiedades mecánicas. La tecnología HiPIMS es en esencia un tipo de sputtering, pero utiliza pulsos de alto voltaje en ciclos cortos dando lugar a altas densidades electrónicas de pico y por tanto una más alta ionización del material evaporado. Esta tecnología se ha emplea en algunos casos únicamente como pre-tratamiento del sustrato de cara a mejorar la adhesión del recubrimiento [137]. El proceso supone una mayor implantación de los iones metálicos en la superficie del sustrato. Se forma una interfase rica en átomos del metal empleado para el pre-tratamiento, lo que proporciona un cambio gradual de las tensiones internas, mejorando la adherencia de la capa depositada. La combinación del HiPIMS con un alto voltaje Bias puede ser de gran utilidad como pre-tratamiento para conseguir una mejor adhesión incluso a bajas temperaturas [138].

Bakoglidis y co. [114] han ido más allá empleando el HiPIMS para la aplicación no sólo de la capa de adherencia sino del recubrimiento en sí. Han estudiado por primera vez la respuesta tribológica en condiciones de rodadura, así como la fatiga en contacto a rodadura de rodillos recubiertos con CNx mediante HiPIMS. Se ha visto que la combinación del recubrimiento CNx con un pre-tratamiento de tungsteno (capa de adherencia), ambos mediante HiPIMS, incrementa la vida de los rodamientos de rodillos.

Finalmente, es interesante mencionar las tendencias de mercado que las grandes empresas recubridoras ofrecen para rodamientos. HAUZER ha desarrollado, en colaboración con el fabricante de rodamiento FAG, toda una serie de recubrimientos, entre ellos los TRIONDUR® en base carbono (CN, CNN, C, C+, CX+, CH) [138]. Además, HAUZER también cuenta con los Me-DLCs en su portfolio para este tipo de aplicación. La empresa BALZERS, por su parte, recomienda el recubrimiento Balinit C (WC/C, un tipo de Me-DLC), que mejora la vida de los componentes en condiciones de baja lubricación o en presencia de partículas contaminantes y fatiga superficial.

Por último, en cuanto a las grandes empresas de rodamientos, tanto FAG como SKF cuentan con rodamientos de alto rendimiento en los que se aplican recubrimientos. Así se puede mencionar la serie X-Life de FAG o los productos de SKF recubiertos con DLC. De hecho, SKF colabora en los estudios más recientes y punteros sobre recubrimientos HiPIMS en rodamientos [114].

Las aportaciones que hace este trabajo se dan en las distintas líneas de investigación establecidas. A lo largo de su ejecución, se han definido y ensayado composiciones que no estaban descritas con anterioridad en la literatura. Por un lado, **con relación al desarrollo de materiales poliméricos, se ha estudiado el efecto de la adición de grafeno y óxido de circonio en la poliamida 66 con fibra de vidrio. Si bien es cierto que los beneficios de estos compuestos habían sido estudiados por separado, no existía constancia en la bibliografía de su aplicación como aditivos en matrices poliméricas. Así mismo, se ha analizado el efecto del texturizado**

de superficies en los valores de coeficiente de fricción y desgaste. Dentro de las referencias consultadas, esta solución había sido aplicada en materiales metálicos, pero no así en plásticos de ahí la importancia de los resultados obtenidos. También en el campo de los polímeros, se ha realizado un estudio sistemático para obtener una comparativa representativa del potencial efecto positivo de diferentes lubricantes sólidos (grafito, grafeno, MoS2 y ZrO2) en el desgaste de distintas matrices poliméricas (PA66, PA46 y PA12) bajo las mismas condiciones de ensayo y no de cada una de forma individual como aparece en la literatura.

Por otro lado, **en referencia al desarrollo de nuevos lubricantes, la principal aportación se ha producido en el estudio del uso de grasas formuladas con espesante basado en sulfonato de calcio para aplicaciones del sector de la automoción.** Su buen comportamiento frente a la corrosión, resistencia al agua y a cargas y su estabilidad al trabajo, demostrado en la industria siderúrgica, derivó en el interés de comprobar si estas características también se daban en otros campos. Además, **se han realizado nuevas formulaciones de aceites semisintéticos para aunar las buenas propiedades de los sintéticos pero con un coste más reducido**, similar al de los minerales. Por último, se han desarrollado 2 nuevos paquetes de aditivos para mejorar el rendimiento de las grasas con espesante de complejo de litio. En particular, **se formularon 2 aditivos, uno cuya función era conseguir mejores prestaciones en las grasas minerales, pero sin encarecer su precio final, propio de las grasas con ese tipo de aceite, y el segundo aditivo cuyo objetivo era obtener un producto con características de alta gama y biodegradable para, a pesar de usar complejo de litio como espesante, desarrollar una grasa más sostenible**.

En lo relativo a los recubrimientos en aceros al carbono, apenas se habían realizado estudios previos con la combinación del recubrimiento de carbonitruro de circonio aplicada en rodamientos. Aunque puede encontrarse alguna referencia que indique su uso, los resultados descritos se centran más en las propiedades del material del rodamiento y en la geometría obtenida tras su deposición que en los resultados funcionales, como el par de fricción o el desgaste, abordados en la presente tesis.

El **análisis del estado del arte realizado ha permitido identificar dos líneas de trabajo en cuanto a la modificación superficial de rodamientos mediante la aplicación de recubrimientos PVD. Por un lado, el desarrollo de nuevas formulaciones de recubrimientos con base CNx y, por otro, el estudio del uso de recubrimientos DLC en soluciones distintas a las mencionadas en la bibliografía. La innovación de ambos desarrollos radica, además, en su aplicación en rodamientos de rodillos cónicos.**

Finalmente, **cabe destacar la importante contribución de este trabajo para aumentar el nivel de madurez de las innovaciones planteadas gracias a la posibilidad de ensayar los desarrollos conseguidos no solo en probetas a nivel de laboratorio sino también en prototipos de rodamientos en instalaciones industriales**, lo que justifica la mención de doctorado industrial solicitada para esta tesis. Como se ha comentado con anterioridad, esta posibilidad ha dado lugar a una nueva familia de producto permitiendo que la transferencia de los resultados del presente doctorado a mercado pueda realizarse en el corto plazo.

3. CONCLUSIONES

Una vez finalizadas las distintas fases del trabajo de investigación, se fueron extrayendo numerosas conclusiones, publicadas, la mayoría de ellas, en artículos de revistas de alto impacto.

Tal y como se explicaba al comienzo de esta memoria, la presente tesis doctoral se ha dividido en 3 líneas de investigación: (i) nuevos materiales poliméricos, (ii) nuevos tratamientos superficiales en aceros al carbono y (iii) nuevos lubricantes avanzados.

A nivel general, con relación al desarrollo de **materiales poliméricos**, se ha podido ampliar el conocimiento en nuevos materiales poliméricos, descartando aditivos e identificando las mejores formulaciones a partir de las siguientes conclusiones:

- A nivel de probeta:
    - En las muestras con nanopartículas (NPs) de ZrO2 se obtuvieron resultados negativos como consecuencia del desprendimiento de estas NPs, que, debido a su alta dureza, provocaron un desgaste abrasivo en el disco de 100Cr6. Por ello, este aditivo no sería el más adecuado para el objetivo que se perseguía.
    - En los ensayos tribológicos realizados (block-on-ring y ball-on-disc), los materiales que mejor comportamiento presentaron, tanto en fricción como en desgaste, fueron los compuestos con matriz PA12 (aditivados tanto con 5%grafeno como con 5% MoS2, con y sin 10%FV), el PEEK y la PA66 con un 5% de grafeno. Por el contrario, los que peor comportamiento mostraron fueron la PA66 con 5% MoS2 y el PEI.
    - Los texturizados aplicados no produjeron ninguna mejora en el comportamiento tribológico del material que se seleccionó como base (PA66+ 5% grafeno).
- A nivel de producto final:
    - La inserción de fibra no supuso una variación destacable en ninguno de los parámetros fundamentales del proceso de inyección (temperatura de fundido, fuerza de cierre, tiempo de ciclo, etc.), ni modificó la contracción volumétrica de manera destacable por lo que solo supone una mejora general en las propiedades mecánicas.
    - En lo referente a las medidas de temperatura, no se obtuvieron resultados muy concluyentes que mostraran tendencias claras o grandes mejoras respecto a la grasa de referencia.
    - Con respecto al par de fricción, se observó que la muestra con que se obtuvo un par de fricción menor fue, en primer lugar, la fabricada con jaula de PA66 aditivada con fibra de vidrio y grafeno con un valor de par de 7,39 Nm, es decir, una reducción del 1,20% respecto al *baseline*. En segundo lugar, se situó el demostrador con jaula de PA12 modificada con fibra de vidrio y grafeno con un valor de 7,42 Nm, es decir, una reducción del 0,80% respecto al *baseline*.

En vista de lo expuesto anteriormente, se puede concluir que el material PA66 aditivado con fibra de vidrio y grafeno fue el que obtuvo mejores resultados y sería el candidato seleccionado. Además de los buenos valores de fricción y temperatura obtenidos, y dada la situación económica actual, cabe destacar la importancia de que la matriz del polímero con mejores prestaciones sea un material técnico (PA66) pero con unas economías de escala bien establecidas. Esto provoca que su coste no sea muy elevado y, por lo tanto, que su industrialización pueda ser una realidad para las empresas del sector de la automoción.

En lo relativo a la formulación de **nuevos lubricantes** se han desarrollado nuevas grasas teniendo en cuenta no solo la mejora de las prestaciones de temperatura y resistencia si no también la situación económica y de recursos de materiales actual de cara a obtener un producto más sostenible:

- A nivel de probeta:
  - En la caracterización tribológica inicial, las nuevas formulaciones que mostraron mejores resultados en su coeficiente de fricción fueron las que incluían espesante complejo de litio con aceite semisintético y espesante complejo de litio con aceite mineral. Por otro lado, las grasas compuestas de espesante complejo de litio con aceite mineral y espesante sulfonato de calcio con aceite semisintético tuvieron mejor comportamiento frente a desgaste.
  - Todas las grasas evaluadas tenían comportamientos muy parecidos y cumplieron con los valores especificados en la norma ASTM D-4950-14.
  - Durante la caracterización tribológica a diferentes temperaturas de trabajo, destacó la respuesta de la nueva grasa desarrollada compuesta de espesante sulfonato de calcio con aceite semisintético que obtuvo mejores resultados tanto en el coeficiente de fricción como en el desgaste en altas temperaturas de operación.
  - Por otro lado, destacar el incorrecto comportamiento de las grasas a -20ºC, las cuales solo consiguieron mantener una correcta lubricación durante unos pocos segundos antes de que se produjera el fallo. De entre todas, la grasa formada por espesante complejo de litio con aceite sintético mostró un comportamiento ligeramente mejor, ya que el tiempo transcurrido hasta que se produjo el fallo fue mayor que en el resto.
  - Con relación a la compatibilidad entre las nuevas formulaciones de materiales, las nuevas grasas desarrolladas y la grasa de referencia mencionar que se obtuvieron valores muy diferentes. De entre todos los materiales poliméricos desarrollados, las formulaciones híbridas mostraron valores de compatibilidad con las nuevas grasas más favorables, destacando, las especies poliméricas con matriz PA12 que presentaron los valores más estables de los parámetros mecánicos analizados. De forma general, la incidencia de la temperatura en las variables mecánicas analizadas es menor que la influencia de la grasa.
- A nivel de producto final:
  - En los ensayos de fricción realizados, en general, se observó una disminución de la temperatura máxima alcanzada con todas las nuevas grasas. La mayor reducción se obtuvo con la grasa compuesta por espesante complejo de litio y aceite sintético siendo esta de un 8,1%. Sin embargo, cabe destacar que la temperatura de estabilización de todas las nuevas grasas fue mayor que el valor baseline.
  - Por otro lado, en lo referente al par de fricción, no se obtuvo una reducción para ninguna de las nuevas grasas desarrolladas respecto a la grasa *baseline* formada por espesante complejo de litio y aceite mineral. A pesar de ello, señalar que el comportamiento de todos los lubricantes fue correcto y muy similar al valor de referencia.

Finalmente, en base a los resultados obtenidos en los ensayos a fatiga de los lubricantes seleccionados, se pudo inferir que la grasa formulada con espesante complejo de litio y aceite sintético, si bien alcanzaba unas temperaturas máximas superiores a la grasa de referencia, presentó unas propiedades óptimas ya que el estado del rodamiento tras el ensayo fue muy similar al obtenido con la muestra *baseline*.

Considerando los resultados de fricción y fatiga expuestos anteriormente, se puede concluir que los nuevos desarrollos han obtenido un comportamiento similar desde el punto de vista funcional al de las grasas de referencia de las que se partía, sin apreciarse mejoras evidentes de funcionamiento. No obstante, sería interesante destacar los valores obtenidos con la grasa compuesta por espesante sulfonato de calcio y aceite semisintético. Por un lado, es cierto que su comportamiento a fatiga fue peor que el de la grasa *baseline* Shell (formada por espesante complejo de litio y aceite mineral) ya que la temperatura máxima alcanzada fue un 105,2% mayor y que el de la grasa que obtuvo mejores resultados (compuesta por espesante complejo de litio y aceite sintético) puesto que la temperatura máxima respecto a ella fue un 49,3% mayor. Sin embargo, los resultados del par de fricción arrojados por la grasa formulada con espesante sulfonato de calcio y aceite semisintético, los cuales solo superaban en un 0,26% al par de la grasa *baseline* y mejoraban en un 1,28% al de la grasa formada por espesante complejo de litio y aceite sintético, hacen pensar que pueda ser un buen candidato para su uso en rodamientos de rodillos cónicos teniendo en cuenta aspectos de sostenibilidad al tratarse de una grasa cuyo espesante está basando en el sulfonato de calcio, en lugar de un material crítico como el litio.

Así mismo, en referencia a la investigación en **nuevos recubrimientos** se ha desarrollado un proceso completo de deposición de recubrimientos sobre acero al carbono definiendo no solo los parámetros de deposición si no también el proceso de post-pulido necesario para conseguir las especificaciones de rugosidad requeridas para asegurar el comportamiento a fatiga de los rodamientos:

- La caracterización geométrica y morfológica de los recubrimientos arrojó resultados positivos ya que todas las variables analizadas cumplían las especificaciones fijadas. Especialmente importantes fueron los resultados conseguidos para la rugosidad (gracias al proceso de post-pulido) y para el mantenimiento de la dureza del sustrato (muy afectada por la temperatura del proceso de deposición PVD). Estos valores resultan críticos para asegurar una correcta vida útil de los rodamientos por lo que su cumplimiento supuso un avance en el desarrollo de los recubrimientos Zr(C,N) para rodamientos.
- De los resultados obtenidos durante la caracterización tribológica de las muestras recubiertas, se pudo concluir que, aunque la geometría de los recubrimientos se encontraba de acuerdo con las especificaciones definidas, el comportamiento tribológico de estas no mejoró frente a las muestras no recubiertas.

Con todo ello, se ha definido un nuevo *roadmap* de producto para la empresa Fersa Bearings el cual permitirá mejorar su posicionamiento en el mercado frente a posibles competidores y cambios en las directivas de eficiencia energética.

4. FUTURAS LÍNEAS DE INVESTIGACIÓN

A continuación, se incluyen futuras líneas de investigación y trabajo complementario al realizado durante la presente tesis doctoral. Esto permitiría continuar con las investigaciones realizadas, actualizándolas y ampliándolas con temas interesantes que no se han podido abarcar en este doctorado.

Con relación al desarrollo de **materiales poliméricos**, por un lado, sería interesante ensayar, en la geometría del producto final, otras formulaciones con las que se obtuvieron buenos resultados a nivel de probeta como el PEEK. Por otro lado, también se podría analizar el comportamiento de matrices poliméricas aditivadas con una mayor cantidad de fibra de vidrio, estudiando valores cercanos a la referencia (25%).

En lo relativo a la investigación en **nuevos lubricantes**, se podría continuar con el desarrollo de nuevos aceites sintéticos que mejorasen los valores del coeficiente de fricción, permitieran reducir la dependencia del petróleo y cuyo coste de fabricación fuera menor que el actual. Así mismo, se podrían formular nuevos paquetes de aditivos que mejorasen el comportamiento a baja temperatura de las grasas. Además, se podría ampliar la investigación en espesantes distintos al complejo de litio ya que este material fue considerado crítico en la lista publicada a partir del cuarto estudio de materias primas críticas realizado por la Comisión Europea en el año 2020. Este hecho pone de manifiesto la necesidad de buscar alternativas ya que el litio juega un papel importante para lograr la transición energética puesto que es usado mayoritariamente en la fabricación de vehículos eléctricos.

Por último, en referencia a la formulación de **nuevos recubrimientos**, inicialmente, y de cara a poder realizar el análisis de la respuesta a fricción de la referencia comercial seleccionada, sería necesario adecuar la máquina en que se realiza el proceso PVD para poder obtener muestras del producto final y proceder con dichos ensayos. A continuación, sería interesante estudiar el comportamiento a fatiga de los recubrimientos desarrollados tanto a nivel de probeta como a nivel de producto final. Finalmente, y en base al estudio del estado del arte, también sería interesante profundizar en las prestaciones de los recubrimientos DLC.

Todo ello permitiría, a la empresa Fersa Bearings, desarrollar nuevas gamas de producto lo que mejoraría su imagen y situación frente a la concesión de nuevos proyectos.

5. BIBLIOGRAFÍA

[1] Jost, H.P. et al. Tribology: origin and future. *Wear* **1990**, *136* (1), 1-17. https://doi.org/10.1016/0043-1648(90)90068-L

[2] https://www.tekniker.es/es/la-importancia-del-analisis-tribologico-para-ahorrar-costes

[3] ISO. 683-17:2014 Heat Treated Steels, Alloy Steels and Free-Cutting Steels—Part 17: Ball and Roller Bearing Steels; ISO: Geneva, Switzerland, 2015.

[4] Dinkel, M. Bearing Steels and Heat Treatment. *Proceedings of the ABMA Webinar Series*, **2015**. https://www.americanbearings.org/events/EventDetails.aspx?id=654049&hhSearchTerms=%22bearing+steels+and+heat+treatment%22

[5] Ai, S; Wang, W; Wang, Y; Zhao, Z. Temperature rise of double-row tapered roller bearings analyzed with thermal network method. *Tribology International* **2015**, 87, 11-22. DOI:10.1016/j.triboint.2015.02.011

[6] Bassani, R. Levitation of passive magnetic bearings and systems. *Tribology International* **2006**, *39* (9), 963-970. https://doi.org/10.1016/j.triboint.2005.10.003

[7] Garg, A.C; Mai, Y. Failure mechanisms in toughened epoxy resins—a review. *Composites Science and Technology* **1988**, *31* (3), 179–223. https://doi.org/10.1016/0266-3538(88)90009-7

[8] Chandra, R; S.P. Singh, K. Gupta, Damping studies in fiber-reinforced composites—a review. *Composites Structures* **1999**, *46* (1) 41–51. https://doi.org/10.1016/S0263-8223(99)00041-0

[9] Friedrich, K; Lu, Z; Hanger, A.M. Recent advances in polymer composites' tribology. *Wear* **1995**, *190* (2), 139–144. https://doi.org/10.1016/0043-1648(96)80012-3

[10] Friedrich, K; Zhang, Z; Schlarb, A.K. Effects of various fillers on the sliding wear of polymer composites, *Composites Science and Technology* **2005**, *65* (15–16), 2329–2343. https://doi.org/10.1016/j.compscitech.2005.05.028

[11] Hironaka, S. Polymer materials and solid lubrication. *Japanese Society of Tribologists* **2008,** *53*, 712–718.

[12] Brostow, W; Kovačević, V; Vrsaljko, D; Whitworth, J. Tribology of polymers and polymer-based composites. *Journal of Materials Education* **2010**, *32* (5–6), 273–290.

[13] Wetzel, B; Haupert, F; Friedrich, K; Zhang, M.Q.; Rong, M.Z. Impact and wear resistance of polymer nanocomposites at low filler content. *Polymer Engineering and Science* **2002**, *42* (9), 1919–1927. DOI:10.1002/pen.11084

[14] Álvarez-Láinez, M.L; Palacio, R; Jairo A. Correlations between thermal and tensile behavior with friction coefficient in copolyamides 6/12. *Wear* **2017**, *372-373,* 76–80. https://doi.org/10.1016/j.wear.2016.11.018

[15] Ambrosio, J; Balarim, C; Carvalho, G. Preparation, characterization, and mechanical/tribological properties of polyamide 11/Titanium dioxide nanocomposites. *Polymer Composites* **2016**, *37* (5), 1415–1424. DOI:10.1002/pc.23310

[16] Semielaborados. Productos plásticos de Ingeniería. *Ensinger* **2014/15**.

[17] Radhesh, K; Helmut, M. Silver ion release from antimicrobial polyamide/silver composites. *Biomaterials* **2005**, *26* (14), 2081–2088. https://doi.org/10.1016/j.biomaterials.2004.05.030

[18] Mens, J.W.M.; de Gee, A.W.J. Friction and wear behaviour of 18 polymers in contact with steel in environments of air and water. *Wear* **1991**, *149* (1-2), 255–268. https://doi.org/10.1016/0043-1648(91)90378-8

[19] Lawrence, C.C.; Stolarski, T.A. Rolling contact wear of polymers: a preliminary study. *Wear* **1989**, *132* (1), 183–191. https://doi.org/10.1016/0043-1648(89)90211-1

[20] Hooke, C.J.; Kukureka, S.N.; Liao, P; Rao, M; Chen, Y.K. The friction and wear of polymers in non-conformal contacts. *Wear* **1996**, *200* (1-2), 83–94. https://doi.org/10.1016/S0043-1648(96)07270-5

[21] Rao, M; Hooke, C.J.; Kukureka, S.N.; Liao, P; Chen, Y.K. The effect of PTFE on the friction and wear behavior of polymers in rolling–sliding contact. *Polymer Engineering and Science* **1998**, *38* (18), 1946–1958.

[22] Apichartpattanasiri, S; Hay, J.N.; Kukureka, S.N. A study of the tribological behaviour of polyamide 66 with varying injection-moulding parameters. *Wear* **2001**, *251* (1-12), 1557–1566. https://doi.org/10.1016/S0043-1648(01)00794-3

[23] Hooke, C.J.; Kukureka, S.N.; Liao, P; Rao, M; Chen, Y.K. Wear and friction of nylonglass fibre composites in non-conformal contact under combined rolling and sliding. *Wear* **1996**, *197* (1-2), 115–122. https://doi.org/10.1016/0043-1648(95)06828-7

[24] Hooke, C.J.; Kukureka, S.N.; Liao, P; Rao, M; Chen, Y.K. The friction and wear of polymers in non-conformal contacts. *Wear* **1996**, *200* (1-2), 83–94. https://doi.org/10.1016/S0043-1648(96)07270-5

[25] Chen, Y.K.; Kukureka, S.N.; Hooke, C.J. The wear and friction of short glass-fibre reinforced polymer composites in unlubricated rolling–sliding contact. *Journal of Materials Science* **1996**, *31* (21), 5643–5649. DOI: 10.1007/BF01160809

[26] Kukureka, S.N.; Hooke, C.J.; Rao, M; Liao, P; Chen, Y.K. The effect of fibre reinforcement on the friction and wear of polyamide 66 under dry rolling–sliding contact. *Tribology International* **1999**, *32* (2), 107–116. https://doi.org/10.1016/S0301-679X(99)00017-1

[27] Chen, Y.K.; Kukureka, S.N.; Hooke, C.J.; Rao, M. Surface topography and wear mechanisms in polyamide 66 and its composites. *Journal of Materials Science* **2000**, *35* (5) 1269–1281. DOI:10.1023/A:1004709125092

[28] Yamada, Y; Kurobe, T; Toyooka, Y. XPS study of transfer films of MoS2 filled nylon46 composites sliding against steel counterfaces. *Journal of Materials Science Letters* **2001**, *20* (6), 577–579. https://doi.org/10.1023/A:1010901221866

[29] Kurokawa, M; Uchiyama, Y; Iwai, T; Nagai, S. Performance of plastic gear made of carbon fiber reinforced polyamide 12. *Wear* **2003**, *254* (5-6), 468–473. https://doi.org/10.1016/S0043-1648(03)00020-6

[30] Xiang, T; Li, X; Liu, P; Cong, R. Effect of compatibilizer on the transfer and tribological behaviors of PA46/HDPE polyblends. *Tribology Letters* **2006**, *22* (3), 279–288. https://doi.org/10.1007/s11249-006-9090-z

[31] Cong, P; Xiang, F; Liu, X; Li, T. Morphology and microstructure of polyamide 46 wear debris and transfer film: in relation to wear mechanisms. *Wear* **2008**, *265* (7-8), 1100–1105. https://doi.org/10.1016/j.wear.2008.03.004

[32] Cong, P; Xiang, F; Liu, X; Li, T. Effect of crystalline form on the tribological properties of PA46/HDPE polyblends. *Wear* **2008**, *265* (7-8) 1106–1113. https://doi.org/10.1016/j.wear.2008.03.005

[33] Unal, H; Mimaroglu, A; Serdar, V. Dry sliding performance of thermoplastics against reinforced unsaturated polyester (BMC): in use in electrical contact breakers components. *Wear* **2006**, *261* (7-8) 841–847. https://doi.org/10.1016/j.wear.2006.01.021

[34] Sandler, J; Pegel, S; Cadek, M; Gojny, F; van Es, M; Lohmar, J; Blau, W.J.; Schulte, K; Windle, A.H.; Shaffer, M. A comparative study of melt spun polyamide-12 fibers reinforced with carbon nanotubes and nanofibers. *Polymer* **2004**, *45* (6) 2001–2015. DOI:10.1016/j.polymer.2004.01.023

[35] Lecouvet, B; Gutierrez, J; Sclavons, M; Bailly, C. Structure-property relationships in polyamide 12/halloysite nanotube nanocomposites. *Polymer Degradation and Stability* **2011**, *96* (2) 226–235. https://doi.org/10.1016/j.polymdegradstab.2010.11.006

[36] Chatterjee, S; Nüesch, F.A; Chu, B.T.T. Comparing carbon nanotubes and graphene nanoplatelets as reinforcements in polyamide 12 composites. *Nanotechnology* **2011**, *22* (27), 275714. DOI: 10.1088/0957-4484/22/27/275714

[37] https://www.victrex.com/es/

[38] Bhmdell, D.J; Osborn, B.N. The morphology of poly(arylether ether-ketone). *Polymer* **1983***, 24* (8), 953-958. https://doi.org/10.1016/0032-3861(83)90144-1

[39] Jones, D.P; Leach, D.C.; Moore, D.R. Mechanical properties of poly(ether-ether-ketone) for engineering applications. *Polymer* **1985***, 26* (9) 1385-1393. https://doi.org/10.1016/0032-3861(85)90316-7

[40] LNP-Plastics: Lubricomp, internally lubricated reinforced thermoplastics and fluoropolymer composites **1988**, *LNP-Bulletin,* 254-988. VM Raamsdonksveer, The Netherlands.

[41] https://www.sabic-ip.com/gep/Plastics/es/ProductsAndServices/ProductLine/ultem.html

[42] Friedrich, K; Karger-Kocsis, J; Lu, Z. Effects of counterpart roughness and temperature on friction and wear of PEEK composites. *Wear* **1991**, *148* (1991) 235-247.

[43] Friedrich, K; Lu, Z; Häger, A.M. Overview on polymer composites for friction and wear application. *Theoretical and Applied Fracture Mechanics* **1993**, *19* (1), 1-11. https://doi.org/10.1016/0167-8442(93)90029-B

[44] Schelling, A; Kausch, H.H. Reciprocating dry friction and wear of short fibre reinforced polymer composites, in K. Friedrich (ed.), Advanced in Composite Tribology. *Composite Materials Series* **1993**, *8*, 65-105. https://doi.org/10.1016/B978-0-444-89079-5.50007-6

[45] Jenkins M.J. Relaxation behaviour in blends of PEEK and PEI. *Polymer* **2000**, *41* (18), 6803-6812. https://doi.org/10.1016/S0032-3861(00)00033-1

[46] Choon Kang, S; Won Chung, D. Improvement of frictional properties and abrasive wear resistance of nylon/graphite composite by oil impregnation. *Wear* **2003**, *254* (1-2), 103–110. https://doi.org/10.1016/S0043-1648(02)00302-2

[47] Samyn, P; De Baets, P; Schoukens, G; Hendrickx, B. Tribological behavior of pure and graphite-filled polyimides under atmospheric conditions. *Polymer Engineering and Science* **2003**, *43* (8), 1477–1487. https://doi.org/10.1002/pen.10125

[48] Chen, J; Jia, J; Zhou, H; Chen, J; Yang, S; L. Fan, L. Tribological behavior of short-fiber-reinforced polyimide composites under dry-sliding and water-lubricated conditions. *Journal of Applied Polymer Science* **2008**, *107* (2), 788–796. https://doi.org/10.1002/app.27127

[49] Sung, N.H.; Suh, H.P. Effect of Orientation on Friction and Wear of Fiber Reinforced Polymeric Composites. *Wear* **1979**, *53* (1979), 129–141.

[50] Kowandya, C; Richarda, C; Chen, Y.M. Characterization of Wear Particles for Comprehension of Wear Mechanisms Case of PTFE against Cast Iron. *Wear* **2008**, *265* (11-12), 1714–1719. https://doi.org/10.1016/j.wear.2008.04.036

[51] Li, F; Hu, K; Li, J; Zhao, B. The friction and wear characteristics of nanometer ZnO filled polytetrafluoroethylene. *Wear* **2002**, *249* (10-11), 877–882. https://doi.org/10.1016/S0043-1648(01)00816-X

[52] Kukureka, S.N.; Chen, Y.K.; Hooke, C.J.; Liao, P. The wear mechanisms of acetal in unlubricated rolling-sliding contact. *Wear* **1995**, *185* (1-2), 1–8. https://doi.org/10.1016/0043-1648(94)06575-6

[53] Franke, R; Lehmannb, D; Kunze, K. Tribological behaviour of new chemically bonded PTFE polyamide compounds. *Wear* **2007**, *262* (3-4), 242–252. https://doi.org/10.1016/j.wear.2006.05.001

[54] Hooke, C.J.; Kukureka, S.N.; Liao, P; Rao, M; Chen, Y.K. The friction and wear of polymers in non-conformal contacts. *Wear* **1996**, *200* (1-2), 83–94. https://doi.org/10.1016/S0043-1648(96)07270-5

[55] Lancaster, J.K. Composites for increased wear resistance: Current achievements and future prospects. *NASA Lewis Research Center Tribology in the 80's* **1984**, *1*, 333-355. https://apps.dtic.mil/sti/pdfs/ADA305066.pdf#page=339

[56] Lingesh, B.V; Rudresh, B.M.; Ravikumar, B.N. Effect of Short Glass Fibers on Mechanical Properties of Polyamide66 and Polypropylene (PA66/PP) Thermoplastic Blend Composites. *Procedia Materials Science* **2014**, *5*, 1231-1240. https://doi.org/10.1016/j.mspro.2014.07.434

[57] Imaddahen, M.A; Shirinbayan, M; Ayari, H; Foucard, M; Tcharkhtchi, A; Fitoussi, J. Multi-scale analysis of short glass fiber-reinforced polypropylene under monotonic and fatigue loading. *Polymer Composites* **2020**, *41* (11), 4649– 4662. https://doi.org/10.1002/pc.25740

[58] Autay, R.; Missaoui, S; Mars, J; Dammak, F. (2019). Mechanical and tribological study of short glass fiber-reinforced PA 66. *Polymers and Polymer Composites* **2019**, *27* (9), 587–596. https://doi.org/10.1177/0967391119853956

[59] Junaedi, H.; Baig, M.; Dawood, A.; Albahkali, E.; Almajid, A. (2020). Mechanical and Physical Properties of Short Carbon Fiber and Nanofiller-Reinforced Polypropylene Hybrid Nanocomposites. *Polymers* **2020**, *12*(12), 2851. https://doi.org/10.3390/polym12122851

[60] Luise, R. R. Applications of High Temperature Polymers. *CRC Press* **2018**, 225-227.

[61] Basavaraj, E; Ramaraj, B; Lee, J.H. Siddaramaiah. Polyamide 6/carbon black/molybdenum disulphide composites: friction, wear and morphological characteristics. *Materials Chemistry and Physics* **2013**, *138* (1-2), 658-665. https://doi.org/10.1016/j.matchemphys.2012.12.035

[62] Hunke, H; Soin, N; Gebhard, A; Shah, T; Kramer, E; Witan, K; Narasimulu, A.A; Siores, E. Plasma modified Polytetrafluoroethylene (PTFE) lubrication of alpha-olefin-copolymer impact-modified Polyamide 66. *Wear* **2015**, *338-339*, 122-132. https://doi.org/10.1016/j.wear.2015.06.003

[63] Mhadhbi, M. Introductory Chapter: Phase Change Material. Phase Change Materials and Their Applications, edited by Mohsen Mhadhbi. *IntechOpen, London* **2018**. DOI: 10.5772/intechopen.79432

[64] Jiménez-Suárez, A.; Prolongo, S.G. Graphene Nanoplatelets. *Applied Sciences* **2020**, *10* (5), 1753. https://doi.org/10.3390/app10051753

[65] Meng, Jianling & Shi, Dong-Xia & Zhang, Guangyu. A review of nanographene: Growth and applications. *Modern Physics Letters B* **2014**. *28,* 1430009. DOI: 10.1142/S0217984914300099.

[66] Dai, Yafei & Yi, Liu & Ding, Kai & Yang, Jinlong. A short review of nanographenes: structures, properties and applications. *Molecular Physics* **2018**, *116*, 1-16. DOI: 10.1080/00268976.2018.1433881.

[67] Balmes X.B. Zirconio, la respuesta. *Dental Dialogue* **2006**, *3*, 56-63.

[68] Guazzato, M; Albakry, M; Ringer, S.P; Swain, M.V. Strength, fracture toughness and microstructure of a selection of all-ceramic materials. Part 2. Zirconia-based dental ceramics. *Dental Materials* **2004**, *20* (5), 449-456. https://doi.org/10.1016/j.dental.2003.05.002

[69] Rizkalla, A.S; Jones D.W. Mechanical properties of commercial high strength ceramic core materials. *Dental Materials* **2004**, *20* (2), 207-212. https://doi.org/10.1016/S0109-5641(03)00093-9

[70] Yilmaz, H; Aydin, C; Gul B.E. Flexural strength and fracture toughness of dental core ceramics. The Journal of Prosthetic Dentistry **2007**, *98* (2), 120-128. https://doi.org/10.1016/S0022-3913(07)60045-6

[71] Manicone, P.F; Rossi, I.P; Raffaelli, L. An overview of zirconia ceramics: basic properties and clinical

applications. *Journal of dentistry* **2007**, *35*(11), 819–26. DOI: 10.1016/j.jdent.2007.07.008.

[72] Koszela, W et al. The effect of oil pockets size and distribution on wear in lubricated sliding. *Wear* **2007**, *263* (7-12), 1585-1592. https://doi.org/10.1016/j.wear.2007.01.108

[73] Moshkovith, A.; Perfiliev, V.; Gindin, D.; Parkansky, N.; Boxman, R; Rapoport, L. Surface Texturing Using Pulsed Air Arc Treatment. *Wear* **2007**, *263*, 1467–1469.

[74] Andersson, P; Koskinen, J; Varjus, S; Gerbig, Y; Microlubrication effect by laser-textured steel surfaces. *Wear* **2007**, *262*, 369-379.

[75] Erdemir, A. Review of engineered tribological interfaces for improved boundary lubrication. *Tribology International* **2005**, *38*, 249-256. DOI: 10.1016/j.triboint.2004.08.008

[76] Etsion, I et al. The effect of various surface treatments on piston pin scuffing resistance. *Wear* **2006**, *261*, 785-791. DOI: 10.1016/j.wear.2006.01.032

[77] Etsion, I; E. Sher, E. Improving fuel efficiency with laser surface textured piston rings. *Tribology International* **2009**, *42*, 542-547.

[78] Wos, P; Hichalski, J. Effect of Initial Cylinder Liner Honing Surface Roughness on Aircraft Piston Engine Performances. *Tribology Letters* **2011**, *41*, 555-567.

[79] http://www.gehring.de/enpdf/LaserHoning.pdf

[80] Popp, U et al. Proceedings of the institution of mechanical engineers part B. *Journal of engineering manufacture* **2006**, *220*, 27-33.

[81] Gualtieri, E et al. Increasing nanohardness and reducing friction of nitride steel by laser surface texturing. *Tribology International* **2009**, *42*, 699-705.

[82] Etsion, I; Kligerman, Y; Ronen, A. Friction-reducing surface-texturing in reciprocating automotive components. *Tribology Transactions* **2001**; *44* (3), 359-366. DOI: 10.1080/10402000108982468

[83] Etsion, I; Halperin, G. Analytical and Experimental Investigation of laser-textured mechanical seal faces. *Tribology Transactions* **1999**; *42* (3), 511-516. DOI: 10.1080/10402009908982248

[84] Segu, D.Z; Hwang, P. Friction control by multi-shape textured surface under pin-on-disc test. *Tribology International* **2015**, *91*, 111-117.

[85] Kovalchenko, A.; Ajayi, O.; Erdemir, A., et al. Friction and wear behavior of laser textured surface under lubricated initial point contact. *Wear* **2011**, *271*, 1719–1725.

[86] Kovalchenko, A; Ajayi, O; Erdemir, A; Fenske, G; Etsion, I. The effect of laser surface texturing on transitions in lubrication regimes during unidirectional sliding contact. *Tribology International* **2005**, *38* (3), 219-225. https://doi.org/10.1016/j.triboint.2004.08.004.

[87] Hoppermann, A; Kordt, M. Tribological optimisation using laser-structured contact surfaces. *O+P Oethydraulik and Pneumatik* **2002**, *46*, 1-23.

[88] S. Cupillard et al. Computational fluid dynamics analysis of a journal bearing with surface texturing. *Proceedings of the Institution of Mechanical Engineers, Part J: Journal of Engineering Tribology* **2008**, *222* (J2), 97-107. DOI10.1243/13506501JET319

[89] Schubert, A; Neugebauer, R; Sylla, D; Avila, M; Hackert, M. Manufacturing of surface microstructures for improved tribological efficiency of powertrain components and forming tools. *CIRP Journal of Manufacturing Science and Technology* **2011**, *4* (2), 200-207. https://doi.org/10.1016/j.cirpj.2011.01.010.

[90] Hu, T; Hu, L; Ding, Q. Effective solution for the tribological problems of Ti-6Al-4V: Combination of laser surface texturing and solid lubricant film. *Surface and Coatings Technology* **2012**, *206* (24), 5060-5066. https://doi.org/10.1016/j.surfcoat.2012.06.014

[91] Podgornik, B; Vilhena, L; Sedlacek, M; Rek, Z; Zun, I. Effectiveness and design of surface texturing for different lubrication regimes. *Meccanica* **2012**, *47* (7), 1613-1622. DOI:10.1007/s11012-012-9540-7.

[92] Marian, V.G; Kilian, M; Scholz, W. Theoretical and experimental analysis of a partially textured thrust bearing with square dimples. *Proceedings of the Institution of Mechanical Engineers, Part J: Journal of Engineering Tribology* **2007**, *221* (7), 771-777. https://doi.org/10.1243/13506501JET292

[93] Trujillo Flores et al. Nuevas Técnicas de Mecanizado. *Universidad de Córdoba* **2005**.

[94] Petkov, P.V; Dimov, S.S; Minev, R.M; Pham, D.T. Laser milling: Pulse duration effects on surface integrity. *Proceedings of the institution of mechanical engineers part B: Journal of Engineering Manufacture* **2008**, *222* (1), 35-45. https://doi.org/10.1243/09544054JEM840

[95] Giboz, J; Copponnex, T; Mélé, P. Microinjection molding of thermoplastic polymers: a review. *Journal of Micromechanics and Microengineering* **2007**, *17*, (2007), R96-R109. https://doi.org/10.1088/0960-1317/17/6/R02

[96] Fleischer, J; Schmidt, J; Haupt, S. Combination of electric discharge machining and laser ablation in microstructuring of hardened steels. *Microsystem Technologies* **2006**, *12*, 697-701. https://doi.org/10.1007/s00542-006-0095-1

[97] Ettefaghi, E; Ahmadi, H; Rashidi, A; Nouralishahi, A; Mohtasebi, S.S. Preparation and thermal properties of oil-based nanofluid from multi-walled carbon nanotubes and engine oil as nano-lubricant. *International Communications in Heat and Mass Transfer* **2013**, *46*, 142–147. https://doi.org/10.1016/j.icheatmasstransfer.2013.05.003

[98] www.subtech.com

[99] Lubricación de rodamientos. *FAG Sales Europe Iberia España* **1997**.

[100] Martín-Alfonso, J.E; A. Romero, A; Valencia, C; J.M. Franco. Formulation and processing of virgin and recycled polyolefin/oil blends for the development of lubricating greases. *Journal of Industrial and Engineering Chemistry* **2013**, *19* (2), 580-588. https://doi.org/10.1016/j.jiec.2012.09.012

[101] Hashimura, S; Miki, T; Otsu, T; Komatsu, K; Inoue, S; Yamashita, S; Omiya, Y. Robustness of polyisobutylene for friction coefficients between bearing surfaces of bolted joints. *Proceedings of the Institution of Mechanical Engineers, Part J: Journal of Engineering Tribology* **2019**, *234* (1), 50-64. https://doi.org/10.1177/1350650119854245

[102] Daudi, D.I.; Kilyakova, A.Y.; Kalyanova, O.A.; Korotaev, A.F.; Aleksanyan, K.G. The development of polyurea greases based on paraffin-naphthenic lubricating oil VHVI-4. *E3S Web of Conferences* **2021**, *266*, 02017. https://doi.org/10.1051/e3sconf/202126602017

[103] Deshmukh, V.; Pagare, C. The study of relationships of urea groups in polyurea greases and their properties. *NLGI SPOKESMAN* **2019**, *84* (1), 22-31.

[104] Bosman, R; Lugt, P. The Microstructure of Calcium Sulfonate Complex Lubricating Grease and Its Change in the Presence of Water. *Tribology Transactions* **2018**, *61* (5), 842-849. https://doi.org/10.1080/10402004.2018.1431752

[105] https://www.stle.org/images/pdf/STLE_ORG/BOK/LS/Grease/Calcium%20sulfonate%20complex%20greases.pdf

[106] Wu, Y.Y.; Tsui, W.C.; Liu, T.C. (2007). Experimental analysis of tribological properties of lubricating oils with nanoparticles additives. *Wear* **2007**, *26* (7-8), 819-825. https://doi.org/10.1016/j.wear.2006.08.021

[107] Liu, L; Fang, Z; Gu, A; Guo, Z. Lubrication Effect of the Paraffin Oil Filled with Functionalized Multiwalled Carbon Nanotubes for Bismaleimide Resin. *Tribology Letters* **2011**, *42* (1), 59–65. https://doi.org/10.1007/s11249-011-9749-y

[108] Peng, Y; Hu, Y; Wang, H. Tribological behaviors of surfactant-functionalized carbon nanotubes as lubricant additive in water. *Tribology Letters* **2007**, *25* (3), 247–253. https://doi.org/10.1007/s11249-006-9176-7

[109] Shen, M; Luo, J; Wen, S; Yao, J. Nano-tribological properties and mechanisms of the liquid crystal as an additive. *Chinese Science Bulletin* **2001**, *46* (14), 1227–1232. https://doi.org/10.1007/BF02900609

[110] Ji, X; Chen, Y; Zhao, G; Wang, X; Liu, W. Tribological properties of CaCO3 nanoparticles as an additive in lithium grease. *Tribology Letters* **2011**, *41* (1), 113–119. https://doi.org/10.1007/s11249-010-9688-z

[111] Hwang, Y.; Lee, C.; Choi, Y.; Cheong, S; Kim, D; Lee, K; Lee, J; Kim, S.H. Effect of the size and morphology of particles dispersed in nano-oil on friction performance between rotating discs. *Journal of Mechanical Science and Technology* **2011**, *25* (11), 2853–2857. https://doi.org/10.1007/s12206-011-0724-1

[112] Ma, S; Zheng, S; Cao, D; Guo, H. Anti-wear and friction performance of ZrO2 nanoparticles as lubricant additive. *Particuology* **2010**, *8* (5), 468-472. https://doi.org/10.1016/j.partic.2009.06.007

[113] Alberdi, A.; Hatto, P; Díaz, B; Csillag, S. Tribological behavior of nanocomposite coatings based on fullerene-like structures. *Vacuum* **2011**, *85* (12), 1087-1092. https://doi.org/10.1016/j.vacuum.2010.11.019

[114] Stewart, S; Ahmed, R. Rolling contact fatigue of surface coatings—a review. *Wear* **2002**, *253* (11-12), 1132–1144. https://doi.org/10.1016/S0043-1648(02)00234-X

[115] Bakoglidis, K.D; Nedelcu, I; Schmidt, S; Greczynski, G; Ehret, P; Hultman, L. Rolling contact fatigue of bearing components coated with carbon nitride thin films. *Tribology International* **2016**, *98*, 100–107. https://doi.org/10.1016/j.triboint.2016.02.017

[116] Igartua, A; Laucirica, J; Aranzabe, A; Leyendecker, T; Lemmer, O; Erkens, G, Weckc, M; Hanrathc, G. Application of low temperature PVD coatings in rolling bearings: Tribological tests and experiences with spindle bearing systems. *Surface and Coatings Technology* **1996**, *86-87* (2), 460-466. https://doi.org/10.1016/S0257-8972(96)03050-2

[117] Holmberg, K; Matthews, A. Coatings tribology: properties, mechanisms, techniques, and applications in surface engineering. *Tribology and Interface Engineering Series* **2009**, *56*.

[118] Klaffke, D; Santner, E; Spaltmann, D; Woydt, M. Influences on the tribological behavior of slip-rolling DLC-coatings. *Wear* **2005**, *259* (1-6),752-758. DOI: 10.1016/j.wear.2005.01.008

[119] Thom, R; Moore, L; Sproul, W.D; Peter Chang, T. Rolling contact fatigue tests of reactively sputtered nitride coatings of Ti, Zr, Hf, Cr, Mo, Ti–Al, Ti–Zr and Ti– Al–V on 440 C stainless steel substrates. *Surface and Coatings Technology* **1993**; *62* (1-3), 423-427. https://doi.org/10.1016/0257-8972(93)90278-V

[120] Novak, R; Polcar, T. Tribological analysis of thin films by pin-on-disc: evaluation of friction and wear measurement uncertainty. *Tribology International* **2014**; *74,* 154–163. https://doi.org/10.1016/j.triboint.2014.02.011

[121] Michalczewski, R; Piekoszewski, W; Szczerek, M; Tuszynski, W. The lubricant-coating interaction in rolling and sliding contacts. *Tribology International* **2009**, *42* (4), 554-560. https://doi.org/10.1016/j.triboint.2008.05.001

[122] Kuhn, M; Gold, P.W; Loos, J. Wear and friction characteristics of PVD-coated roller bearings. *Surface and Coatings Technology* **2004**, *177 –178*, 469–476. https://doi.org/10.1016/S0257-8972(03)00914-9

[123] Ciarsolo, I; Fernández, X; Ruiz de Gopegui, U; Zubizarreta, C; Abad, M.D; Mariscal, A.; Caretti, I; Jiménez, I; Sánchez-López, J.C. Tribological comparison of different C-based coatings in lubricated and unlubricated conditions. *Surface and Coatings Technology* **2014**, *257*, 278–285. https://doi.org/10.1016/j.surfcoat.2014.07.068

[124] Sasaki, S. Environmentally friendly tribology (Eco-tribology). *Journal of Mechanical Science and Technology* **2010**, *24*, 67-71. https://doi.org/10.1007/s12206-009-1154-1

[125] Mabuchi, Y; Okuda, S. Super-low Friction Technology with Hydrogen-free DLC Film. *Journal-Society of Automotive Engineers of Japan* **2008**, *62*(4), 44-48.

[126] Saito, T. Vacuum clean lubricant film V-DFO. *NSK Technical Journal* **2002**, *673*, 22-25.

[127] Podgornik, B; Sedlacek, M; Vizintin, J. Influence of contact conditions on tribological behaviour of DLC coatings. *Surface and Coatings Technology* **2007**, *202* (4-7), 1062–1066. https://doi.org/10.1016/j.surfcoat.2007.07.040

[128] Erdemir, A; Donnet, C. Tribology of diamond-like carbon films: recent progress and future prospects. *Journal of Physics D: Applied Physics* **2006**, *39* (18), R311. https://doi.org/10.1088/0022-3727/39/18/R01

[129] Field, S.K.; Jarratt, M; Teer, D.G. Tribological properties of graphite-like and diamond-like carbon coatings. *Tribology International* **2004**, *37* (11-12), 949-956. https://doi.org/10.1016/j.triboint.2004.07.012

[130] Ban, M; Ryoji, M; Fujii, S; Fujioka, J. Tribological characteristics of Si-containing diamond-like carbon films under oil-lubrication. *Wear* **2002**, *253* (3-4), 331-338. https://doi.org/10.1016/S0043-1648(02)00156-4

[131] Kalin, M; Vizintin, J. The tribological performance of DLC-coated gears lubricated with biodegradable oil in various pinion/gear material combinations. *Wear* **2005**, *259* (7-12), 1270-1280. https://doi.org/10.1016/j.wear.2005.02.028

[132] Kalin, M; Vizintin, J; Barriga, J; Vercammen, K; Acker, K.V.; Arnsek, A. The effect of doping elements and oil additives on the tribological performance of boundary-lubricated DLC/DLC contacts. *Tribology Letters* **2004**, *17* (4), 679–688. https://doi.org/10.1007/s11249-004-8073-1

[133] Podgornik, B; Vizintin, J; Jacobson, S; Hogmark, S. Tribological behaviour of WC/C coatings operating under different lubrication regimes. *Surface and Coatings Technology* **2004**, *177–178*, 558-565. https://doi.org/10.1016/S0257-8972(03)00927-7

[134] Podgornik, B; Jacobson, S; Hogmark, S. DLC coating of boundary lubricated components—advantages of coating one of the contact surfaces rather than both or none. *Tribology International* **2003**, *36* (11), 843-849. https://doi.org/10.1016/S0301-679X(03)00102-6

[135] Salvadori, M.C.; Martins, D.R.; Cattani, M. DLC coating roughness as a function of film thickness. *Surface and Coatings Technology* **2006**, *200* (16–17), 5119-5122. https://doi.org/10.1016/j.surfcoat.2005.05.030

[136] Manier, C-A; Ziegele, H; Barriga, J; Goikoetxea, J; Woydt, M. Zirconium-based coatings in highly stressed rolling contacts as alternative solution to DLC and ta-C coatings. *Wear* **2010**, *269* (11-12) 770–781. https://doi.org/10.1016/j.wear.2010.08.004. IK4-TEKNIKER Patent P1767DE00.

[137] Ehiasarian, A; Wen, J; Petrov, I. Interface microstructure engineering by high power impulse magnetron sputtering for the enhancement of adhesion. *Journal of Applied Physics* **2007**, *101* (5), 0–10. https://doi.org/10.1063/1.2697052

[138] Drábik, M; Ballo, V; Truchlý, M; Frkáň, J; Roch, T; Kvetková, L; Satrapinskyy, L; Kúš, P. Influence of plasma pretreatment on the performance of industrial tungsten carbide coatings deposited at low temperature on 100Cr6 bearing steel substrates. *Surface and Coatings Technology* **2016**, *293*, 2-9. https://doi.org/10.1016/j.surfcoat.2016.01.035

[139] Hauzer Conference 2012 | Triondur® Coatings as a design element for highly stressed engine components

6. Publicaciones

6.1. Tribology International: Analysis of self-lubrication enhancement via PA66 strategies: Texturing and nano-reinforcement with ZrO2 and graphene

En el artículo “*Analysis of self-lubrication enhancement via PA66 strategies: Texturing and nano-reinforcement with ZrO2 and graphene*”, se estudió la influencia de la adición de nanoflakes de grafeno y de dióxido de circonio (ZrO_2) a los compuestos de poliamida 66 con fibra de vidrio para mejorar sus propiedades autolubricantes y hacerlos aptos para aplicaciones de rodamientos de alto rendimiento. También se investigó la influencia del texturizado de las superficies. Para cada una de las diferentes combinaciones de compuestos poliméricos híbridos, porcentajes de aditivo y geometrías de texturización generadas, se analizó su comportamiento tribológico mediante ensayos ball-on-disc. Los resultados mostraron que los coeficientes de fricción más bajos se obtienen para la combinación híbrida de PA66 con un 30% de fibra de vidrio y un 5% de grafeno. Además de ensayos tribológicos, las superficies desgastadas fueron analizadas mediante microscopía electrónica de barrido (Scanning Electron Microscopy, SEM) y microscopía óptica confirmando la mejora de las propiedades tribológicas con la adición de grafeno y la falta de relevancia del texturizado bajo lubricación seca.

Contribución del doctorando: Revisión del estado del arte. Análisis e interpretación de resultados. Redacción y revisión del artículo.

Tribology International 131 (2019) 332–342

Contents lists available at ScienceDirect

Tribology International

journal homepage: www.elsevier.com/locate/triboint

Analysis of self-lubrication enhancement via PA66 strategies: Texturing and nano-reinforcement with ZrO_2 and graphene

Isabel Clavería[a,*], Daniel Elduque[a], Aleida Lostalé[a], Ángel Fernández[a], Pere Castell[b], Carlos Javierre[a]

[a] Mechanical Department, University of Zaragoza EINA, María de Luna 3, 50018, Zaragoza, Spain
[b] AITIIP Foundation, Romero 12, 50720, Zaragoza, Spain

ARTICLE INFO

Keywords:
ZrO_2
Graphene
Friction
Texturing

ABSTRACT

Graphene nanoflakes and zirconium dioxide (ZrO_2) were added to polyamide 66-based composites with glass fibre in order to improve their self-lubricating properties and make them suitable for high-performance bearing applications. The influence of texturing the surfaces was also investigated. The tribological behaviour was analysed for different combinations of hybrid polymeric composites, percentages of additive, and texturing geometries. The results show that the lowest low friction coefficients are obtained for PA66 + 30GF with 5% graphene. Worn surfaces, analysed by scanning electron microscopy and optical microscopy confirm the enhancement of the tribological properties with the addition of graphene. Texturing results under dry lubrication are not relevant for tribological purposes.

1. Introduction

It is estimated that almost 30% of the energy consumed worldwide is lost in the form of heat due to friction [1]. Traditionally, tribological properties such as friction, wear, and lubrication have been investigated by focusing on the development of new surface treatments [2,3], e.g., nitriding and carburizing, grease lubricants, and hard coatings. Nitriding and carburizing significantly increase the hardness, which leads to better tribological behaviour [4–7]. Owing to their composition [8] and industrial applications [9], new grease lubricants are continuously investigated to optimise the tribological performance. Hard coatings such as nanocomposites of silver containing carbon films (a-C:H/Ag) [10], Molibdenum dysulfide with mixture of titanium and tungsten (MoS_2TiW) [11], (Zr,Ti)N deposited via physical vapour deposition (PVD) [12], and diamond films deposited via chemical vapour deposition (CVD) [13,14], as well as plasma spray techniques [15,16], are used to reduce heat generation. Some friction and wear phenomena are controlled by processes at the atomic or molecular scale, and others are controlled by processes at a scale of roughness of approximately 1–20 μm [17]. Consequently, one of the challenges that tribology research faces with regard to new surface treatments based on coatings is the difficulty of studying microscopic phenomena resulting in macroscopic wear and friction. Additionally, the interacting forces between the coating and substrate surface determine the adherence properties and coating detachment. Thus, new self-lubricating materials with optimal properties for each application without coating requirements are a good solution, as they allow the elimination of external lubricants, simplifying the design and reducing maintenance costs.

Polymers are extensively used in active engineering components such as gears and cams, and their self-lubricating properties are exploited to avoid the need for oil or grease lubrication, which present the problems of sealing and possible contamination [18]. Bearings are one of the most widely used mechanical components in industry and it is one of the components to which tribology research can be most directly applied. New trends in bearings are focused on obtaining high-performance bearings capable of operating under high-speed and high-temperature conditions [19,20]. These features are directly related to the friction during bearing performance caused by rolling and/or sliding between rolling elements and the bearing cage [21–23]. Cages for small-to medium-size bearings can be made of metallic materials or polymer composites, which minimise the inertial effects [24]. Different polymers have been studied from a tribological viewpoint, such as polyether ether ketone (PEEK)/polytetrafluoroethylene (PTFE) [25] and polyamide (PA), which is the most promising material for this purpose [26–30]. PAs are usually mixed with glass fibre (GF) to improve their mechanical properties. The tribological behaviour of these

* Corresponding author.
E-mail addresses: isabel.claveria@unizar.es (I. Clavería), delduque@unizar.es (D. Elduque), aleida.lostale@fersa.com (A. Lostalé), afernan@unizar.es (Á. Fernández), pere.castell@aitiip.com (P. Castell), carlos.javierre@unizar.es (C. Javierre).

https://doi.org/10.1016/j.triboint.2018.10.044
Received 20 July 2018; Received in revised form 25 October 2018; Accepted 27 October 2018
Available online 02 November 2018
0301-679X/

composites under sliding conditions was reported in Refs. [31,32] long ago, indicating the ability of PA to form a thin and uniform transfer film while sliding against steel counterparts, which helps to reduce the coefficient of friction (COF). The tribological behaviour of the composite is affected by the different contents of GF in the PA matrix during sliding, as described in Ref. [33]. While few investigations of the behaviour of PA under rolling conditions have been reported, studies have revealed the negative effect of GF on wear [34–36].

Therefore, new bearing applications demand new composites combining the good mechanical properties of GF, good processability of polymers, and good wear behaviour that can be achieved by adding nano-particles to the polymer matrix.

Carbon nanotubes provide effective reinforcement for polymers, improving the mechanical properties [37] and reducing the friction and specific wear rate for a range of loads [38]. Additionally, alumina has been added to PTFE to reduce the COF and wear, and titanium dioxide (TiO_2) has been proven to reduce the COF, especially under high-load/speed conditions [27].

Graphene, which was first obtained from graphite in 2004 [39], is one of the most promising additives owing to its special bidimensional layered structure, whose atomic thickness is 0.1 nm. The most relevant properties of graphene are its high conductive capacity, hardness, and strength as a very thin layered structure. Regarding the tribological behaviour, it has been dispersed on an oil lubricant to reduce the wear and friction of mechanical elements immersed in the lubricant [40] and applied to silicon dioxide (SiO_2) substrates [41]. Literature concerning the tribological behaviour of graphene applied to polymers is limited to the study of PEEK [42], acrylonitrile butadiene rubbers (NBRs) [43], PTFE [44], and polyphenylene sulphide (PPS) [45], with graphene used for coating purposes.

ZrO_2 particles are also a promising material owing to their high hardness and stiffness, as well as their optimum thermal stability. When they are applied to coatings for metallic materials, a higher working temperature can be reached [46], and the mechanical properties are significantly improved [47]. The modification of the tribological properties of ZrO_2 itself was analysed in Ref. [48], as well as its influence on ceramic metal materials (CerMet) materials [49], but few investigations have focused on the improvement of the tribological properties of polymers doped with ZrO_2 [50].

A technique that has not been thoroughly explored for improving the self-lubricating properties is surface modification by texturing. In the past few years, new mechanical [51], pulsed air arc [52], and energetic beam [53] techniques for surface modification have led to innovative surface treatments that can replace the current ones for improving the tribological properties. One of the most promising techniques is the micromachining of geometrical shapes on lubricated surfaces, which act as small lubricant reservoirs [54]. Laser micromachining is the most advanced technique for surface modification in tribological applications and is a clean, rapid, and highly accurate process. Even when micromachining is combined with other surface techniques, the best tribological results are due to the micromachined geometry [55–57]. However, studies show that the tribological improvement depends strongly on the main micromachining parameters, such as the shape, dimensions, and density of the motif. The typical micromachined geometry suitable for improving the tribological properties consists of dimples that act as cells of hydrodynamic pressure to ensure heat removal in the case of wet lubrication [58] or as reservoirs for preventing the accumulation of the wear material in contact areas [59,60] in the case of dry lubrication. These dimples also allow the modification of the width and height of the limit lubrication area achieving lower friction values that are close to hydrodynamic lubrication values [61]. Another advantage of this kind of micromachining is the non-interference with the surface macro-geometry produced by material roughness [62]. Most of the literature regarding the improvement of the tribological behaviour via surface geometry modification is focused on metals.

In the present study, the effect of graphene and ZrO_2 additivation on the friction and wear behaviour of a GF PA66 composite is investigated. A second strategy for improvement involves texturing the surfaces of the additived samples exhibiting the best tribological behaviour with dimples having two different geometries in order to analyse their influence on the COF and wear results.

2. Experimental

2.1. Materials

Polymer nano-reinforced composites based on PA 66 + 30% GF from INVISTA (TORZEN® G3000 NC01) [63] were analysed. Glass fibre is sized 10 µm diameter and an average length of 150 µm.

The additives used were ZrO_2 and graphene. The graphene used was Avangraphen Plat 40, which is a two-dimensional carbon atom structure obtained via the mechanical exfoliation of graphite, with an oxygen content (X-ray photoelectron spectroscopy) of < 0.5%, a hydrogen content of < 1%, a nitrogen content of < 1%, an average thickness of 10 nm, a side size (Laser Diffraction) of 40 µm, a surface area (Brunauer–Emmett–Teller) of 282 m^2/g, and an average number of layers of < 30. It is specially designed to be mixed with polymeric materials, and a low dosage is required to reach the percolation level. The other additive used was general-purpose ZrO_2 supplied by TORRECID [64], sized 750 nm and with a tensile strength of 450 MPa.

2.2. Specimen preparation

Five different nano-reinforced composite materials were prepared, as shown in Table 1, via extrusion compounding in a co-rotating twin screw extruder (Coperion ZS26K) equipped with two gravimetric feeders (Brabender). The maximum torque was 100 Nm, maximum screw speed was 1200 rpm, and maximum pressure was 180 bar. A screw diameter of 25 mm and a length/diameter ratio of 40 were used in the different test procedures. The optimum level of additive dispersion into the polymeric matrix was determined using an ultrasonic device specially designed for this purpose, fully described in Refs. [65,66]. The morphology of the samples was analysed via scanning electron microscopy (SEM, Hitachi S-3400 N) and energy-dispersive X-ray spectroscopy (EDX, Röntec XFlash de Si(Li)), at an acceleration voltage of 15 kV and a working distance of 17.6 mm. The samples were previously sputtered with a thin layer of gold in vacuum before observation. Scanning electron images of the microstructure of the resulting PA66GF30 composites are shown in Fig. 1. Fig. 1a shows the morphology of the samples without additives. Fig. 1b and c shows samples doped with ZrO_2, and Fig. 1d and e shows samples doped with graphene. It can be observed for samples doped with low percentages (1%) in Fig. 1b and d that laminar morphology of these samples do not change significantly regarding to morphology of sample 1a without doping. When percentages of additive are increased up to 5% graphene (figure 1e) and 10 ZrO_2 (Fig. 1c), a change in sample morphology is clearly appreciated. In case of samples doped with ZrO_2 an alveolar structure is induced into the polymer due to the spherical shape of the ZrO_2. In case of samples doped with graphene, a flaked structure is induced into the polymer matrix due to the laminar structure of the graphene. All the samples doped with any of the additives do not

Table 1
Hybrid composites tested.

Composite	Base polymer	additive
PA66GF30	PA 66 + 30% GF	–
PA66GF30ZrO$_2$1	PA 66 + 30% GF	1% ZrO_2
PA66GF30ZrO$_2$10	PA 66 + 30% GF	10% ZrO_2
PA66GF30G1	PA 66 + 30% GF	1% graphene
PA66GF30G5	PA 66 + 30% GF	5% graphene

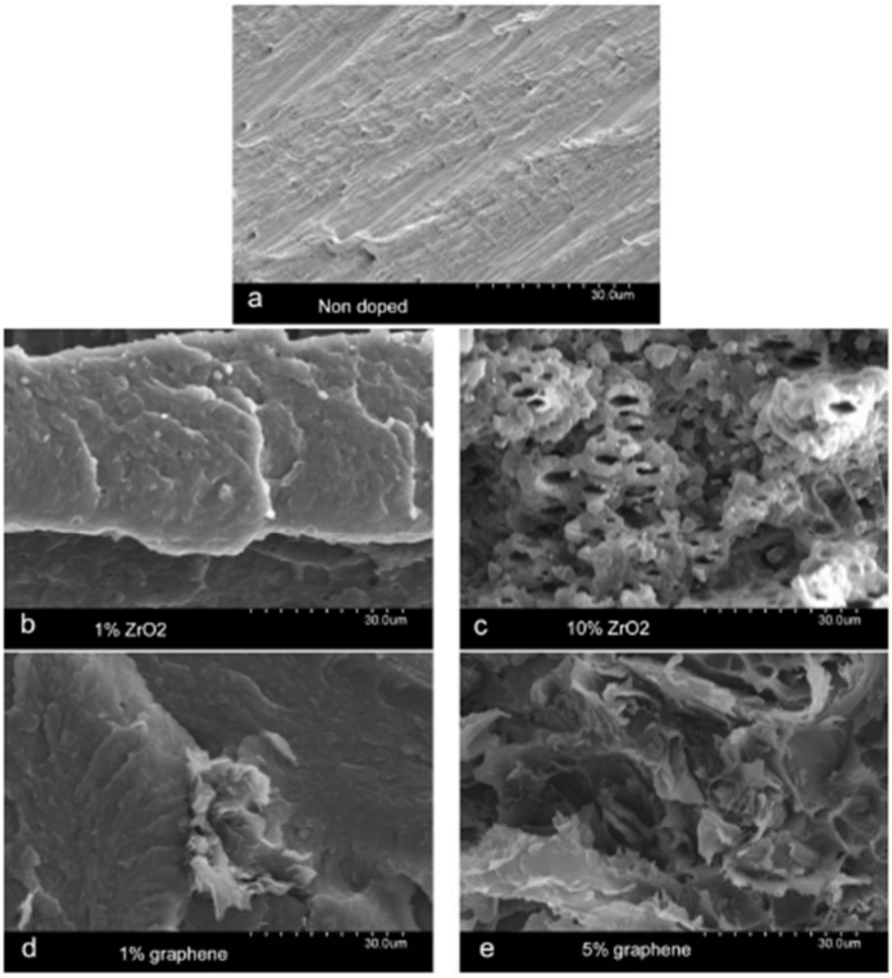

Fig. 1. SEM images of the microstructure for hybrid PA66GF30 nanocomposites.

exhibit aggregates which could imply a good dispersion of the additives for both low and high percentages of additive.

Samples of 45 × 45 × 3 mm^3 from the resulting composite materials were injected using an electric injection machine (JSW 85 EL II) with a clamping force of 85 tons, a maximum injection pressure of 1960 bar, a maximum injection volume of 97 cm^3, and a screw diameter of 32 mm. The process conditions were as follows: an injection temperature profile of 240/260/280 °C, a mould temperature of 70 °C, an injection time of 1 s, a packing pressure of 50 MPa for 5 s, and a cooling time of 7 s.

2.3. *Friction and wear test*

Ball-on-disk wear experiments were conducted using a tribometer (Falex Multispecimen) according to the ASTM G99 standard. Because the purpose of the study was to obtain a self-lubricating material for bearing cages, the ball specimen was an AISI 52100 100Cr6 ball with hardness of HRC 60 and roughness of R_a = 0.010 μm, directly obtained from rolling bearings, with a diameter of 12.7 mm. The counterface material was obtained from the different composite-injected samples at a sliding speed of 249 mm/s at 80 °C. A test normal load of F_N = 22.5 N was applied for 1800 s in an attempt to avoid plastic deformation on the polymeric disc surface. The following results were recorded: the COF evolution over time, the roughness measured using a MARSURF XCR 20 device, and the wear determined both by the weight difference and the wear track measured via optical microscopic techniques. The microscope used was a SEM EDX Hitachi S-3400 N, and the mass loss of the samples was weighed using an electric balance in order to calculate the specific wear rate via the following equation:

$$w_s = \frac{\Delta m}{\rho F_N L}\left(\frac{mm^3}{Nm}\right), \quad (1)$$

where F_N is the normal force applied during the test, ρ is the material density, L = 447.63 m is the sliding distance according to the sliding speed and test duration, and Δm is the mass loss obtained experimentally from the weight difference of the sample before and after the test.

Density values (ρ) are calculated from equation:

$$\rho = (\%_{matrix} {}^{*} \rho_{matrix}) + (\%_{additive} {}^{*} \rho_{additive}) \quad (2)$$

Where ρ is density for the sample material, $\%_{additive}$ is mass percentage of additive (ZrO_2 or graphene) added to the sample composite, $\%_{matrix}$ is mass percentage of polymer material (PA66 + 30% glass fiber), ρ_{matrix} is density of polymer, and $\rho_{additive}$ is density of additive.

2.4. *Texturing*

Surface microstructuring was performed by using a picosecond-pulse Nd:YVO_4 laser, which was integrated in a micromachining workstation

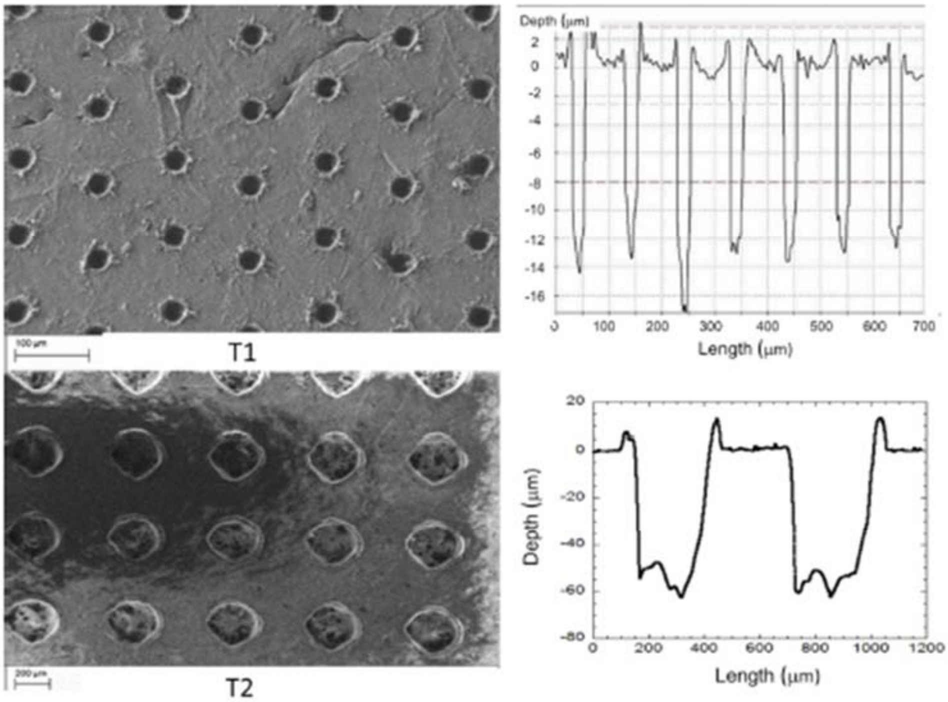

Fig. 2. Morphology and dimple configuration for texturing T1 (up) and texturing T2 (down).

(3D MICROMAC). Dimples were created on the material by applying 355 nm wavelength. Two different dimple configurations were obtained by varying the frequency, the overlapping distance between laser pulses, energy, and number of laser passes. The first dimple configuration, which was called T1, was generated by applying a frequency of 10 kHz, an overlapping distance between pulses of 100 µm, an energy of 50 µJ, and five passes, leading to the formation of dimples 20 µm in diameter and 15 µm in depth. The second dimple configuration—T2—was obtained by applying a frequency of 250 kHz, an overlapping distance between pulses of 2 µm, an energy of 1.5 µJ, and 12 passes, yielding dimples 300 µm in diameter and 60 µm in depth. The laser beam was focused onto the sample by a focusing lens placed in the air. The lens had a focal length of 103 mm for 355 nm-wavelength light. Fig. 2 shows the distribution of the circular dimples on the samples obtained by SEM.

3. Results

3.1. Friction and wear

Fig. 3 shows the evolution of the COF during the wear test for the hybrid composite materials described in Table 1. The results exhibit an increasing trend at times under approximately 60 s for the running-in stage of all composites, except for PA66GF30ZrO$_2$1, whose increasing trend lasts for 400 s and exhibits instability until the test was half-complete. Then, once the transfer film has been developed and remains intact, the curve reaches a steady stage, exhibiting a constant value. PA66GF30 has an average COF of 0.3. The addition of ZrO_2 has a negative effect, increasing the COF up to 0.5 and 0.6 for ZrO_2 concentrations of 1% and 10%, respectively. The lower average COFs resulted from the addition of graphene to PA66GF30: 0.15 in the case of 1% graphene and 0.1 in the case of 5% graphene. The results show more stable behaviour during the test with graphene than during the test with ZrO_2.

Table 2 summarises the average values of the COF, which were calculated by averaging the experimental values from the steady-state stage in Fig. 3. It also indicates the specific wear rate ω_s calculated using Equation (1), the width of the wear track, and the roughness induced by wear.

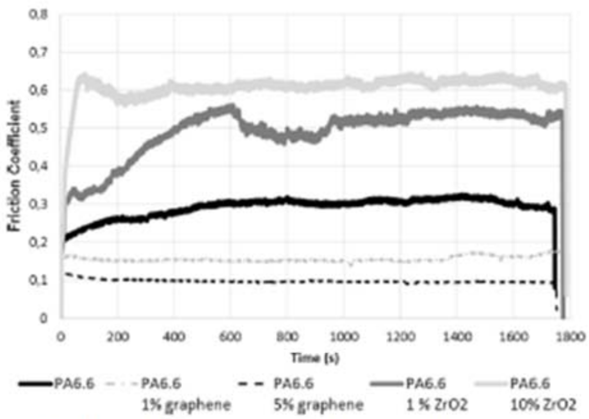

Fig. 3. Evolution of friction coefficient as a function of the wear test time for PA66 hybrid composites.

According to Fig. 4, the mass loss is reduced from 17.8 mg for the samples without additives to 10.5 mg for the samples with 1% graphene and to 7.5 for the samples with 5% graphene. When PA66GF30 is doped with ZrO_2, a smaller reduction in the mass loss is achieved: up to 12 mg for 1% ZrO_2 samples and up to 17 mg for 10% ZrO_2 samples.

It can be stated that the PA66GF30 + graphene exhibits better tribological behaviour than PA66GF30, with lower COFs and a lower wear rate. The best results are achieved by adding 5% graphene to PA66GF30, reducing the COF from 0.3 to 0.098 and reducing the wear rate from 1.54 to 0.65. Consequently, a shallow wear track is obtained, as indicated by Table 2 and Fig. 5. As stated previously, the addition of ZrO_2 has a negative effect on the COF, yielding values approximately

Table 2
Summary of wear test results for hybrid composites.

Material	μ		ρ (g/cm³)	w_s 10^{-3} (mm³/Nm)	Ra (μm) Before test	Ra (μm) After test	Width of Wear track (mm)
	Average	Standard deviation					
PA66GF30	0.309	0.016	1.37	1.289	0.167	0.219	1.186
PA66GF30 + 1% graphene	0.157	0.024	1.3783	0.757	0.149	0.257	1.001
PA66GF30 + 5% graphene	0.098	0.008	1.4115	0.527	0.153	0.489	1.072
PA66GF30 + 1% ZrO_2	0.519	0.069	1.4123	0.853	0.109	0.126	1.240
PA66GF30 + 10% ZrO_2	0.606	0.063	1.793	0.941	0.114	0.128	1.122

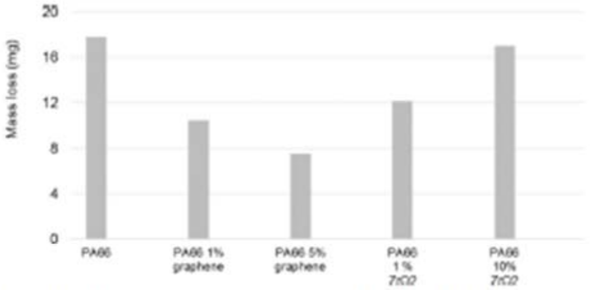

Fig. 4. Mass loss measured after wear tests for PA66GF30 hybrid composites.

twice those for PA66GF30, although the wear rate is reduced, especially for low fractions of ZrO_2. The friction and wear results become worse when high percentages of zirconia (10%) are added.

In spite of the low friction values achieved for the samples doped with graphene, the roughness values remain higher than those for the non-doped samples (0.25 μm for PA66GF30G1 and 0.489 μm for PA66GF30G5). The high roughness values are attributed to material deposition onto the sharpest polymer peaks during sliding, similar to the phenomenon reported in Ref. [67].

3.2. Characterisation of worn surface

The wear track in PA66GF30, with a width of 1.080 mm, is clearly observed in Fig. 5a. Samples 5d and 5e, which were doped with 1% and 5% graphene, respectively, exhibit a shallower wear path owing to their smaller width of 1.001 and 0.809 mm, respectively. The samples doped with ZrO_2 exhibit a wider wear path, as shown in Fig. 5b and c, with values of 1.105 mm for 1% ZrO_2 and 1.202 mm for 10% ZrO_2.

Using optical microscopy, images of the worn surface were obtained to better analyse the generated tracks (Fig. 6).

The worn surface exhibits a wavy morphology for PA66GF30, as shown in Fig. 6a, indicating the presence of a transfer film with PA66 debris on top of the sample due to plastic softening. This is caused by local plastic deformation, which indicates the viscous flow of the polymer induced by the high flash temperature occurring in the real contact area and the stress concentration near the sample borders. The stress concentration is mainly caused by the GF interface, although the optical image cannot identify the typical shiny spots of GF needles disrupting the transfer film [33]. This softening of the polymeric material is reduced in Fig. 6d and e, showing less debris for samples doped with 5% graphene. Owing to the graphene nanoflakes, the COF is reduced and the debris is eliminated under a normal process of fibre thinning, fibre fracture, or fibre peeling-off. Therefore, the fibres can effectively undertake the load and be gradually removed via a normal process [27].

The PA66GF30ZrO$_2$10 samples in Fig. 6c exhibit a worn surface with slight grooves parallel to the sliding direction, indicating mechanical interaction. This suggests that the wear process is partially governed by an abrasive wear mechanism. In this case, the polymer generally obtains a high wear rate, depending on the original roughness of the harder counterparts and the contact pressure [27]. The wear rate for these samples is higher than that for other additived samples, as shown in Table 2, but hardly lower than the values obtained for non-doped ones. This is probably because of the positive effects of both the additives, which reduced the temperature in the contact area owing to the high thermal conductivity, and the low ball counterpart roughness (R_a = 0.010 μm), which compensated for the effect of the abrasive wear mechanism.

3.3. Results for micromachined samples

According to the aforementioned results, PA66GF5G exhibits the best tribological behaviour. Therefore, the surfaces of these samples were textured with two different dimple geometries, as described in Section 2.3. The results for the COF are shown in Fig. 7, indicating an increasing trend until reaching a steady state. The steady state is reached quickly, except for the textured T2 samples, which require 500 s and exhibit instability during the running-in stage. The T1 and T2 samples have average COFs of 0.15 and 0.38, respectively. Micromachining does not appear to have a positive effect; the results are even worse than those for the non-doped texturised T2 samples. Table 3 summarises the average values of the COFs, which were calculated by averaging the experimental values from the steady-state stage in Fig. 7, and the wear results for the specific wear rate ω_s calculated using Equation (1). All the micromachined samples exhibit worse tribological behaviour than the non-textured samples with the same composition. The COFs are 1.5 and 3.8 times higher for T1 and T2, respectively, and the wear rate is almost twice as high for both textured cases compared with the non-textured ones.

The worn surfaces analysed via SEM are shown in Fig. 8. They exhibit a wavy morphology, indicating plastic softening. The SEM images show dimples filled by the plasticised material detached during rolling wear, especially for the T1 samples, where the dimples are smaller and closer. For the T2 samples, the refilling of the dimples with debris and detached material is clearly observed.

4. Discussion

4.1. Wear mechanism

The polymer selected for the research has very good tribological properties to begin with. It also forms a good transfer film on the counterfaces during sliding, which is generally a prerequisite for good tribological properties. Thus, it is a challenge to improve its tribological properties further.

The main cause of rolling wear is adhesion, which leads to the formation of a transfer film. Fig. 9a shows an optical image of the ball and Fig. 9b shows SEM image of the ball where transferred polymer can be observed. An EDX analysis has been carried out to confirm this presence of polymer. Fig. 10c shows EDX spectrum (named in the figure as spectrum 5) for a local area of the ball where sample material has not been transferred. Materials detected in this area were Fe (89.66% weight), Cr (1.31% weight) and C (9.03% weight). Fig. 10d shows EDX spectrum (named in the figure as spectrum 1) for a local area of the ball

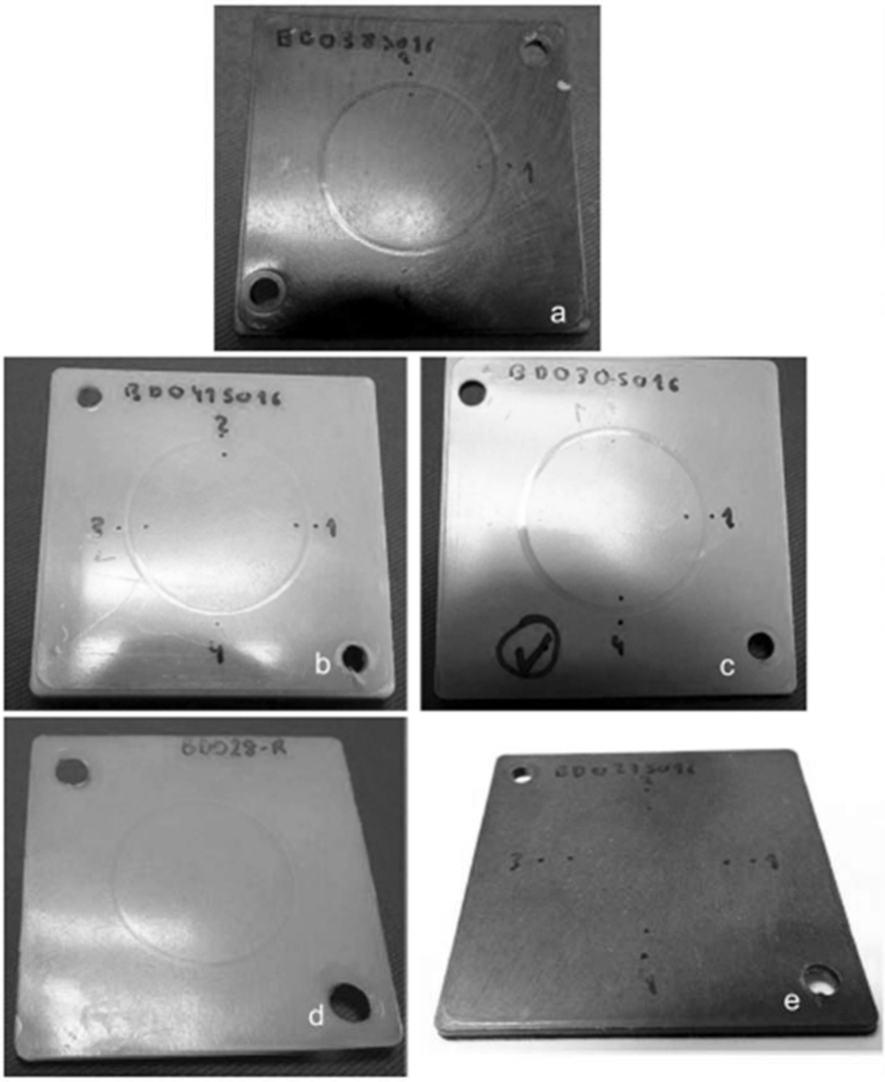

Fig. 5. Wear paths generated during wear tests for PA66GF30 (a), PA66GF30ZrO$_2$1 (b), PA66GF30ZrO$_2$10 (c), PA66GF30G1 (d), and PA66GF30G5 (e).

where polymer sample material has been transferred. Materials detected in this area were Fe (26.06% weight), Cr (0.54% weight), O (9.34% weight) and C (64.04% weight). High presence of C confirms the presence of polymeric material transferred from the sample to the ball.

The wear adhesion mechanism is as follows: owing to the low load-carrying capacity of polymers, the cohesive forces inside the polymer are weaker than the adhesion power between the steel counterpart and the polymer. This leads to the development of a transfer film on the counterface in the transient wear state, through the microfragmentation of the polymeric material, because of the interaction with metal asperities. Owing to the lower wear resistance of the polymeric composite, small wear particles are rapidly removed from the softened polymeric surface by the hard asperities of the metallic counterpart surface almost from the beginning of the wear test. As stated in Ref. [68], the friction component resulting from adhesion is equal to the product of the real contact area and the shear strength of the polymer for the sliding contact of polymers against metals. The adhesion ability of polymers can differ significantly because of the specific surface characteristics of the material, which are expressed by its surface energy. PA has one of the highest surface energies in the literature [69] owing to the strongly increased polar component caused by its chemical structure and the strong interactions (hydrogen bonds) between adjacent polymer chains, which is correlated with high adhesion work between PA contacts. The formation and growth of this transfer film is usually followed by the moderate stabilisation of the COF, once the sharp asperities of the hard counterpart cease to abrade, after being covered by the fragments of the polymer [70,71]. Once the transfer film is formed on the counterpart, wear arises from the loss of transfer-film fragments during repetitive sliding and the occasional separation of the material from the sample surface, which causes it to escape from the interface rather than building up the transfer film. At the transfer film, shearing is accompanied by the detachment of fragments of polymer, with a large amount of broken polymer sticking to the metal counterpart.

Fig. 3 shows the increasing trend of the COF values during the running-in stage, which is probably caused by the increase of the real contact area and the contact temperature due to frictional heating [27]. The duration of this stage is determined by the speed of the formation of the stable transfer film, owing to the accelerated generation of wear debris and the easier formation of the transfer film.

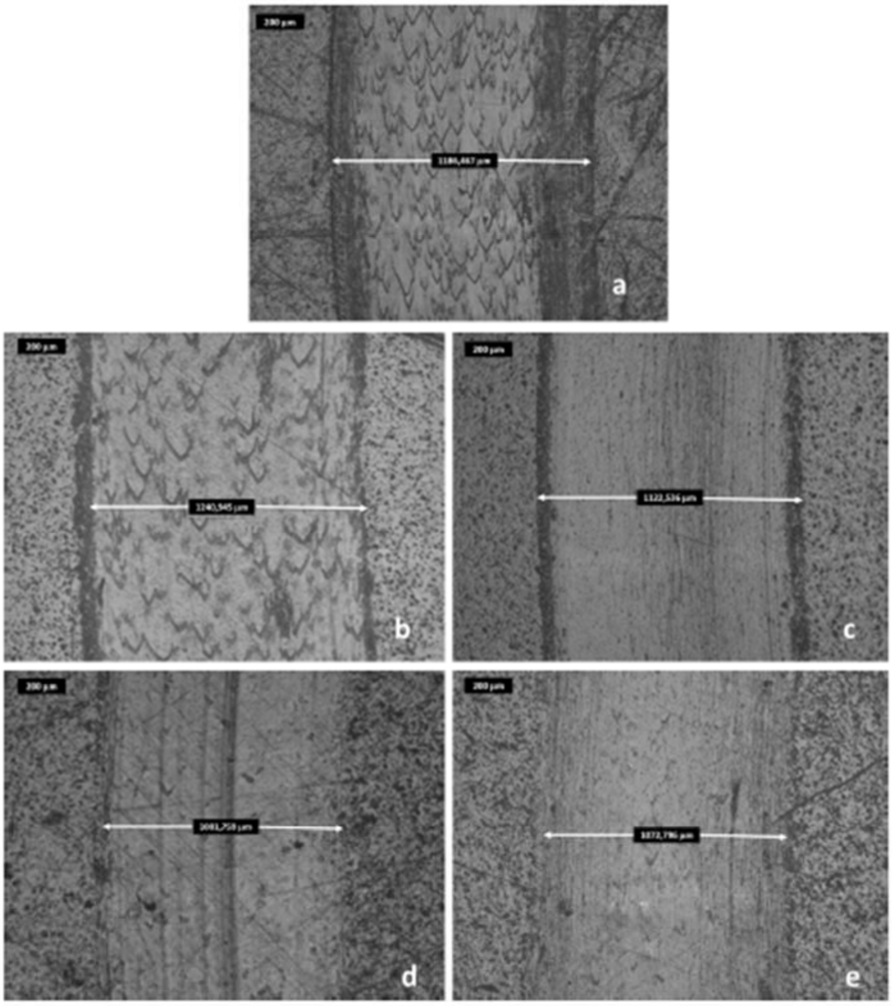

Fig. 6. Worn surfaces after wear tests for PA66GF30 (a), PA66GF30$ZrO_2$1 (b), PA66GF30$ZrO_2$10 (c), PA66GF30G1 (d), and PA66GF30G5 (d).

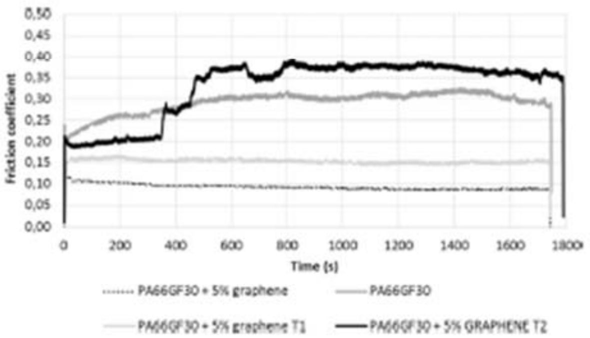

Fig. 7. Evolution of friction coefficient as a function of the wear test time for PA66 textured hybrid composites.

Table 3
Summary of wear test results for the textured hybrid composites.

Material	μ	w_s 10^{-3} (mm^3/Nm)
PA66GF30	0.309	1.549
PA66GF30 + 5% graphene	0.098	0.653
PA66GF30 + 5% graphene T1	0.153	1.167
PA66GF30 + 5% graphene T2	0.38	1.211

4.2. Influence of nanoadditives

Under dry sliding, the temperature of the polymer surface increases owing to the accumulation of frictional heat, and a softening point is reached because of the relaxation of polymer molecular chains. Therefore, the Young's modulus decreases, leading to higher plastic deformation and thus an increased real contact area, making the predominant adhesive mechanism friction and increasing the COF until the total formation of the transfer film [68].

Samples based on PA + 30% GF are studied. Although GF has the advantage of a high thermal conductivity, providing good heat dissipation, it has a negative effect on the friction behaviour because it prevents the formation of a good transfer film, forms abrasive tracks on the counterpart surfaces, and increases the contact temperature. The good results obtained with samples containing graphene are expected because this additive significantly improves the dissipation of accumulated frictional heat owing to its high thermal conductivity of 3000 W/mK (compared with 0.5 W/mK for PA66GF30), thereby reducing the influence of the adhesive friction mechanism. Although a better heat dissipation in the tribocontact seems to have a key for the

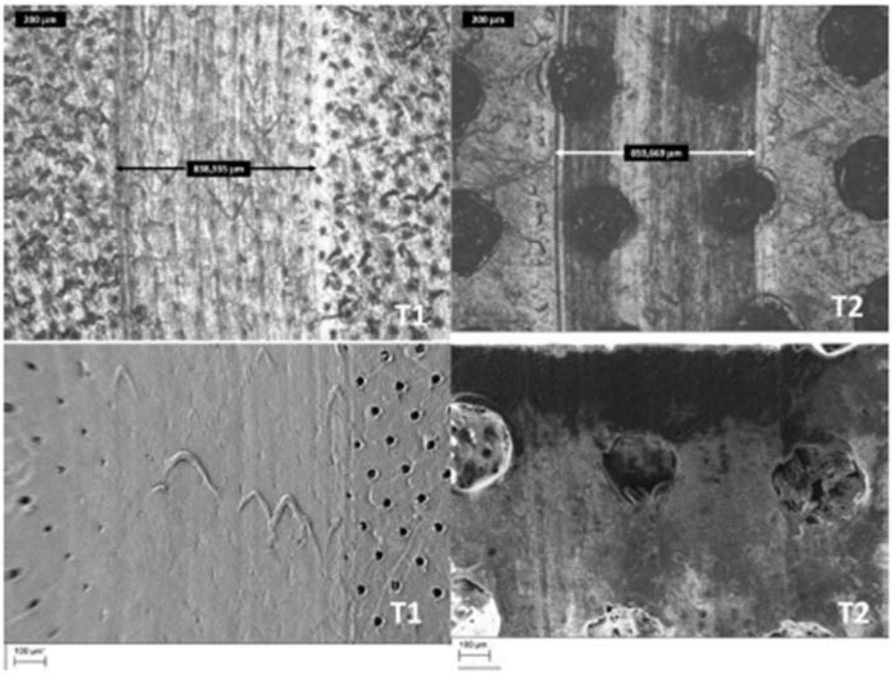

Fig. 8. Worn surfaces after wear tests for textured PA66GF30G5 T1 samples (left) and for PA66GF30G5 T2 samples (right).

decreasing of coefficient of friction, morphology of the graphene seems to play an important role in the tribological behaviour of the composite doped with it as well. Layers of graphene act as a lubricant allowing soft sliding instead of wear [72,73]. All of this contributes to the reduced COF for PA66GF30 doped with graphene. Besides, Young's modulus (E) is improved by the addition of graphene and ZrO_2, as described in Table 4, which leads to a higher wear resistance and a lower wear rate, as shown in Table 2.

On the other hand, during wear test, the increasing of temperature in the contact area leads to a reduction of Young modulus resulting into an increasing of contact area, and so and higher coefficient of friction. In case of samples doped with graphene, improvement of mechanical properties due to graphene addition is dominant compared to the effect of reducing Young modulus due to temperature and contact area increasing, therefore, a lower coefficient of friction is achieved. In case of samples doped with ZrO2, improvement of mechanical properties due to additive presence is not dominant compared to the effect of reducing Young modulus due to temperature and contact area increasing, so a higher coefficient of friction is induced.

A second consequence of the increasing of temperature in the contact area is the reduction of the shear strength (τ), which theoretically leads to lower COFs. Thus, depending on the polymer composition, one of these two effects, reducing Young modulus or reducing shear strength, can be predominant leading to opposite effects. For the samples doped with ZrO_2, reduction of Young modulus seems to be dominant, leading to higher values of the COF.

4.3. *Worn surfaces*

Composites containing GF exhibit a worn surface with shear lips owing to the softening and stress concentrations near the sample borders and at the interfaces between the PA66 matrix and the GF, where crack growth initiation at the interfaces between particles of GFs and the polymeric matrix is observable, as described in Ref. [34]. The cracks

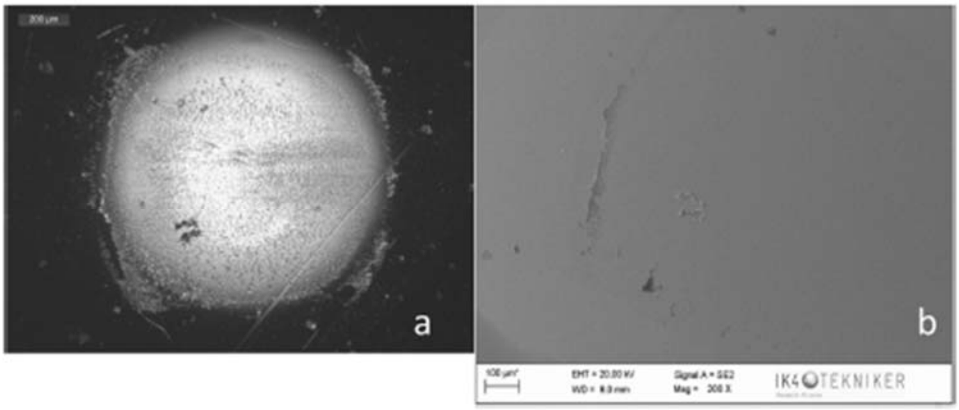

Fig. 9. Optical image (a) and SEM image (b) of the steel ball with transferred polymer.

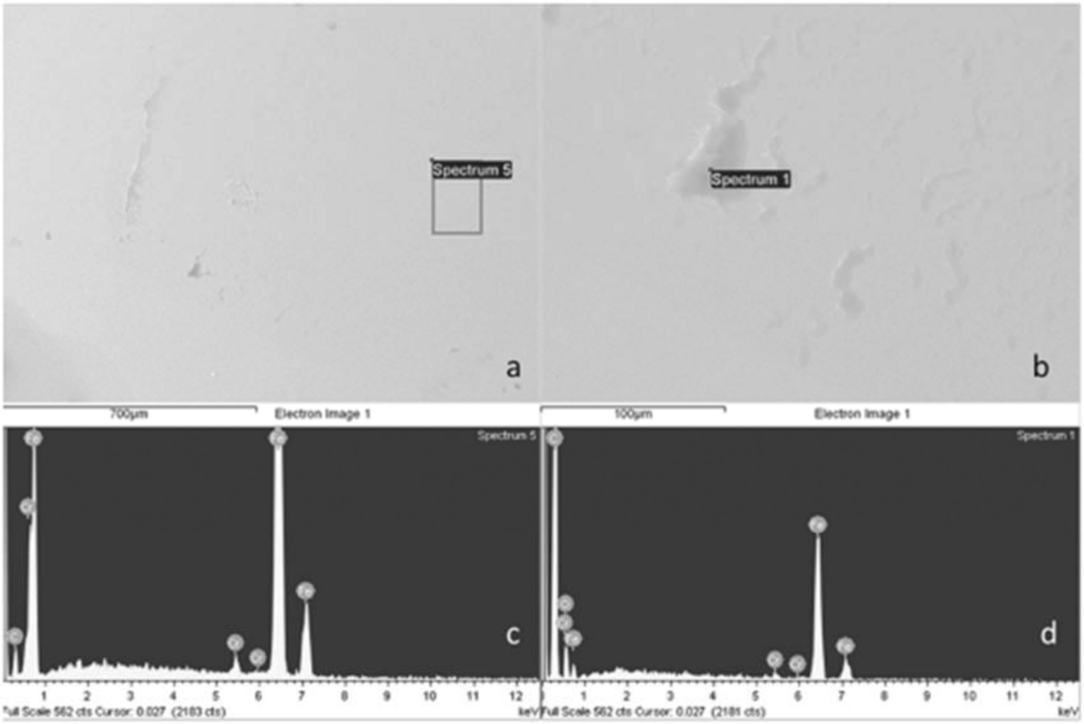

Fig. 10. EDX spectrums for an area of the ball without polymer transferred (c) and with polymer transferred (d).

Table 4
Summary of mechanical properties for the samples tested.

	E (MPa)		Tensile strength (MPa)	
	Average	Standard deviation	Average	Standard deviation
PA66GF30	9800	975	195	9.75
PA66GF30G1	10687	1050	189	9.072
PA66GF30G5	11711	1208	169	8.52
PA66GF30ZrO$_2$1	9996	990	189	9.45
PA66GF30ZrO$_2$10	10030	998	182	9.24

do not grow straight; rather, they join together—thus, wear debris is formed and removed. The PA66GF30, PA66GF30G1, and PA66GF30ZrO$_2$1 materials exhibit a wrinkled and wavy surface morphology owing to the heating effect of friction, which softens the polymer surface.

In GF composites without nanoadditives, all the effects of the counterpart asperities are usually loaded on the fibre, and there is no interface damage, because of the major interfacial bonding of the PA matrix and the GF. The transfer film is disrupted in areas under which there is an accumulation of GF. PA is removed in large flakes, and GF is detached as separate needles [29].

With the addition of nanoparticles, the real contact area is reduced by the three bodies of contact instead of surface contact; thus, a lower adhesive force is achieved. Consequently, the frictional coefficient is effectively reduced, limiting the increase of the contact temperature. This reduction enhances the load-carrying capacity of the composite. On the other hand, according to [27,74], in three-component composites, the rolling effect appears, replacing the sliding and preventing the fibre from being detached; rather, it is only grooved, which reduces the shear stress, frictional coefficient, contact temperature, and matrix damage. In spite of this, the COF can be increased for high percentages of nanoadditives owing to their abrasive effect on the composite, as observed for PA66GF30ZrO$_2$10. When nanocomposite particles slide against a smoother counterpart, the nanoparticles cannot provide the aforementioned rolling effect, because the particle dimensions should agree with the gap between the mating surfaces, which is mostly determined by the roughness of the steel counterpart. In this case, the COF can even be increased, as observed for the PA66GF30ZrO$_2$1 and PA66GF30ZrO$_2$10 samples.

4.4. *Micromachined samples*

Dimple micromachining appears to be a more efficient way of improving the tribological properties under wet lubrication. The dimples play the role of lubricant reservoirs, which act as hydrodynamic cells, ensuring efficient heat dissipation. In the case of dry lubrication, this advantage cannot be exploited to improve the tribological behaviour. On the other hand, the presence of intercalated dimples along the wear track can hinder the development of a homogeneous and continuous transfer film that allows easy detachment of the polymeric material.

5. Conclusions

The improvement of the tribological behaviour of hybrid polymer composites based on PA + 30% GF via two strategies was analysed.

The first strategy employs additive composites containing 1% and 5% graphene and 1% and 10% ZrO_2. Wear tests reveal that the composites doped with graphene exhibit lower values of the COF and wear rate, especially those doped with 5% graphene, which achieve reductions of 30% and 35% in the COF and wear rate, respectively compared to non-doped samples. This improvement is attributed to the high thermal conductivity of graphene, which contributes to better dissipation of frictional heat, and to its high Young's modulus and tensile strength, which reduce the wear rate. The addition of ZrO_2 does not improve the wear performance of the composite. In this case, the increase of the real contact area appears to be dominant compared with the reduction of the shear strength due to the increase of the frictional temperature, leading to worse tribological behaviour.

The second strategy involves microtexturing the surface of the best hybrid nanocomposite, i.e., PA66G30 + 5% graphene. Two different configurations of dimples were laser-micromachined, but no significant improvement was observed in the tribological results.

Acknowledgements

This work was supported by the Regional Government of Aragon, Spain (INNOVA-A1-008-15) and the University of Zaragoza (BOA10-OTRI 2016/0172). The authors are members of the I+AITIIP (DGA-T08_17R) research group of the FEDER 2014-2020 "Construyendo Europa desde Aragón" program, which is recognised by the Regional Government of Aragon. The authors acknowledge the AITIIP Foundation in Spain for providing facilities for sample preparation and the TEKNIKER Foundation in Spain for the loan of equipment for tribological measurements.

References

[1] Jost HP. Tribology:origin and future. Wear 1990;136(1):1–17.
[2] Holmberg K, Matthews A, Ronkainen H. Coatings tribology—contact mechanisms and surface design. Tribol Int 1998;31:107–13.
[3] Davidov SV, Gorienko AO. Friction surface modification by nanodiamonds of detonational synthesis. IOP Conf Ser Mater Sci Eng 2016;24. UNSP 012154.
[4] Morita T, Andatsu K, Hirota S, Kumakiri T, Ikenaga M, Kagaya C. Effect of hybrid surface treatment composed of plasma nitriding and DLC coating on friction coefficient and fatigue strength of stainless steel. Mater Trans 2013;54:732–5.
[5] Morita T, Inoue K, Ding X, Usui Y, Ikenaga M. Effect of hybrid surface treatment composed of nitriding and DLC coating on friction-wear properties and fatigue strength of alloy Steel. Mater Sci Eng, A 2016;661:105–9.
[6] Ceschini L, Chiavari C, Marconi A, Martini C. Influence of the countermaterial on the dry sliding friction and wear behaviour of low temperature carburized AISI316L Steel. Tribol Int 2013;67:36–7.
[7] Farzalipour F, Shakib N, Shokuhfar A, Nushari N. Effect of nitro-carburizing treatment on wear mechanism and friction of steel/WC-Co sliding couple. J Tribol 2012;134. 014501-1.
[8] Lugt P. A review on grease lubrication in rolling bearings. Tribol Trans 2009;52. 470-10.
[9] Mota V, Ferreira LA. Influence of grease composition on rolling contact wear: experimental study. Tribol Int 2009;42. 569-5.
[10] Cousseau T, GraÇa B, Campos A, Seabra J. Friction torque in grease lubricated thrust ball bearings. Tribol Int 2011;44:523–8.
[11] Venkatesh M, Taktak S, Meletis EI. Wear and friction properties of nanocomposite a-c:h/ag thin films deposited by a hybrid pvd-pecvd process. J Balkan Tribol Assoc 2014;20:409–14.
[12] Golabczak M, Jacquet P, Nouveau C, Fliti R. Low friction MoS2TiW coatings manufactured on X38CrMoV5-1 steel using PVD method. Mater Werkst 2013;44:395–7.
[13] Pei Y, Jiaxin D, Ze W, Shipeng L, Youqutang X, Jun Z. Friction and wear behavior of the PVD (Zr,Ti)N coated cemented carbide against 40Cr hardened Steel. Int J Refract Met Hard Mater 2012;35:213–7.
[14] Lin Z, Sun F, Shen B. Friction properties of polished cvd diamond films sliding against different metals. Surf Rev Lett 2016;23. 1550096.
[15] Miki H, Tsutsui A, Takeno T, Takagi T. Friction properties of partially polished CVD diamond films at different sliding speeds. Diam Relat Mater 2012;24. 167-3.
[16] Gee MG, Nunn JW, Muntz-Piniella A, Orkney LP. Micro-tribology experiments on engineering coatings. Wear 2011;271:2673–7.
[17] Holmberg K, Ronkainen H, Matthews A. Tribology of thin coatings. Ceram Int 2000;26(7):787–95.
[18] Singh PK, Siddhartha, Singh AK. An investigation on the thermal and wear behavior of polymer based spur gears. Tribol Int 2018;118:264–72.
[19] Ai S, Wang W, Wang Y, Zhao Z. Temperature rise of double-row tapered roller bearings analyzed with thermal network method. Tribol Int 2015;87:11–22.
[20] Bassani R. Levitation of passive magnetic bearings and systems. Tribol Int 2006;39:263–7.
[21] Zhao X, Liang L, Liu Z. Tapered roller bearings cage to improvement design. Indonesian J Electr Eng 2014;12(3). 1855-4.
[22] Lauman S, Jisa R, Deinhofer G, Franek F. Tribological properties of brass materials and their application for cages in rolling bearings. Tribol 2014;8(1):35–6.
[23] Seiler K, Stadler M, Tremmel S, Hahn B, Wartzack S, Graf-Goller O. Modeling of cage guidance in a rolling bearing multi-body dynamic simulation program for a power efficient bearing design. STLE annul meeting and exhibition 2014.
[24] Sreenilayam-Raveendran RK, Azarian MH, Morillo C, Petch MG, Kida K, Santos EC, et al. Comparative evaluation of metal and polymer ball bearings. Wear 2013;302. 1499-05.
[25] Burris DL, Sawyer WG. A low friction and ultra low wear rate PEEK/PTFE composite. Wear 2006;261:410–8.
[26] Unal H, Sen U, Mimaroglu A. Dry sliding wear characteristics of some industrial polymers against steel counterface. Tribol Int 2004;37. 727-5.
[27] Chang L, Zhang Z, Zhang H, Schlarb AK. On the sliding wear of nanoparticle filled polyamide 66 composites. Compos Sci Technol 2006;66. 3188-10.
[28] Kukureka SN, Hooke CJ, Rao M, Liao P, Chen YK. The effect of fiber reinforcement on the friction and wear of polyamide 66 under dry rolling–sliding contact. Tribol Int 1999;32:107–9.
[29] Xing Y, Zhang G, Ma K, et al. Study on the friction and wear behaviors of modified PA66 composites. Pol-Plastic Tech Eng 2009;48(6):633–8.
[30] Abdelbart A. Fatigue wear of unfilled polymers. In: Abdelbart A. Wear of polymers and composites, Cambridge: Woodhead Publishing; 2014, p.67-92.
[31] Demirci MT, Durzukoglu H. Wear behaviors of Polytetrafluoroethylene and glass fiber reinforced Polyamide 66 journal bearings. Mater Des 2014;57:560–7.
[32] Shibata K, Fukuda M, Yamaguchi T. Relationship between sliding-induced wear and severity of sliding contact for polyamide 66 filled with hard filler. Proc Inst Mech Eng, Part J: J Eng Tribol 2017;231(6):783–90.
[33] Chen YK, Modi OP, Mhay AS, Chrysanthou A, O'Sullivan JM. The effect of different metallic counterface materials and different surface treatments on the wear and friction of polyamide 66 and its composite in rolling–sliding contact. Wear 2003;255:714–7.
[34] Palabiyik M, Bahadur S. Tribological studies of polyamide 6 and high-density polyethylene blends filled with PTFE and copper oxide and reinforced with short glass fibers. Wear 2002;253. 369-7.
[35] Harrass M, Friedrich K, Almajid AA. Tribological behavior of selected engineering polymers under rolling contact. Tribol Int 2010;43. 635-11.
[36] Pinney Charles D, Gnanamoorthy R, Ravindran P. Rolling contact fatigue behavior of polyamide clay reinforced nanocomposite—effect of load and speed. Wear 2010;269:565–6.
[37] Blanco M, Sarasua JA, López M, Gonzalo O, Marcaide A, Muniesa M, et al. Ultrasound assisted extrusion of polyamide 6 nanocomposites based on carbon nanotubes. Macromol Symp 2012;321–322:80–3.
[38] Lee SM, Shin MW, Jang H. Effect of carbon-nanotube length on friction and wear of polyamide 6,6 nanocomposites. Wear 2014;320:103–10.
[39] Novoselov K, Geim AK, Morozov SV, Jiang D, Zhang Y, Dubonos SV, et al. Electric field effect in atomically thin carbon films. Science 2004;306. 666-3.
[40] Dou X, Koltonow AR, He X, Jang HD, Wang Q, Chung YW, et al. Self-dispersed crumpled graphene balls in oil for friction and wear reduction. Proc Natl Acad Sci USA 2016;113. 1528-5.
[41] Sun CF, Zhang Y, Wang YJ, Chen YF. Investigation on friction performance of graphene. 2013 Int conf manipulation manuf meas nanoscale (3m-NANO) 2013; 224-227.
[42] Kalin M, Zalaznik M, Novak S. Wear and friction behavior of poly-ether-ether-ketone (PEEK) filled with graphene, WS2 and CNT nanoparticles. Wear 2015;332–333:855–7.
[43] Agrawal N, Parihar AS, Singh JP, Goswami TH, Tripathi DN. Efficient nano-composite formation of acrylo nitrile rubber by incorporation of graphite and graphene layers: reduction in friction and wear rate. Procedia Mater Sci 2015;10. 139-9.
[44] Khandanur SS, Rafiee MA, Yavari F, Schrameyer M, Yu Z, Blanchet TA, et al. Suppression of wear in graphene polymer composites. Carbon 2012;50. 3178-5.
[45] Pan BL, Zhao J, Zhang YQ, Zhang YZ. Wear performance and mechanisms of polyphenylene sulfide/polytetrafluoroethylene wax composite coatings reinforced by graphene. J Macromol Sci Part B-Phys 2012;6:1218–9.
[46] Quian L, Xu F, Voisey KT, Nekouie V, Zhou Z, Silberschmidt VV, et al. Incorporation and evolution of ZrO2 nano-particles in Pt-modified aluminide coating for high temperature applications. Surf Coating Technol 2017;311:238–9.
[47] Karimi M, Baharvandi HR, Abdizadeh H, Beyrami BP, Bonab M. Microstructure and mechanical properties of Al-nano ZrO2 composites produced by casting route. Int Conf Smart Mater Nanotech Eng 2007;6423. UNSP 64235Y.
[48] Zhang FF, Zheng SH, Yin YS, Liu B. Anti-wear and friction-reducing behavior of nano-ZrO2 additive. Second Int Conf Multi Funct Mater Struct 2009;79-82:605.
[49] Ma J, Xu CH, Yi MD, Xiao GC, Wang XH. Friction and wear property of Ti(C,N)/ZrO2/WC nano-composite cermet die material. Adv Mater Res 2013;834-836:23–5.
[50] Mordina B, Tiwari RK. A comparative study of mechanical and tribological properties of poly(ether ether ketone) composites filled by micro- and nano-Ni and ZrO2 fillers. J Compos Mater 2013;47. 2835-10.
[51] Adjemount F, Andrieux A, Bouyer J, Brunetière N, Marcos G, Czerwiek T. Influence of the real dimple shape on the performance of a textured mechanical seal. Tribol Int 2017;115:409–16.
[52] Moshkovith A, Perfiliev V, Gindin D, Parkansky N, Boxman N, Rapoport L. Surface texturing using pulsed air arc treatment. Wear 2007;263:1467–9.
[53] Lu L, Zhang Z, Guan Y, Zheng H. Comparison of the effect of typical patterns on friction and wear properties of chromium alloy prepared by laser surface texturing. Optic Laser Technol 2018;106:272–9.
[54] Erdemir A. Review of engineered tribological interfaces for improved boundary lubrication. Tribol Int 2005;38:249–56.
[55] Etsion I, Halperin G, Becker E. The effect of various surface treatments on piston pin scuffing resistance. Wear 2006;261:785–91.
[56] Etsion I. State of the art in laser surface texturing. J Tribol 2005;127:248–53.
[57] Gualtieri E, Borghi A, Calabri L, Pugno N, Valeri S. Increasing nanohardness and reducing friction of nitride steel by laser surface texturing. Tribol Int 2009;42. 699-6.
[58] Cupillard S, Glavatskih S, Cervantes MJ. Computational fluid dynamics analysis of a journal bearing with surface texturing. J Eng Tribol 2008;222(2). 97-10.
[59] Etsion I, Kligerman Y, Ronen A. Friction-reducing surface-texturing in reciprocating

automotive components. Tribol Trans 2001;44(3). 359-7.
[60] Segu DZ, Hwang P. Friction control by multi-shape textured surface under pin-on-disc test. Tribol Int 2015;91. 111-7.
[61] Kovalchenko A, Ajayi O, Erdemir A, Fenske G, Etsion I. The effect of laser surface texturing on transitions in lubrication regimes during unidirectional sliding contact. Tribol Int 2005;38. 219-6.
[62] Hoppermann A, Kordt M. Tribologische Optimierung durch laserstrukturierte Kontaktflächen. O + P Ölhydraulik und Pneumatik 2002;46:560–4.
[63] PROSPECTOR. TORZEN® G3000 NC01 DATA SHEET, https://plastics.ulprospector.com/es/datasheet/e156315/torzen-G3000-nc01.
[64] MICROZIR® ULTRAFINE DATA SHEET, http://www.chirchesmaterials.com/producto/microzir-ultrafine-2/.
[65] Blanco M, Sarasua JA, López M, Gonzalo O, Marcaide A, Muniesa M, et al. Ultrasound assisted extrusion of polyamide 6 nanocomposites based on carbon nanotubes. Macromol Symp 2012;321–322:80–3.
[66] Muniesa M, Fernández A, Clavería I, Javierre C, Sarasua JA, Blanco M. A new extrusion head with integrated ultrasonic device and online process parameters measurements system—design and testing. Polimery 2015;60:209–16.
[67] Samyn P, De Baets P, Shoukens g, Van Peteghem AP. Large-scale tests on friction and wear of engineering polymers for material selection in highly loaded sliding systems. Mater Des 2006;27. 535-20.
[68] Meng H, Sui GX, Sie GY, Yang R. Friction and wear behavior of carbon nanotubes reinforced polyamide 6 composites under dry sliding and water lubricated condition. Compos Sci Technol 2009;69. 606-5.
[69] Zsidai L, De Baets P, Samyn P, Kalacska G, Van Peteghem AP, Van Parys F. The tribological behavior of engineering plastics during sliding friction investigated with small-scale specimens. Wear 2002;253:673–715.
[70] Bahadur S. The development of transfer layers and their role in polymer tribology. Wear 2000;245:92–101.
[71] Quaglini V, Dubini P, Ferroni D, Poggi C. Influence of counterface roughness on friction properties of engineering plastics for bearing applications. Mater Des 2009;30:1650–8.
[72] Berman D, Erdemir A, Sumant AV. Graphene: a new emerging lubricant. Mater Today 2014;17(1):31–42.
[73] Peng Y, Wang Z, Zou K. Friction and wear properties of different types of graphene nanosheets as effective solid lubricants. Langmuir 2015;31:7782–91. https://doi.org/10.1021/acs.langmuir.5b00422.
[74] Chang L, Zhang Z. Tribological properties of epoxy nanocomposites Part II. A combinative effect of short carbon fibre with nano-TiO2. Wear 2006;260:869–78.

6.2. Coatings: Enhancement of Tribological Behavior of Rolling Bearings by Applying a Multilayer ZrN/ZrCN Coating

El artículo "*Enhancement of Tribological Behavior of Rolling Bearings by Applying a Multilayer ZrN/ZrCN Coating*" se centra en el comportamiento tribológico del recubrimiento de ZrN/ZrCN aplicado sobre sustratos de acero para rodamientos 100Cr6 (según ISO 683-17 [3]). Los recubrimientos se aplicaron en procesos a temperatura ambiente mediante Deposición Física de Vapor (Physical Vapour Deposition, PVD) y, en concreto, con el método de Evaporación por Arco Catódico (Cathodic Arc Evaporation, CAE). Así mismo, para lograr un compromiso satisfactorio entre la adhesión del recubrimiento al sustrato y los requisitos de rugosidad de la superficie de los aros del rodamiento, se diseñó un post-proceso de pulido. Con todo ello, se definieron diferentes tiempos de aplicación de PVD y condiciones del post-proceso de pulido. Las muestras se caracterizaron, antes y después de ser recubiertas y pulidas, y se ensayaron bajo protocolos de prueba de par de fricción con distintas condiciones de carga y velocidad. Estas pruebas mostraron que la aplicación del recubrimiento no suponía una mejora significativa en el comportamiento a la fricción del rodamiento.

Contribución del doctorando: Revisión del estado del arte. Análisis e interpretación de resultados. Redacción y revisión del artículo.

coatings

MDPI

Article

Enhancement of Tribological Behavior of Rolling Bearings by Applying a Multilayer ZrN/ZrCN Coating

Isabel Clavería [1,*], Aleida Lostalé [1,2], Ángel Fernández [1], Pere Castell [3], Daniel Elduque [1], Gemma Mendoza [4] and Cristina Zubizarreta [4]

1 Department of Mechanical Engineering, University of Zaragoza EINA, Maria de Luna 3, 50018 Zaragoza, Spain
2 FERSA BEARINGS S.A., Bari 18, 50197 Zaragoza, Spain
3 AITIIP Foundation, Calle Romero 12, 50720 Zaragoza, Spain
4 Fundación Tekniker, Calle Iñaki Goenaga 5, 20600 Eibar, Spain
* Correspondence: isabel.claveria@unizar.es; Tel.: +34-876-555-234

Received: 14 May 2019; Accepted: 8 July 2019; Published: 10 July 2019

check for updates

Abstract: This paper focuses on the tribological behaviour of ZrN/ZrCN coating on bearing steel substrates DIN 17230, 100Cr6/1.3505. Coatings are applied at room temperature processes by means of Cathodic Arc Evaporation (CAE), a kind of Physical Vapor Deposition (PVD) technique. In order to achieve a satisfactory compromise between coating-substrate adhesion and the surface roughness requirement of the bearing rings, a polish post-processing is proposed. Different polish post-processing times and conditions are applied. The coated and polished bearing rings are tested under real friction torque test protocols. These tests show that the application of the coating does not entail a significant improvement in friction performance of the bearing. However, fatigue tests in real test bench are pending to evaluate the possible improvement in bearing life time.

Keywords: PVD; polishing; Zr(C,N); coating; bearing; roughness; adhesion; friction torque

1. Introduction

Roller bearings are components with numerous uses for rotating applications, particularly in the automotive industry. According to recent studies [1], for every liter of fuel used in an average vehicle, 5% is consumed in mechanical losses, and 1% of the total is lost in the simple operation of the bearings. Energy efficiency, the reduction of fuel consumption, and polluting emissions are aspects increasingly demanded. This trend is observed with the emergence of more efficient products, which may even differ from the standard versions in terms of dimensions, assembly, or new materials [2,3].

Despite the aforementioned bearing losses, these mechanical components exhibit very low friction in lubricated conditions (friction coefficient < 0.05), also provided by the rectangular shaped "line contact" among the roller, and the outer and inner rings [4–7]. The contact pressures may vary from 0.5 up to 3 GPa, depending on the application [4,5]. The rolling operation follows the elastohydrodynamic (EHD) theory, and it is characterized by the thickness of the lubricant film formed during the rolling [8–11]. Important factors defining the conditions of rolling operation are the surface roughness of the counterparts, [12] and the stress distribution on the subsurface (from 50 to 150 µm underneath the surface) resulting from the contact between the counterparts [13–16]. Therefore, nowadays, it is commonly expected that tribology can lead to the following technical considerations: improvements of the fuel consumption efficiency through friction reduction; lightweight construction; downsizing of some components through a resistance increase leading to higher Hertzian contact pressures; waste reduction due to a lower wear and less frequent oil changes; as well as the use of more environment-friendly lubricants (Bio-no-tox).

Coatings **2019**, *9*, 434; doi:10.3390/coatings9070434 www.mdpi.com/journal/coatings

There are different methods for reducing friction on bearings. They go from updating internal bearing geometry or changing bearing component materials (e.g., plastic cages made of nano-additivated plastics to achieve a self-lubricant behavior) [17], to the development of new lubricants or coatings for the rolling bearing surface.

Thin coatings are nowadays an interesting and low-cost approach for solving technical problems since their properties can be highly varied and combined without implying a complete change of the original conception of mechanical components. The deposition of a protective low friction coating on the surface of the rollers extends the lifetime of the component [4,18–20]. In many cases, where a coating is deposited on a steel component, the lifetime of the component is increased, and its tribological response improved [21–25]. The overall performance of the coated surfaces is also determined by the coating/substrate interface tolerance to crack propagation [18,21]. It has been demonstrated that coatings produced by physical vapor deposition (PVD) may withstand higher shear stress levels during the rolling phase than coatings produced by chemical vapor deposition (CVD) or thermal spray [20–27]. TiN, TiAlN, TiC, CrN, Cu, and diamond-like carbon (DLC) coatings, produced by PVD [28–31], have already been studied in rolling-contact fatigue (RCF) tests improving the lifetime of the components [21–23,32–34]. DLC and carbon nitride (CN) coatings are considered good candidates for its use in rolling components as they provide low friction and high wearing resistance [35–37].

In this study, Zr(C, N) thin coatings are considered because they have been successfully tested at a lubricant temperature of 120 °C and, thus reach average Hertzian pressures of 1.94 GPa [38]. From these results, this composition arises as a promising coating to be used in bearings for the automotive industries (differential applications) because they withstand similar working temperatures and contact stresses. Hardly any previous studies have been carried out with the combination of ZrCN coating on bearings. In Kuhn et al. [19], ZrC and ZrN are used for rolling bearings, but the results measured are more focused on the properties of the bearing material than on the functional results such as friction torque, as revealed in this paper.

2. Materials and Methods

2.1. Materials

2.1.1. Substrate

Bearing steel 100Cr6 (according to ISO 683-17 [39]) has been used as a PVD substrate. In this study, a through hardened bearing steel with the following chemical composition was used: carbon (0.93–1.05%), manganese (0.25–1.20%), chromium (0.90–1.60%), molybdenum (0–0.10%), nickel (0–0.25%), and Fe (95.75–97.92%) to balance. Other residuals are: oxygen (max. 10–15 ppm), aluminum (max. 0.050%), titanium (max. 30–50 ppm), and calcium (max. 10 ppm) [40].

Due to its endurance strength, the distribution must compensate an equivalent stress level and, therefore, steel has to be subjected to a martensitic transformation through a hardening treatment, adjusting the hardness of the surface to 59–63 HRC (Rockwell Hardness C scale) at a temperature of 180–200 °C. These HRC values are minimum for a dynamic capacity of 100%.

2.1.2. Bearing Samples

Tapered roller bearing (TRB) 594A/592A belonging to the TRB inches family from FERSA BEARINGS SA (Zaragoza, Spain) and used for differential applications in heavy-duty vehicles was chosen as the sample to be coated. Shape and dimensions are shown in Table 1. Coated surfaces are the contact surfaces between Components 2 and 3 in Figure 1.

Coatings **2019**, *9*, 434

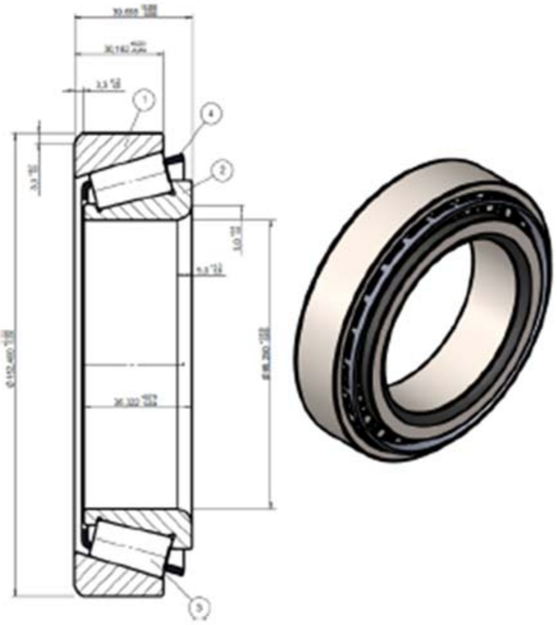

Figure 1. Tapered roller bearing 594A/592A.

2.1.3. Coating Layer

Materials used for the coating layer deposition were Zr target from Robeko (Šibenik, Croatia), purity R60702 ≥ 99.5 wt%; and Ti target from Robeko, purity grade 2, 99.5% in weight. Hydrogen in Argon (20%); Alphagaz 2 Argon (purity ≥ 99.9999 mol%); Alphagaz 2 Nitrogen (purity ≥ 99.9999 mol%), and Alphagaz 1 Acetylene (purity ≥ 99.6 mol%) from Air Liquide (Paris, France) were used as reactive gases.

2.2. Equipment and Experimental

2.2.1. PVD Coating Process

The process was carried out with an industrial equipment MIDAS 775 designed and manufactured by Tekniker (Eibar, Spain) [41]; including a vacuum chamber, 12 circular arc evaporators in four columns; a pulsed DC bias power supply system, consisting of two MDX II DC and one SPARC-VS pulsing unit from Advanced Energy (Fort Collins, CO, USA). Table 1 summarizes the technical data of the equipment.

Table 1. Technical data of MIDAS 775 equipment.

Vacuum Chamber	Cicular Arc Evaporators Diameter	Pulsed DC Bias Power Supply System			Maximum Temperature	Reactive Gases
		Power	Bias	Pulsing Unit Intensity		
Ø750 mm × 750 mm	Ø100 mm	45 kW	Up to 1000 V	60–200 A	500 °C	N_2, C_2H_2, O_2

ZrCN coatings were deposited by a physical vapor deposition (PVD) technique using the cathodic arc evaporation (CAE) method to apply titanium-zirconium-based coatings on the rolling bearing surface. CAE method consists of applying a low voltage and a high current between an anode and an arc cathode in the presence of argon gas in a vacuum chamber, melting or evaporating tiny quantities of material. Approximately 90% of the evaporated cathode particles form positively charged metal ions. A negative bias voltage was then applied between the vacuum chamber and the substrate. This accelerates the metal ions in the direction of the sample surface. A reaction between metal ions and a reactive gas (nitrogen and hydrocarbon) fed in externally was produced, leading to the deposition of the ions on the sample as a fine carbonitride layer.

Prior to PVD deposition, the sample substrates were cleaned in a degreasing-solvent sequence. Once loaded in the vacuum chamber, it was evacuated up to a pressure of 10^{-4} mbar. Then, a Glow Discharge cleanliness stage was implemented. It consists of applying a current of 4 A under vacuum conditions (0.4 mbar) on the samples in an atmosphere of argon mixed with hydrogen (140 sccm) during 30 min. Subsequently, a high negative bias step to promote adhesion was introduced. A voltage of −600 V was applied to the samples in an argon atmosphere (100 sccm) with two Ti arcs at 120 A.

After the cleanliness stage, four different PVD coating designs were developed by using 4 metallic evaporators (2Ti, 2Zr), and introducing Nitrogen gas (N_2, 300 sccm) and acetylene (C_2H_2, 10–20 sccm) in a reactive process (pressure 10^{-2} mbar). 400 V of Bias voltage was initially applied, decreasing gradually to 30 V in 4 min, voltage which was maintained during the rest of the process. The arc intensity of Titanium and Zirconium targets during the growing steps was set at 120 and 140 A, respectively. As it is described in Table 2, each coating design consists of a first adhesion layer followed by the functional coating multilayer. A first robust thick Ti metallic layer followed by a Ti–Zr transition was applied as an adhesion layer in D1. A thinner adhesion sequence (Ti + Ti–Zr) was performed for D2 and, in D3, after a very brief Ti metallic step, nitrogen was introduced followed by the last step including Zr.

Regarding the functional coating, a multilayer was deposited consisting of three ZrN/ZrCN bilayer sequences (10/5 min, respectively) for D1, D2, and D3. In D4, a fourth identical bilayer was added. The different adhesion sequences were designed to guarantee a proper substrate-coating adhesion. The functional multilayer was designed to provide the tribological properties required to reduce friction during the bearing performance.

Table 2. Composition of PVD coating designs.

Coating Design	Adhesion Layer Sequence	Adhesion Layer Deposition Time (min)				Functional Layer Configuration	Resistance Temperature (°C)
		Ti	Ti–Zr	TiN	Ti–Zr–N		
D1	Ti + Ti–Zr	60	5	0	0	ZrN/ZrCN multilayer	250
D2	Ti + Ti–Zr	5	1	0	0	ZrN/ZrCN multilayer	250
D3	Ti + TiN + Ti–Zr–N	1	0	4	1	ZrN/ZrCN multilayer	250
D4	Ti + Ti–Zr	60	5	0	0	ZrN/ZrCN multilayer + ZrN/ZrCN bilayer	250

2.2.2. Polish Post-Processing

A polish post-processing stage was carried out on those coated bearings samples with R_a values exceeding the bearing specifications (R_a < 0.15 µm). Two different methods were followed. Method A used the walnut shell (0.2–0.4 mm) as an abrasive material in an OTEC DF 35 machine (OTEC Präzisionsfinish GmbH, Straubenhardt-Conweiler, Germany), which is a spindle abrasive finishing machine, with 3 workplace holders, 0.75 kW, and a 230 volt motor with octagonal stainless-steel process container and controls. Method B used the walnut shell (0.8–1.7 mm) additivated with a silica base abrasive (80%) in a Pardus Drag Finish Unit from PD2i machine (Paris, France). In both types of equipment, samples were introduced in a vessel full of abrasive material in order to polish the surface of the piece. Method A was defined by applying 30 min steps (15 min each way) at 20 rpm; and Method B was characterized by applying 15 min (1.5 min each way) at 35 rpm. Three different configurations were employed according to Table 3.

Table 3. Polish post-processing configuration parameters.

Configuration	Method	Time (min)	Rotation Speed (rpm)
A1	A	180	20
A2	A	360	20
B	B	15	35

2.2.3. Geometric Analysis

Before testing coating quality parameters, a complete metrological analysis including shapes, profiles, and roundness of bearing raceway and flange is done. Profile characterization is carried out by using a Form Talysurf 120 (Taylor Hobson Ibérica, Barcelona, Spain). This analysis is crucial to know if coated bearing samples to be tested are comparable to the baseline design bearing according to the allowed limits and shapes agreed by FERSA BEARINGS SA (Zaragoza, Spain). Figure 2 shows the inner ring raceway profile (a), and the flange profile (b) where the geometric analysis is performed.

A second test testing the roundness of the raceway is performed according to ISO 1101:2017 [42] with a Talyrond 365 with software Ultra by Taylor Hobson V5.21.9.36, both from TAYLOR HOBSON (Taylor Hobson Ibérica, Barcelona, Spain). Roundness (RONt) is defined as the separation of two concentric circles that enclose the circular section of interest, that is, the circular raceway section in this study. An accurate roundness measurement is vital to ensure the correct function of the bearings avoiding noise and premature failures.

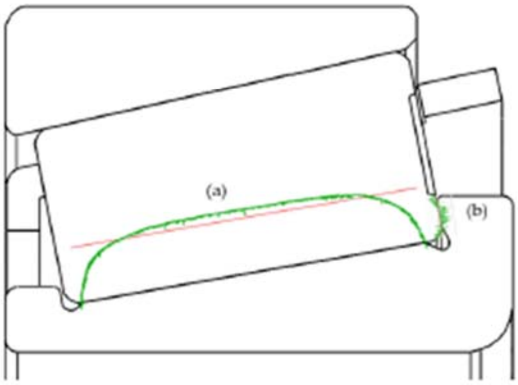

Figure 2. Measured profiles: (**a**) inner ring raceway profile; (**b**) flange profile.

2.2.4. Hardness

A durometer ERGOTEST DIGI 25 R (LFT, Antegnate, Italy) was used to perform an HRC test on the samples before and after applying a PVD coating according to S/UNE-EN ISO 6508-1 [43]. The indentation force was 1471 N with a preload of 98 N, and the diamond indentation angle was 120°. This test has the purpose of verifying that the hardness of the substrate surface was kept within the 59–63 HRC range after the PVD deposition process. In case the coating detaches during the bearing performance, the substrate must keep its initial properties and performance conditions of a standard bearing without coating. Initial properties of the substrate could be altered by the increase of temperature on the substrate due to PVD deposition process, which could lead to a hardness decreasing on the substrate.

2.2.5. Coating Properties

Coating properties measured to ensure its validity are roughness (R_a), thickness, adhesion, and bearing friction torque.

- Roughness

Perthometer M2 from Mahr (Barcelona, Spain), with a maximum range of 150 µm and a maximum cut-off length of 17.5 mm, was used for measuring roughness of coated samples as R_a (arithmetical mean deviation of the assessed profile), used in standards such as DIN EN ISO 4287:1998 [44], or JIS B 0601:1994 [45]. This equipment uses a mapping method for a 2D surface analysis in which a surface is horizontally crossed at a constant speed. The mapping profile is the superficial profile drawn with an analysis needle (ø 2 µm). Quantification is made by measuring the vertical deviations of a real surface compared to its ideal shape. The cut-off parameter is a profile filter that sets which wavelength refers to roughness and which one to waviness. Cut-off parameters set for the tests according to R_a ranges are shown in Table 4. To ensure a proper bearing performance, the arithmetical mean deviation of the assessed profile roughness (R_a) must be lower than 0.15 µm according to FERSA BEARINGS SA specifications.

Table 4. Cut-off selection, λ_c according to ISO 4288:1996 [46].

Profile R_a (µm)	Cut-off, λ_c (mm) × n	R_a Evaluation Length, l_n (mm)
$(0.006) < R_a \leq 0.02$	0.08 × 5	0.4
$(0.02) < R_a \leq 0.1$	0.25 × 5	1.25
$0.1 < R_a \leq 2$	0.8 × 5	4
$2 < R_a \leq 10$	2.5 × 5	12.5

Coating surface, as well as cross sections, were analyzed via scanning with an electron microscopy High Resolution FE-SEM Ultra Plus, Zeiss(Oberkochen, Germany).

- Thickness

Coating thickness was determined using a Calostest Test with a Calotest CSEM equipment (DEPHIS, Étupes, France). A ball was turned over the coating until it arrived at the substrate, producing a spherical crater. Microscope measuring of this dimple diameter allows us to know the coating thickness [47]. An adequate thickness measurement ranges between 1 and 10 µm, given that a smaller thickness dimple could be too small, leading to inaccurate measurements.

- Adhesion

A Rockwell C indentation was performed with a durometer WIZHARD HR-522 (Mitutoyo, Kanagawa, Japan) with a load of 1470 N, then trace edges were analyzed with an optical microscope to evaluate adhesion. A chart VDI, Verein Deutscher Ingenieure Normen 3198 indentation test (Figure 3) was used to set the adhesion grade [48]. The chart states that the bigger the crack and delamination number, the worse the adhesion. Values from HF1 to HF4 stand for acceptable adhesion values, and HF5 and HF6 values stand for non-acceptable adhesion values.

- Coating composition

The profiles of composition in coating depth were analyzed with the Glow Discharge Optical Emission Spectrometry (GD-OES) equipment from Horiba Jobin YvonSAS (Palaiseau, France). The equipment analyzes the emitted light by the atoms sputtered from the sample; each one producing a light emission at a characteristic wavelength. The measurement conditions used were 650 Pa and 35 W, with a copper anode of 4 mm of diameter [49]. For this characterization, coatings deposited on stainless steel (AISI 430) were employed.

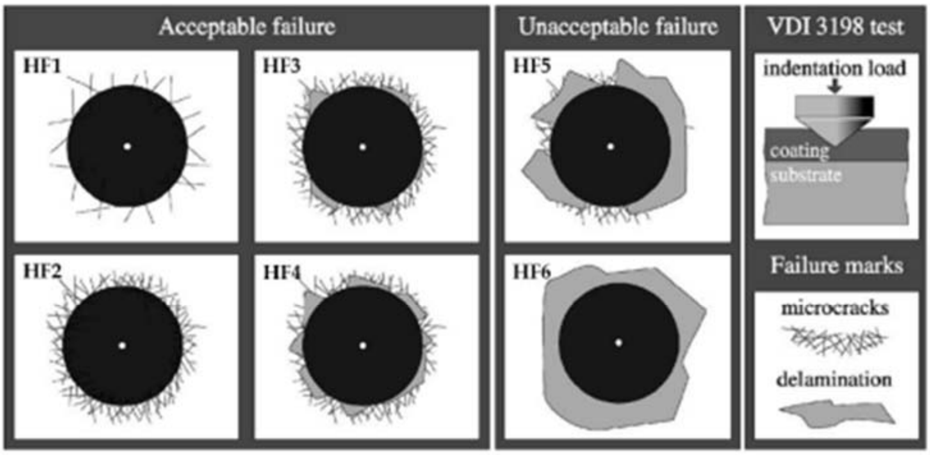

Figure 3. Chart VDI 3198 indentation test.

- Coating structure

The crystal structure of the films was examined by a grazing-incidence X-ray diffraction (XRD) using an angle of 2° and Cu Kα radiation in a Bruker D8 Advance diffractometer with Bragg-Brentano beam geometry. A step size of 0.02 (2θ) with 2.5 s per point was used.

X-ray diffraction is based on a constructive interference of monochromatic X-rays and a crystalline sample. The interaction of the incident rays with the sample produces a constructive interference (and a diffracted ray) when conditions satisfy Bragg's Law ($n\lambda = 2d\sin\theta$). This law relates the wavelength of electromagnetic radiation to the diffraction angle and the lattice spacing in a crystalline sample.

2.2.6. Friction Torque

Two friction torque test protocols, described in Table 5, were performed to know the behavior of bearings samples under both low-load and low-speed conditions. The Stribeck test (ST) determines friction torque at low loads, and it is useful to determine how the lubrication regime is acting, and how much torque bearing is consuming during the running-in. The Torque to Rotate (TTR) test was used to determine how much torque the bearing consumes under different loads and at a low speed. They both offer a GO/NO GO threshold to check if the ZrN/ZrCN coatings peel-off, or they stay on the bearings surface during their lifetime. Three coated bearing pairs, named as Set 1, Set 2 and Set 3, plus a pair of uncoated bearings, named as baseline, were subjected to the tests. Friction torque tests were carried out in collaboration with FERSA BEARINGS SA in an AX-180 TT test rig where tapered roller bearings were assembled in a tandem configuration. Protective oil Shell Ensis RPO 1000 (kinematic viscosity 35 Cst, flash point 192 °C, specific gravity 0.899 g/cm^3) was applied as the bearing lubrication. The test rig characteristics were: test bench size, 450 mm × 1220 mm; No. of stations, 1; No. of bearings, 2; bearing outer diameter size, up to 180 mm; axial load (max.) 15 kN; speed range, 0–1000 rpm; and torque (max.) 100 Nm.

Table 5. Friction torque test protocols.

Test	Preload (kN)	Speed Range (rpm)	Temperature	Test Time (min)
Stribeck test	8	0–200	room	1.5 min
Torque to Rotate test	0–15 (1.5 kN/step)	30	room	10 min (1 min/load step)

3. Results and Discussion

3.1. Geometrical Analysis

Results of a geometrical analysis for the raceway profile defined as (a) in Figure 2 are shown in Figure 4. Although all the samples were tested, Figures 4 and 5 only show the results for D4 coating, since the results for all the configurations of the coating were very similar. Figure 4a shows a raceway profile for uncoated bearings, and Figure 4c shows a raceway profile for coated bearings. It can be observed that the coating has perfectly copied the shape of the raceway logarithmic profile. Figure 4b,d show the roughness of the profile along the dotted area in Figure 4a,c. Roughness is represented on a horizontal axis (different from the axis of the bearing profile) in order to calculate an average of the peaks and valleys, and, thus, the roughness. It is also confirmed in detailed views that the coating reproduces almost exactly the uncoated track.

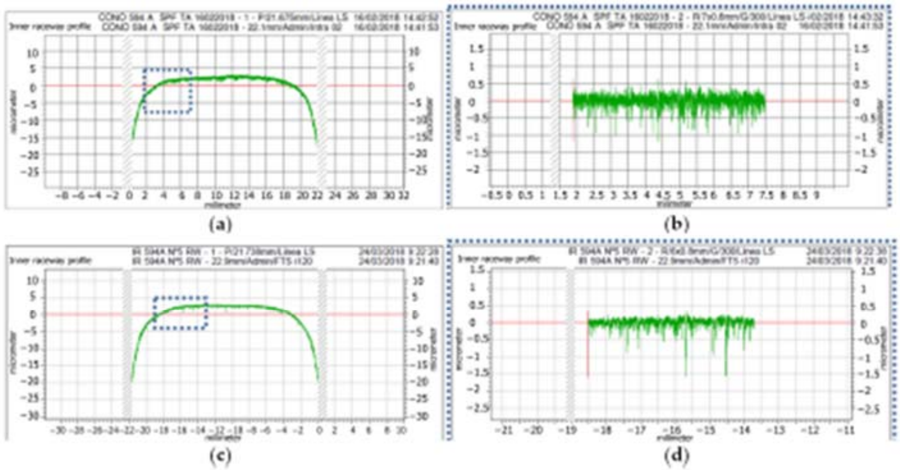

Figure 4. Inner raceway profile (logarithmic) for (**a**) Uncoated bearing; (**b**) uncoated bearing at the selected area in (**a**), (**c**) coated bearing; and (**d**) coated bearing at the selected area in (**c**).

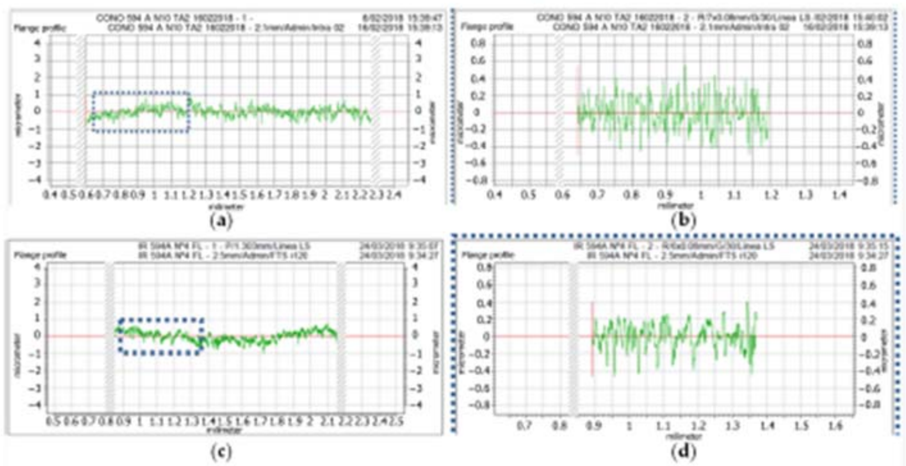

Figure 5. Flange profile for (**a**) Uncoated bearing; (**b**) uncoated bearing at the selected area in (**a**), (**c**) coated bearing; and (**d**) coated bearing at the selected area in (**c**).

The results of a geometrical analysis for flange profile, which is defined as (b) in Figure 2 are shown in Figure 5. Figure 5a shows the flange profile for uncoated bearings, and Figure 5c shows the flange profile for coated bearings. It can be observed that the coating has also perfectly copied the shape of the flange profile. Figure 5b,d show the roughness of the profile along the dotted area in Figure 5a,c. Roughness is represented on a horizontal axis (different from the axis of the bearing profile) in order to calculate an average of the peaks and valleys, and thus the roughness. It is also confirmed in detailed views that the coating reproduces almost exactly the uncoated flange.

Figure 6 shows the RONt distribution at the inner ring raceway. RONt values, obtained after the PVD coating process, range from 0.82 to 2.34 μm, which are under the FERSA BEARINGS SA specifications (RONt < 6 μm).

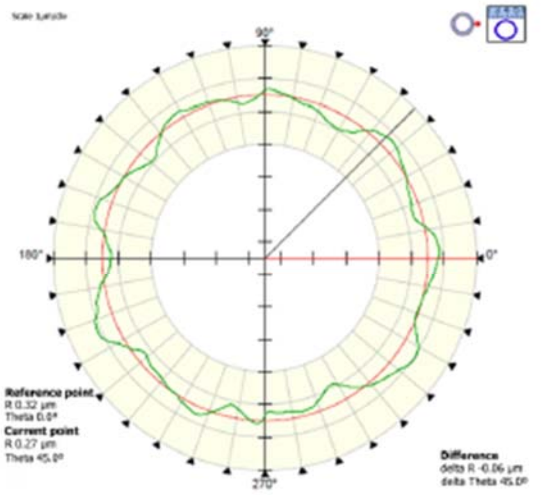

Figure 6. Inner ring raceway diameter shape.

It can be concluded that the obtained shapes are suitable according to FERSA BEARINGS SA specification, so the coating process has no affection on the profile shapes of the bearing. Therefore, it allows proceeding with the roughness, thickness, hardness, and adhesion tests ensuring that the results obtained are comparable to those obtained on the uncoated baseline bearings.

3.2. PVD Coating Characterization

The Zr(C,N) coatings were analyzed by means of XRD, using the Cu K_1 wavelength (0.154075 nm). The corresponding spectrum is represented in Figure 7. Graze Incidence X-Ray Diffraction (GIXRD) was employed, meaning that, as the functional coating is the same for all the studied coating designs, equivalent spectra are obtained in all the cases. That is the reason just one of them is shown.

The spectrum agrees with an equivalent coating reported in a previous work [38], showing clear peaks of cubic Zr_2CN, cubic ZrN, and ZrC, approximately homologous. The coatings investigated are crystalline with a rock salt like a NaCl cubic structure Fm–3m.

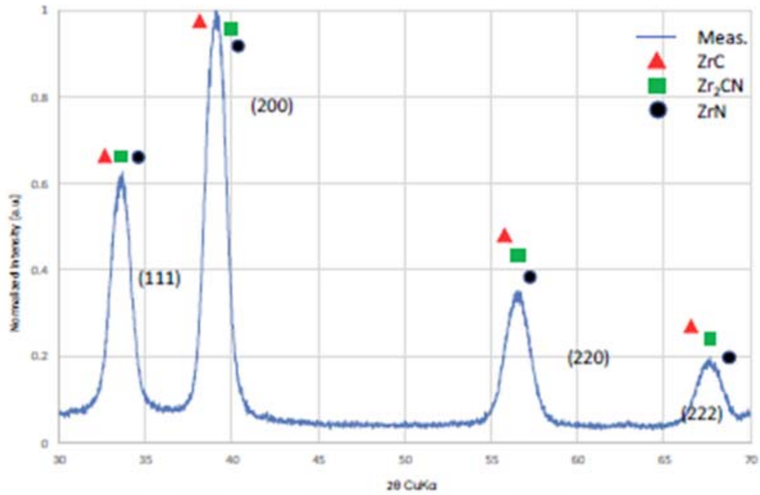

Figure 7. Example of GIXRD spectrum of a ZrCN coating.

The chemical composition profiles of the developed coatings were measured using the GD-OES technique. Figure 8 shows the profile corresponding to D1 design as an example, where the sequence of the adhesion layer and functional layer configuration can be observed. It must be said that the profile gives a qualitative idea of the progression in chemical composition in coating depth because a general PVD method for calibration has been used. On the right of the graph, the main elements of the stainless-steel substrate can be seen, and afterward an increase of the titanium concentration is appreciated due to the first titanium adhesion layer. Finally, regarding the functional layer, the sequence of three ZrN/ZrCN bilayers can be observed by the presence of small "hills" for carbon profile, which correspond to the introduction of acetylene gas during the coating deposition process.

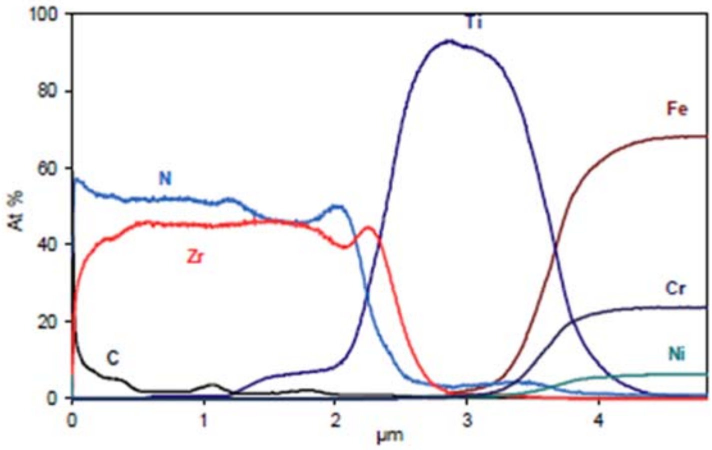

Figure 8. D1 design coating composition graphic obtained by GD-OES.

Table 6 gathers the characterization results obtained for the developed coatings, regarding roughness, thickness, adhesion, and substrate integrity.

Coating design D1 offers a good adhesion result HF1, showing neither cracks nor delamination (Figure 9a). Nevertheless, the roughness R_a is 0.540 μm, above the allowed value (R_a < 0.15 μm) due to the presence of droplets. These droplets are inherent to the Arc Evaporation coating technology in which a very high grade of ionization is achieved. At the same time, these high energies can melt the

Coatings **2019**, *9*, 434

material to be deposited, with the formation and deposition of the consequent droplets. Filters can be used (Filtered Arc Evaporation) to avoid droplets reaching the substrate but, as this variant entails lower deposition rates, it was not considered interesting from an industrial point of view. As can be seen in the cross-section of the adhesion layer (Ti + Ti–Zr) of the D1 coating (Figure 9b,c), the Ti metallic first layer is the main responsible for the high roughness, reason why a strategy to reduce the thickness (1.24 µm) of this adhesion layer is followed in D2 and D3 coating designs.

For the coating design D2, 5 min of Ti instead of 60 min, and 1 min of Ti–Zr instead of 5 min have been applied. An evident lack of adhesion (HF5) is observed. Figure 10a shows grey zones surrounding the indentation, which correspond to the bare substrate, areas where the coating has been detached. Roughness (R_a = 0.240 µm) has been reduced (Figure 10b), although it is not low enough to enter under the specifications. Therefore, applying a thinner adhesion layer (0.21 µm) leads to a lower roughness at the expense of the substrate-coating adhesion.

Table 6. PVD coating results.

Coating Design	R_a (µm)	Thickness (µm)		Adhesion (HF)	Substrate Hardness (HRC)	
		Adhesion Layer	Total		Before PVD Application	After PVD Application
D1	0.540	1.24	3.67	HF1	60.7	59.0
D2	0.240	0.21	2.61	HF5	60.4	59.1
D3	0.080	0.46	2.86	HF5	60.5	59.7
D4	0.533	1.23	4.35	HF1	59.6	59.2

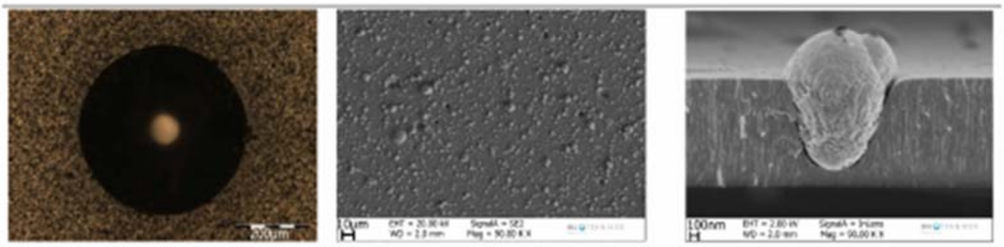

(a) (b) (c)

Figure 9. Optical and SEM images for D1 coating; (**a**) adhesion results (optical); (**b**,**c**) surface, and cross-section micrographs.

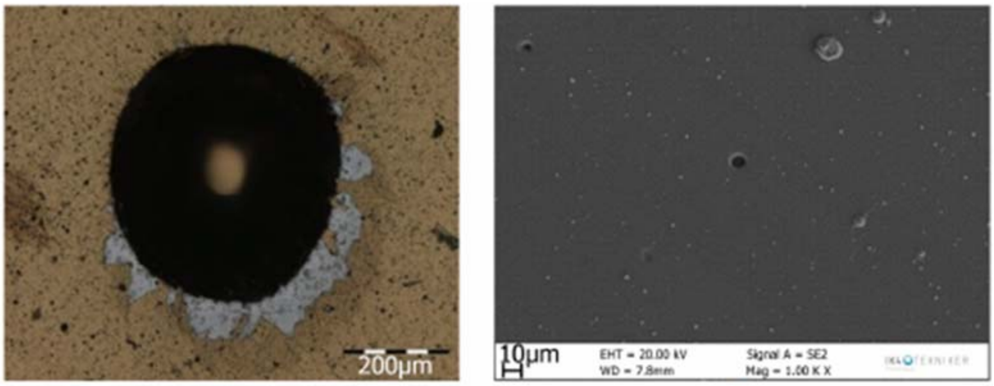

(a) (b)

Figure 10. Optical and SEM images for D2 coating; (**a**) adhesion results (optical); (**b**) surface micrograph.

D3 coating design includes a new structure for the adhesion layer. After a thinner Ti metallic layer of one minute (to reduce roughness), nitrogen is introduced (4 min) before Zr, trying to build a more progressive transition to the functional multilayer starting with ZrN, with the aim of providing the coating an improved adhesion (total thickness of adhesion layer 0.46 μm). A proper R_a value of 0.080 μm is achieved, which can be observed in both the surface and cross-section micrographs (Figure 11b,c), where a lower density and smaller droplets appear. However, once again, the coating results in a lack of adhesion HF5 (Figure 11a).

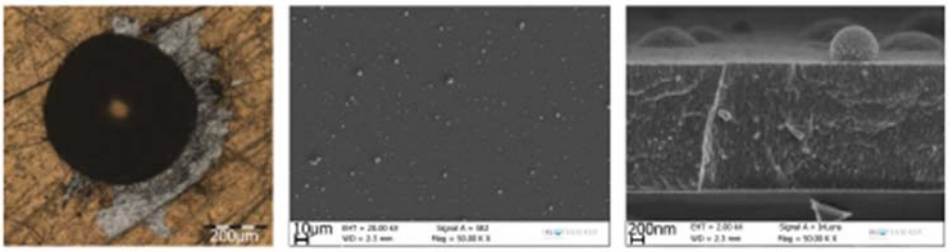

(a) (b) (c)

Figure 11. SEM images for D3 coating; (**a**) adhesion results; (**b**,**c**) D3 surface, and cross-section micrographs.

The D1 structure was reconsidered for the D4 design. However, taking into account the subsequent polish post-processing to be applied for roughness reduction, a fourth ZrN/ZrCN bilayer was added to the functional coating, achieving an adhesion layer thickness of 1.23 μm similar to the D1 adhesion layer, and a total thickness of 4.33 μm. Therefore, the thickness of the functional coating is increased to compensate for the thickness reduction during the polish post-processing. HF1 classification is observed at the adhesion test, as it can be seen in Figure 12, where neither trace of peeling off nor bare substrates are observed. As expected, the roughness of the deposited coating (R_a 0.533 μm) is far from the allowed roughness of 0.15 μm.

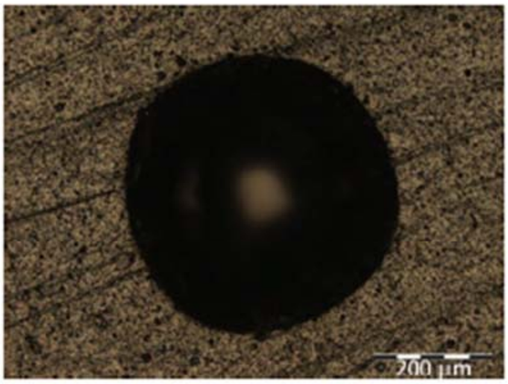

Figure 12. D4 adhesion results.

3.3. Polish Post-Processing

After the analysis of the PVD process carried out at a low-temperature Arc Evaporation, it can be concluded that coating design strategies are not enough to get a proper coating balancing required in terms of roughness and adhesion results. For that reason, a polish post-processing is applied to decrease the surface roughness of the properly adhered coatings D1 and D4. Table 7 shows roughness results after the polish post-processing.

Table 7. Polish post-processing results.

Coating Design	Post-Polishing Configuration	R_a (μm)	
		Before Post-Polishing	After Post-Polishing
D1	A1	0.540	0.371
	A2	0.540	0.226
	B	0.540	0.171
D4	B	0.533	0.148

After applying the polish post-processing Method A during three hours (Polish Configuration A1), samples D1 were measured and then, introduced again in the vessel to continue the polish post-processing up to six hours (Polish Configuration A2). R_a values decrease by 31.30% for Configuration A1 and by 58.15% for Configuration A2, showing that Configuration A is not able to obtain the required roughness. Following the more aggressive polish post-processing Method B (Configuration B), R_a is reduced by 68.33% up to 0.171 μm in 15 min, achieving an adhesion very close to the roughness specification. In case of the D4 coating design, since a fourth Zr/ZrCN bilayer was added, the final thickness after polish post-processing is not significantly changed, and R_a is reduced by 72.33% up to 0.148 μm ($< R_a = 0.15$ required). Figure 13 shows D4 coated samples, post polished under Configuration B.

Figure 13. Bearing samples D4 coating + B polish post-processing.

3.4. Substrate Hardness

HRC on the bearing substrate, before and after the PVD application, is shown in Table 6. Samples before the PVD application show an HRC value around 60 HRC. After the PVD application, they decrease up to values ranging from 59 to 59.7 HRC. The reduction in HRC when applying the PVD process is explained by the increasing temperature on the sample during the cathodic arc application on the bearing steel. This analysis of the hardness of the sample gives relevant information about the performance of bearing steel after a PVD process implementation. HRC values ranging 59–63 HRC after the PVD application indicate that the steel of the bearing sample has not reached 180–200 °C, which is the tempering temperature of the bearing steel, avoiding any deterioration of the substrate properties. Figure 14a shows that the tempering temperature is achieved at 180–200 °C for martensitic bearing steel. Figure 14b gives information about the relation between the tempering temperature and the HRC hardness for martensitic bearing steel. It can be observed that the temperature range of 180–200 °C corresponds to a range of 59–63 HRC [50].

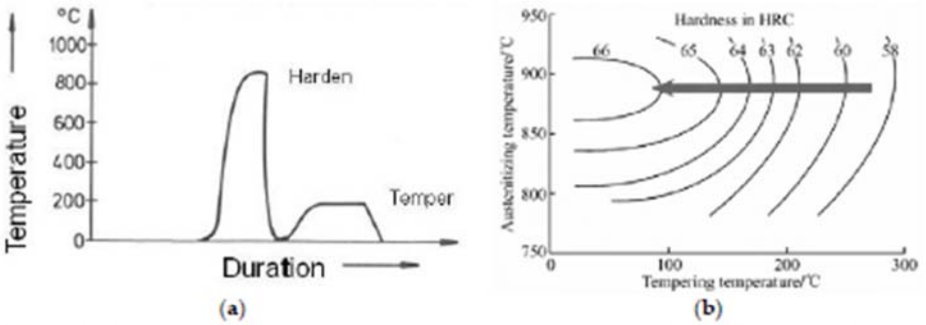

Figure 14. Relation between tempering temperature and hardness (**a**) Martensitic through hardening treatment; (**b**) tempering temperature vs hardness [50].

3.5. *Friction Torque*

Samples with the D4 coating design and the Configuration B polish post-processing, achieving functional requirements of R_a, thickness, hardness, and adhesion, were subjected to friction torque results in order to test if any improvement is achieved in the bearing performance.

3.5.1. Stribeck Tests

Stribeck tests results are shown in Figure 15. At the beginning of the test, the four sets of samples, Set 1, Set 2, Set 3, and baseline reach the initial torque values between 6 and 6.5 Nm. Then, during stabilization, Set 1 torque stabilizes at around 4 Nm, Set 2 torque stabilizes at 3.2 Nm, and Set 3 torque stabilizes at 3 Nm. However, the baseline sample stabilizes at 1.3 Nm, which is a very promising result, much better than the coated and polished bearings. Therefore, as can be checked, the friction of the coated bearings is never lower than the friction consumed by uncoated bearings, so there is no improvement in the tribological behavior of the bearings after coating them at low-load conditions.

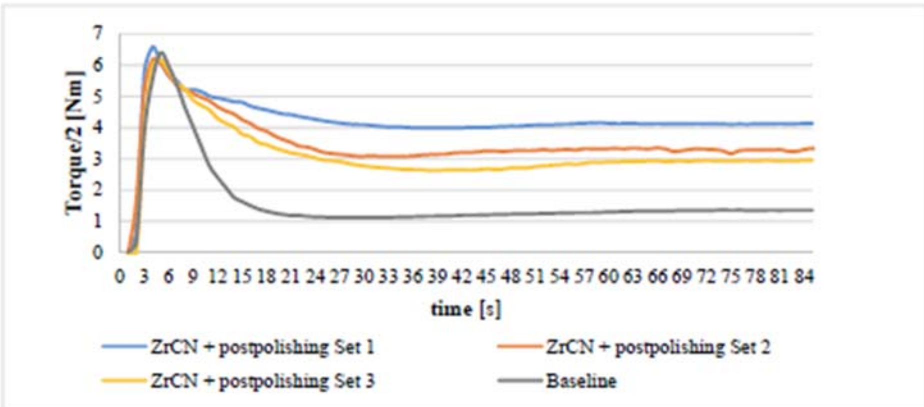

Figure 15. 594A/592A ZrCN + polish post-processing Stribeck friction test 8 kN.

3.5.2. TTR Tests

Figure 16 shows the results for TTR tests. It can be observed that the friction behavior is similar for all the bearing samples (Set 1, Set 2, Set 3, baseline) at low speed and loads. However, slight differences can be observed at high loads, where Set 3 achieves torque values lower than the baseline torque.

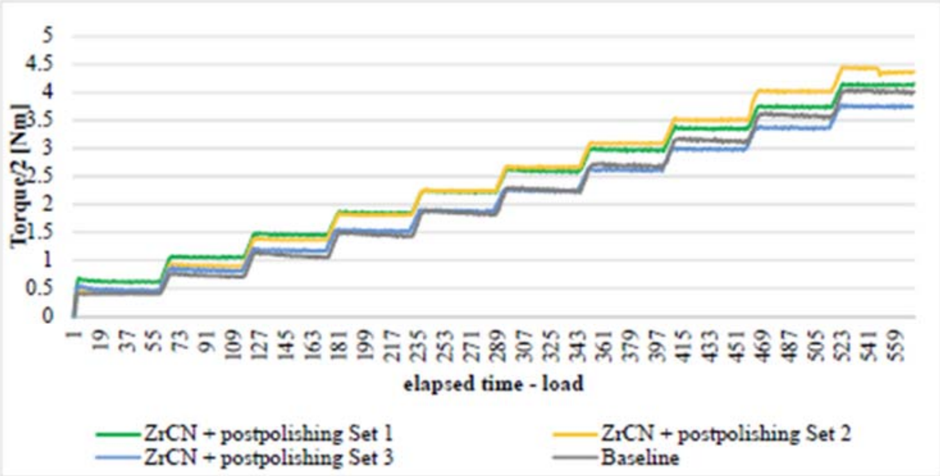

Figure 16. 594A/592A ZrCN + polish post-processing TTR friction test 0–15 kN, 30 rpm.

Analyzing torque vs load in Figure 17, it is shown that Set 3 exhibits a lower torque value than the baseline for all the loads, which is not achieved for Set 1 and Set 2. The dotted line shows the average torque value for the three sets of coated bearings, which confirms that the behavior is quite constant between the samples, and no major torque improvement appears regarding baseline torque.

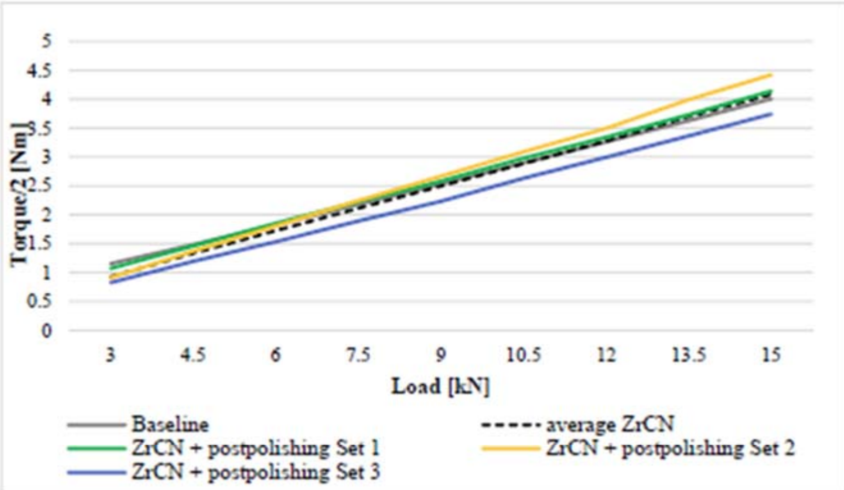

Figure 17. 594A/592A ZrCN + polish post-processing TTR friction test vs Baseline.

4. Conclusions

A strategy based on applying PVD coatings on rolling bearings is proposed in order to improve friction behavior during the bearing performance. Different PVD coating designs have been tested varying mainly the adhesion layer. Coatings with thick interlayer show good adhesion results, although the roughness specification is not achieved. Only samples coated with a thin interlayer of Ti–TiN obtain acceptable roughness values, but at the expense of an inadequate adhesion. A polish post-processing is proposed for the samples with suitable adhesion in order to reduce roughness. The method based on walnut shell additivated with an 80% abrasive silica achieves the required low roughness. Coated rolling bearings are subjected to a friction torque test to evaluate their tribological behavior. However, regarding tribological properties of the coated rolling bearings, hardly any improvement is observed in the friction torque neither at low load nor at low speed. However, fatigue tests in real test bench are pending to evaluate the possible improvement in bearing life time.

Author Contributions: Conceptualization, I.C., C.Z. and G.M.; Data curation, C.Z. and G.M.; Formal analysis, A.L., Á.F. and P.C.; Funding acquisition, Á.F. and P.C.; Investigation, A.L.; Methodology, C.Z. and G.M.; Project administration, Á.F. and P.C.; Resources, I.C., A.L. and D.E.; Software, G.M.; Supervision, I.C.; Validation, C.Z.; Visualization, D.E.; Writing—original draft, I.C. and A.L.; Writing—review & editing, I.C.

Funding: This research was funded by Spanish Ministry of Industry, Economics and Competitivity (RTC-2016-5799-4) and has been performed by members of the I+AITIIP (DGA-T08_17R) research group of the FEDER 2014-2020 "Building Europe from Aragón" program, recognized by the Regional Government of Aragon.

Conflicts of Interest: The authors declare no conflicts of interest. The founding sponsors had no role in the design of the study; in the collection, analyses, or interpretation of data; in the writing of the manuscript, and in the decision to publish the results.

References

1. Holmberg, K.; Andersson, P.; Nylund, N.-O.; Mäkelä, K.; Erdemir, A. Global energy consumption due to friction in trucks and buses. *Tribol. Int.* **2014**, *78*, 94–114. [CrossRef]
2. Ligier, J.L.; Noel, B. Friction Reduction and Reliability for Engines Bearings. *Lubricants* **2015**, *3*, 569–596. [CrossRef]
3. Nirmal, U. Friction Performance of Aged T-BFRP Composite for Bearing Applications. *Polymers* **2018**, *10*, 1066. [CrossRef] [PubMed]
4. Holmberg, K.; Matthews, A. Tribology of coatings. In *Coatings Tribology: Properties, Mechanisms, Techniques, and Applications in Surface Engineering*, 2nd ed.; Elsevier: Amsterdam, The Netherlands, 2009; pp. 41–183.
5. Bhadeshia, H.K.D.H. Steels for bearings. *Prog. Mater. Sci.* **2012**, *57*, 268–435. [CrossRef]
6. Dowson, D.; Higginson, G.R. Analysis of roller bearings. In *Elasto-Hydrodynamic Lubrication*, 1st ed.; Hopkins, D.W., Ed.; Elsevier: Amsterdam, The Netherlands, 1977; pp. 193–215.
7. Dowson, D. Elastohydrodynamic and micro-elastohydrodynamic lubrication. *Wear* **1995**, *190*, 125–138. [CrossRef]
8. Dowson, D.; Higginson, G.R. Theory of roller bearing lubrication and deformation. *Proc. Inst. Mech. Eng.* **1963**, *177*, 67–69.
9. Harris, T.; Mindel, M. Rolling element bearing dynamics. *Wear* **1973**, *23*, 311–337. [CrossRef]
10. Archard, J.F.; Crook, A.W. Apparatus and measurements of film thickness and film shape. In *Elasto-Hydrodynamic Lubrication*, SI ed.; Dowson, D., Higginson, G.R., Eds.; Pergamon Press: Oxford, UK, 1977; pp. 481–495.
11. Katsaros, K.; Bompos, D.A.; Nikolakopoulos, P.G.; Theodossiades, S. Thermal-Hydrodynamic Behaviour of Coated Pivoted Pad Thrust Bearings: Comparison between Babbitt, PTFE and DLC. *Lubricants* **2018**, *6*, 50. [CrossRef]
12. Xie, Z.; Rao, Z.; Liu, H. Effect of Surface Topography and Structural Parameters on the Lubrication Performance of a Water-Lubricated Bearing: Theoretical and Experimental Study. *Coatings* **2019**, *9*, 23. [CrossRef]
13. Morales-Espejel, G.E.; Brizmer, V. Micropitting modelling in rolling-sliding contacts: Application to rolling bearings. *Tribol. Trans.* **2011**, *54*, 625–643. [CrossRef]
14. Miller, G.R.; Keer, L.M.; Cheng, H.S. On the mechanics of fatigue crack growth due to contact loading. *Proc. R. Soc. A* **1985**, *397*, 197–209. [CrossRef]
15. Morales-Espejel, G.; Brizmer, V.; Piras, E. Roughness evolution in mixed lubrication condition due to mild wear. *Proc. Inst. Mech. Eng. Part J J. Eng. Tribol.* **2015**, *229*, 1330–1346. [CrossRef]
16. Oh, H.; Azarian, M.H.; Morillo, C.; Pecht, M.; Rhem, E. Failure mechanisms of ball bearings under lightly loaded, non-accelerated usage conditions. *Tribol. Int.* **2015**, *81*, 291–299. [CrossRef]
17. Claveria, I.; Elduque, D.; Lostalé, A.; Fernández, A.; Javierre, C.; Castell, P. Analysis of self-lubrication enhancement via PA66 strategies: Texturing and nano-reinforcement with ZrO_2 and graphene. *Tribol. Int.* **2019**, *131*, 332–342. [CrossRef]
18. Erdemir, A. Rolling-contact fatigue and wear resistance of hard coatings on bearing-steel substrates. *Surf. Coat. Technol.* **1992**, *54*, 482–489. [CrossRef]

19. Kuhn, M.; Gold, P.W.; Loos, J. Wear and friction characteristics of PVD-coated roller bearings. *Surf. Coat. Technol.* **2004**, *177*, 469–476. [CrossRef]
20. Igartua, A.; Laucirica, J.; Aranzabe, A.; Leyendecker, T.; Lemmer, O.; Erkens, G. Application of low temperature PVD coatings in rolling bearings: Tribological tests and experiences with spindle bearing systems. *Surf. Coat. Technol.* **1996**, *86*, 460–466. [CrossRef]
21. Hochman, R.F. Rolling contact fatigue behavior of Cu and TiN coatings on bearing steel substrates. *J. Vac. Sci. Technol. A* **1985**, *3*, 2348–2353. [CrossRef]
22. Rosado, L.; Jain, V.K.; Trivedi, H.K. The effect of diamond-like carbon coatings on the rolling fatigue and wear of M50 steel. *Wear* **1997**, *212*, 1–6. [CrossRef]
23. Chang, T.-A.P.; Cheng, H.S.; Sproul, W.D. The influence of coating thickness on lubricated rolling contact fatigue life. *Surf. Coat. Technol.* **1990**, *43*, 699–708. [CrossRef]
24. Komori, K.; Umehara, N. Effect of surface morphology of diamond-like carbon coating on friction, wear behavior and tribo-chemical reactions under engine oil lubricated condition. *Tribol. Int.* **2015**, *84*, 100–109. [CrossRef]
25. Yeo, S.M.; Polycarpou, A.A. Fretting experiments of advanced polymeric coatings and the effect of transfer films on their tribological behavior. *Tribol. Int.* **2014**, *79*, 16–25. [CrossRef]
26. Stewart, S.; Ahmed, R. Rolling contact fatigue of surface coatings—A review. *Wear* **2002**, *253*, 1132–1144. [CrossRef]
27. Baptista, A.; Silva, F.; Porteiro, J.; Míguez, J.; Pinto, G. Sputtering Physical Vapour Deposition (PVD) Coatings: A Critical Review on Process Improvement and Market Trend Demands. *Coatings* **2018**, *8*, 402. [CrossRef]
28. Chen, J.; Geng, M.; Li, Y.; Yang, Z.; Chai, Y.; He, G. Erosion Resistance and Damage Mechanism of TiN/ZrN Nanoscale Multilayer Coating. *Coatings* **2019**, *9*, 64. [CrossRef]
29. Geng, M.; He, G.; Sun, Z.; Chen, J.; Yang, Z.; Li, Y. Corrosion Damage Mechanism of TiN/ZrN Nanoscale Multilayer Anti-Erosion Coating. *Coatings* **2018**, *8*, 400. [CrossRef]
30. Vereschaka, A.; Kataeva, E.; Sitnikov, N.; Aksenenko, A.; Oganyan, G.; Sotova, C. Influence of Thickness of Multilayered Nano-Structured Coatings Ti–TiN-(TiCrAl)N and Zr-ZrN-(ZrCrNbAl)N on Tool Life of Metal Cutting Tools at Various Cutting Speeds. *Coatings* **2018**, *8*, 44. [CrossRef]
31. Zhang, P.; Wang, J. Torsional Fretting Wear Behavior of PVD TiCN Coated CuNiAl Blade Bearing in Oil and Artificial Seawater. *Coatings* **2019**, *9*, 140. [CrossRef]
32. Klaffke, D.; Santner, E.; Spaltmann, D.; Woydt, M. Influences on the tribological behaviour of slip-rolling DLC-coatings. *Wear* **2005**, *259*, 752–758. [CrossRef]
33. Thom, R.; Moore, L.; Sproul, W.D.; Peter Chang, T. Rolling contact fatigue tests of reactively sputtered nitride coatings of Ti, Zr, Hf, Cr, Mo, Ti–Al, Ti–Zr and Ti–Al–V on 440 C stainless steel substrates. *Surf. Coat. Technol.* **1993**, *62*, 423–427. [CrossRef]
34. Novak, R.; Polcar, T. Tribological analysis of thin films by pin-on-disc: Evaluation of friction and wear measurement uncertainty. *Tribol. Int.* **2014**, *74*, 154–163. [CrossRef]
35. Grill, A. Tribology of diamondlike carbon and related materials: An updated review. *Surf. Coat. Technol.* **1997**, *94*, 507–513. [CrossRef]
36. Robertson, J. Diamond-like amorphous carbon. *Mater. Sci. Eng. R Rep.* **2002**, *37*, 129–281. [CrossRef]
37. Fiaschi, G.; Rota, A.; Ballestrazzi, A.; Marchetto, D.; Vezzalini, E.; Valeri, S. A Chemical, Mechanical, and Tribological Analysis of DLC Coatings Deposited by Magnetron Sputtering. *Lubricants* **2019**, *7*, 38. [CrossRef]
38. Manier, C.-A.; Ziegele, H.; Barriga, J.; Goikoetxea, J.; Woydt, M. Zirconium-based coatings in highly stressed rolling contacts as alternative solution to DLC and ta-C coatings. *Wear* **2010**, *269*, 770–781. [CrossRef]
39. ISO. *683-17:2014 Heat Treated Steels, Alloy Steels and Free-Cutting Steels—Part 17: Ball and Roller Bearing Steels*; ISO: Geneva, Switzerland, 2015.
40. Dinkel, M. Bearing Steels and Heat Treatment. In Proceedings of the ABMA Webinar Series, 17 September 2015; Available online: https://www.americanbearings.org/events/EventDetails.aspx?id=654049&hhSearchTerms=%22bearing+steels+and+heat+treatment%22 (accessed on 17 September 2015).
41. IK4-Tekniker. Arc Evaporator and Method for Operating the Evaporator. International Patent WO2010072850, 7 January 2010.
42. ISO. *1101:2017 Geometrical Product Specifications (GPS)—Geometrical Tolerancing—Tolerances of Form, Orientation, Location and Run-Out*; ISO: Geneva, Switzerland, 2017.
43. ISO. *6508-1:2016 Metallic Materials—Rockwell Hardness Test—Part 1: Test Method*; ISO: Geneva, Switzerland, 2016.

44. ISO. *4287:1998 Geometrical Product Specifications (GPS)—Surface Texture: Profile Method—Terms, Definitions and Surface Texture Parameters*; Deutsches Institut für Normung: Berlin, Germany, 1998.
45. Japanese Industrial Standard. *JIS B 0601:1994 Surface Roughness: Definitions and Designation*; JSA: Tokyo, Japan, 1994.
46. ISO. *4288:1996 Geometrical Product Specifications (GPS)—Surface Texture: Profile Method—Rules and Procedures for the Assessment of Surface Texture*; ISO: Geneva, Switzerland, 1996.
47. ISO. *26423:2009 Fine Ceramics (Advanced Ceramics, Advanced Technical Ceramics)—Determination of Coating Thickness by Crater-Grinding Method*; ISO: Geneva, Switzerland, 2009.
48. Verein Deutscher Ingenieure Normen. In *VDI 3198*; VDI-Verlag: Dusseldorf, Germany, 1991.
49. Payling, R.; Michler, J.; Aeberhard, M. Quantitative analysis of conductive coatings by radiofrequency-powered glow discharge optical emission spectrometry: Hydrogen, d.c. bias voltage and density corrections. *Surf. Interface Anal.* **2002**, *33*, 472–477. [CrossRef]
50. Ebert, F.-J. Fundamentals of Design and Technology of Rolling Element Bearings. *Chin. J. Aeronaut.* **2010**, *23*, 123–136. [CrossRef]

6.3. POLYMERS: TRIBOLOGICAL PERFORMANCE OF NYLON COMPOSITES WITH NANOADDITIVES FOR SELF-LUBRICATION PURPOSES

En el artículo “*Tribological Performance of Nylon Composites with Nanoadditives for Self-Lubrication Purposes*”, se realizó un estudio sistemático en que se comparó el comportamiento al desgaste de los composites con matriz de de poliamida (PA66, PA46, PA12) y diferentes nanoaditivos y aditivos de refuerzo (grafito, grafeno, MoS2 y ZrO2) con el fin de conseguir un material autolubricante adecuado para jaulas de rodamientos. La caracterización del desgaste se realizó mediante ensayos pin-on-disc, microscopia electrónica de barrido (Scanning Electron Microscopy, SEM) y análisis por dispersión de energías de rayos-X (Energy Dispersive X-ray spectroscopy, EDX). Los resultados mostraron que los mejores resultados se obtenían para los composites basados en PA12 y que la adición de nanopartículas de ZrO_2 provocó valores negativos de desgaste debido a la transferencia de partículas metálicas a la probeta polimérica.

Contribución del doctorando: Revisión del estado del arte. Análisis e interpretación de resultados. Redacción y revisión del artículo.

polymers
MDPI

Article

Tribological Performance of Nylon Composites with Nanoadditives for Self-Lubrication Purposes

Isabel Clavería [1,*], Sofía Gimeno [2], Ignacio Miguel [2], Gemma Mendoza [3], Aleida Lostalé [1], Ángel Fernández [1], Pere Castell [4] and Daniel Elduque [1]

1 Mechanical Department, EINA, University of Zaragoza Maria de Luna, 50018 Zaragoza, Spain; 547686@unizar.es (A.L.); afernan@unizar.es (Á.F.); delduque@unizar.es (D.E.)
2 FERSA BEARINGS S.A., Bari, 50197 Zaragoza, Spain; sofia.gimeno@fersa.com (S.G.); ignacio.miguel@fersa.com (I.M.)
3 Fundación Tekniker, Iñaki Goenaga, 20600 Eibar, Spain; gemma.mendoza@tekniker.es
4 Fundación AITIIP, Calle Romero, 50720 Zaragoza, Spain; pere.castell@aitiip.com
* Correspondence: isabel.claveria@unizar.es

Received: 25 July 2020; Accepted: 21 September 2020; Published: 30 September 2020

Abstract: A systematic study comparing the wear behaviour of composites with nylon matrix (PA66, PA46, PA12) and different nanoadditives and reinforcing additives (graphite, graphene, MoS_2 and ZrO_2) has been carried out in order to achieve a proper self-lubricant material for bearing cages. The wear characterisation was done using pin-on-disc tests, SEM and EDX analysis. The results show that better outcomes are obtained for composites based on PA12. The addition of ZrO_2 offers negative values of wear due to the metallic particle transference from the counterface to the polymeric pin.

Keywords: ZrO_2; graphene; MoS_2; friction; wear; polyamide

1. Introduction

One of the challenges that has arisen during recent years in the industrial field is to make industrial processes and component performance more sustainable. In this sense, one of the most used industrial components is bearings, so improving their energy efficiency may be key to reduce fuel consumption and pollutant emissions. As an example, recent analyses [1] show that for every litre of fuel used in an average vehicle, 5% is consumed in mechanical losses and 1% of the total is lost due to bearing operation. Since a significant part of the energy required for industrial component performance is lost in form of heat due to friction [2], new strategies are required to develop low-friction components. Traditionally, these strategies have been focused on modifying surfaces through different treatments to improve surface hardness [3,4], or to develop hard coatings deposited by physical [5] or chemical vapor deposition (PVD and CVD) [6], and the development of new lubricants [7]. However, some friction and wear phenomena are characterised by different scale processes (ones at atomic or molecular scales and others at a scale of roughness of approximately 1–20 µm [8]) that operate simultaneously. This fact leads to difficulties in studying microscopic phenomena resulting in macroscopic wear and friction and becomes one the biggest challenges of current tribology research. Furthermore, problems related to coating detachment can arise because adherence properties strongly depend on the morphology and composition of the coating layer [5], and also on the interacting forces between the coating layers and the substrate surface. Therefore, the development of new self-lubricant materials without coating requirements seems to be an excellent solution to achieve low-friction properties, minimising maintenance costs due to the presence of additional lubricants.

As stated previously, bearings, and particularly bearing cages, are one of the mechanical applications where low-friction polymers can play an essential role in order to achieve a high

Polymers **2020**, *12*, 2253; doi:10.3390/polym12102253 www.mdpi.com/journal/polymers

performance under high speed and temperature conditions by means of reducing the wear between the cage and rolling elements, as investigated by Fersa Bearings S.A. [5–9] and other authors [10,11].

Polymers have traditionally been investigated for industrial purposes, especially in mechanical components subjected to high speed, because of their light weight and, thus, their low inertial contribution.

Some polymers have also been investigated in relation to their excellent tribological properties, such us nylons (PA) [12,13] and polytetrafluoroethylene (PTFE) [14,15]. However, due to the poor mechanical properties of PTFE, it has usually been used as a self-lubricant additive into other polymeric matrices rather than as a polymeric matrix itself [16–19]. Nylons stand out thanks to their ability to form a proper transfer film when sliding against metallic counterparts [20,21]. PA66 is one of the most commonly used nylons for mechanical purposes [22,23], as well as other relatively new engineering nylons, such as PA12 and PA46 [24]. In the case of PA46, it is expected to show superior performances to other nylons used in engineering parts and components, such as gears, because of its higher modulus and strength as a result of being highly crystalline.

Nevertheless, the engineering performance of nylons can be improved by means of developing new composites, combining the optimum processability of polymers and the excellent wear and mechanical properties of some solid lubricant nanoadditives. Nanostructures derived from carbon allotropes such as graphite and graphene have been widely proven to provide good properties for mechanical and tribological purposes in several polymeric matrices, such as PA [22–27], PTFE [28], PEEK [29] or PES [30].

ZrO_2 can be used as a nanocomponent, usually added to metal and cermet matrices to improve its mechanical and wear behaviour [31,32], or it can also be used as a direct coating for metallic bare substrates [33]. However, few examples are found in literature about the wear performance of polymeric composites containing ZrO_2 [9], and some of the studies refer only to polymeric composites including other components apart from ZrO_2. The results reported by these studies are variable regarding the performance of ZrO_2 in the wear behaviour of the composite, as described in [9,34,35]. Despite these results, few investigations have focused on the improvement of the tribological properties of polymers doped with ZrO_2 and, consequently, this paper aimed to increase the knowledge of this nanocomponent and its behaviour working as a filler in different polyamides.

Due to its lamellar shape made of individual atomically thin planes that can easily slide against each other [36], molybdenum disulphide (MoS_2) has been successfully used as a solid lubricant. MoS_2 can work, alone or with other additives, in different environments, such as: polymeric composites based on PEEK [37,38], ABS [39], PI [40] and PA [19,41–44]; liquid lubricants [45–47] or coatings [48–50], showing promising results in terms of improving friction coefficient and wear rate.

In many of the studies found in the literature, the polymer composites are formed by a combination of several nanoadditives mixed in the same matrix, such as PA12-graphene-paraffine oil in [26]; PEEK-ZrO_2-Ni in [34]; PEEK-graphene-WS_2-CNT in [29]; PI-MoS_2-graphene in [40]; PA6-TiO_2-MoS_2 in [41]; PPSK-graphite-PFTE in [51].

With this background, a systematic study comparing potential solid lubricants for the same polymeric matrix under similar conditions is missing. It seems to be suitable to carry out a study that provides comparable results about the tribological behaviour of some polyamides doped with some of the nanoadditives that have exhibited some wear improvement.

The aim of this research is to provide comparative results about the wear behaviour of different solid lubricants such as graphite, graphene, MoS_2 and ZrO_2 with the same polymeric matrix (PA66, PA46 and PA12) under similar test conditions.

2. Experimental

2.1. Materials

Polymer nano-reinforced composites based on PA66 from Bada Hispanaplast S.A. (PA66 BADAMID A70S, Huesca, Spain) [52], PA46 from DSM Engineering Plastics (STANYL® TW341, Heerlen, Netherland) [53] and PA12 from Bada Hispanaplast S.A. (PA12 BADAMID PA12H) [54] were analysed.

The different polyamides were filled with different additives in order to obtain enhanced tribological properties. In particular, four different fillers were used: ZrO_2, MoS_2, graphene and graphite. The graphene used was Avangraphene Plat 40 (Avanzare, Navarrete, Spain) which is a two-dimensional carbon atom structure obtained via the mechanical exfoliation of graphite, with an oxygen content (X-ray photoelectron spectroscopy) of <0.5%, a hydrogen content of <1%, a nitrogen content of <1%, an average thickness of 10 nm, a width (laser diffraction) of 40 μm, a surface area (Brunauer–Emmett–Teller) of 282 m^2/g and an average number of layers of < 30. It is specially designed to be mixed with polymeric materials, and a low dosage is required to reach the percolation level. General purpose ZrO_2 supplied by Torrecid S.A. (Castellón, Spain) [55], with a size of D50 1.20 ± 0.20 μm (spherical) and with a tensile strength of 450 MPa has also been used. The laminar MoS_2 used was M15 with an average size of D50 = 1.5 μm and a thickness of 10 nm from Brugarolas S.A (Barcelona, Spain) [56]. Two-dimensional graphite, with a similar structure to MoS_2, was provided by GrapheneTech S.L. (Zaragoza, Spain) [57].

2.2. Specimen Preparation

In order to characterise the different composites, the tribological tests were performed using a pin-on-disc configuration. Overall, twelve different nano-reinforced composite materials were prepared, as shown in Table 1. The samples were prepared via extrusion compounding in a co-rotating twin-screw extruder (Coperion ZS26K, Barcelona, Spain) equipped with two gravimetric feeders (Brabender Technologies, Duisburg, Germany). All the samples were prepared using the same experimental conditions: temperature profile (270 °C to 300 °C at the die), screw speed between 100 and 175 rpm, torque between 60 and 80 Nm and pressure between 80 and 85 bar. The screw profile was designed to achieve a high to medium shear profile that was optimised in previous studies [58,59]. A screw diameter of 25 mm and a length/diameter ratio of 40 were used in the different test procedures.

Table 1. Hybrid composites tested.

Composite Name	Base Polymer	Additive (by Weight)	Additive (by Volume)
PA66GN	PA66	5% graphene	4.10% graphene
PA66GT	PA66	5% graphite	4.20% graphite
PA66M	PA66	5% MoS_2	1.75% MoS_2
PA66Z	PA66	5% ZrO_2	3.60% ZrO_2
PA46GN	PA46	5% graphene	4.10% graphene
PA46GT	PA46	5% graphite	4.20% graphite
PA46M	PA46	5% MoS_2	1.75% MoS_2
PA46Z	PA46	5% ZrO_2	3.60% ZrO_2
PA12GN	PA12	5% graphene	4.10% graphene
PA12GT	PA12	5% graphite	4.20% graphite
PA12M	PA12	5% MoS_2	1.75% MoS_2
PA12Z	PA12	5% ZrO_2	3.60% ZrO_2

The optimum level of additive dispersion into the polymeric matrix was determined using an ultrasonic device specially designed for this purpose, fully described in previous studies [58,59]. These studies varied the concentration of nanoadditives and the extrusion conditions in PA6 matrices. Once the materials were processed, mechanical, thermal and morphological studies determined the optimal concentration of additives, which resulted in the best combined properties. The dispersion of the additives determined by Scanning Electron Microscope (SEM) and Transmission electron microscope (TEM) was key to selecting the optimal conditions. From these studies, the authors determined and selected the optimal loading that has been used in the present study.

On the one hand, the content of additives was determined by weight in all the formulations prepared. On the other hand, the quantity of additives was set at 5% since this percentage shows promising results in the literature [9].

Pins of $8 \times 8 \times 4$ mm^3 from the resulting composite materials were injected using an electric injection machine (JSW 85 EL II, Tokyo, Japan) with a clamping force of 85 tons, a maximum injection pressure of 1960 bar, a maximum injection volume of 97 cm^3 and a screw diameter of 32 mm. The process conditions were as follows: an injection temperature profile of 240/260/280 °C, a mould temperature of 70 °C, an injection time of 1 s, a packing pressure of 50 MPa for 5 s and a cooling time of 7 s.

As the purpose of the study was to obtain a self-lubricating material for bearing cages, the disc specimens (dimensions Ø24 × 7.9 mm) were made of an AISI 52,100 100Cr6, the material used in rolling bearings, with a hardness of HRC 59–63 and a roughness of $R_a < 0.15$ µm according to the Fersa Bearings S.A. specification.

2.3. Pin on Disc Tests

The tests were performed on a CETR-UMT tribometer using a polymeric pin oscillating at a constant frequency (5 Hz), a stroke amplitude (4.25 mm) and under a defined load (384 N), against a stationary steel test disc under dry conditions for 1800 s. The sliding speed was 42.5 mm/s. A scheme of the testing configuration is shown in Figure 1.

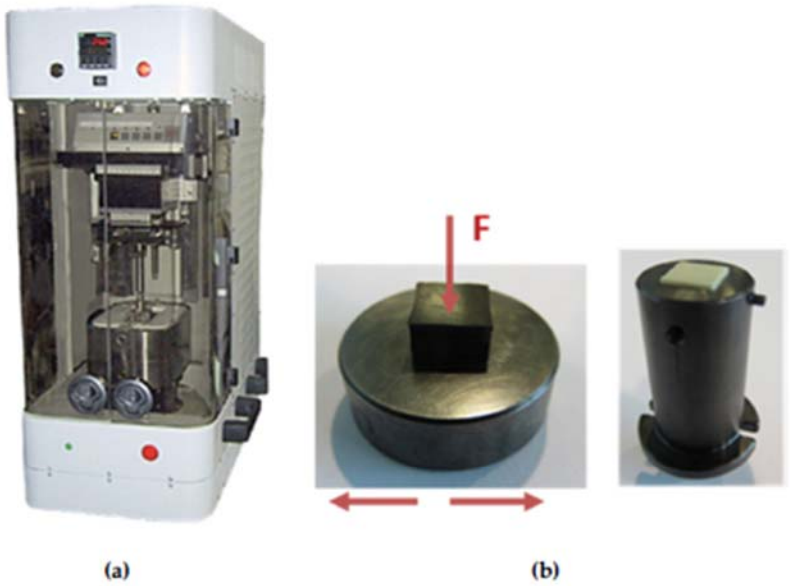

Figure 1. (**a**) CETR-UMT tribometer and (**b**) pin-on-disc testing configuration.

The following results were recorded: the coefficient of friction (CoF) evolution over time, obtained using CETR-UMT tribometer software (Viewer of UMT) which processes measured values, and the wear determined by the samples' mass loss, weighed using an electric balance in order to calculate the specific wear rate via the following equation:

$$w_s = \frac{\Delta m}{\rho F_N L}\left(\frac{\text{mm}^3}{\text{Nm}}\right) \quad (1)$$

where F_N is the normal force applied during the test, ρ is the material density, $L = 76.5$ m is the sliding distance according to the sliding speed and test duration and Δm is the mass loss obtained experimentally. Density values (ρ) are calculated from the equation:

$$\rho = (\%_{\text{matrix}} \times \rho_{\text{matrix}}) + (\%_{\text{additive}} \times \rho_{\text{additive}}) \quad (2)$$

where ρ is the density for the sample material, $\%_{\text{additive}}$ is the mass percentage of additive added to the sample composite, $\%_{\text{matrix}}$ is the mass percentage of polymer material, ρ_{matrix} is the density of the polymer and ρ_{additive} is the density of the additive.

2.4. SEM and EDS Analysis

The microstructure of some of the samples was studied using High-Resolution FE-SEM Ultra Plus Zeiss equipment (Jena, Germany), a scanning electron microscope with field emission gun. The equipment has a complete detection system (EsB® detector with filtering grid (0–1500 V), a high efficiency in-lens SE detector, a chamber-mounted Everhart–Thornley detector, an Integrated AsB® detector EBS, SE). The EDS Oxford INCA Energy 350 system was used for microanalysis. Energy dispersive X-ray spectroscopy (EDS) allowed for elemental and chemical analysis of the samples.

3. Results and Discussion

3.1. Coefficient of Friction and Wear

Figure 2 shows the evolution of the CoF during the wear test for the hybrid composite materials described in Table 1.

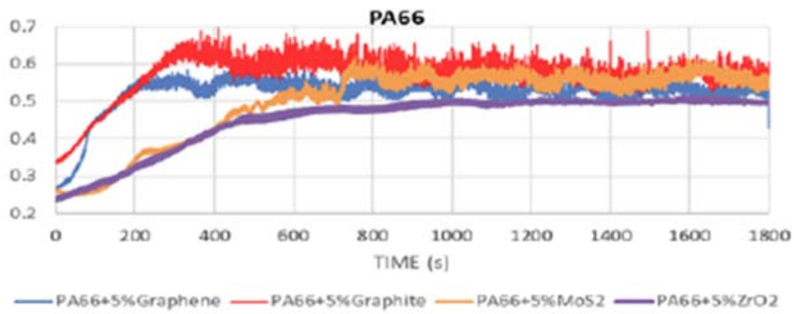

(a)

Figure 2. *Cont.*

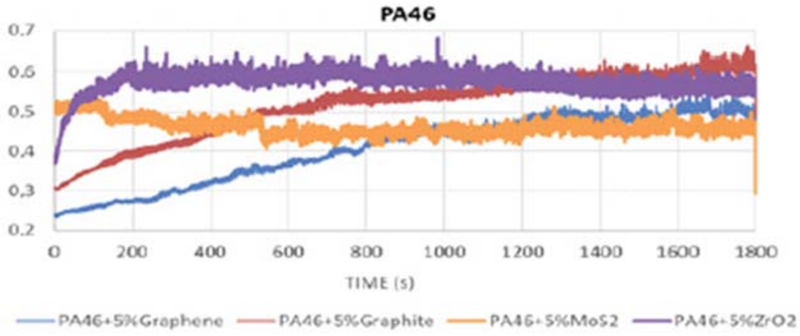

(b)

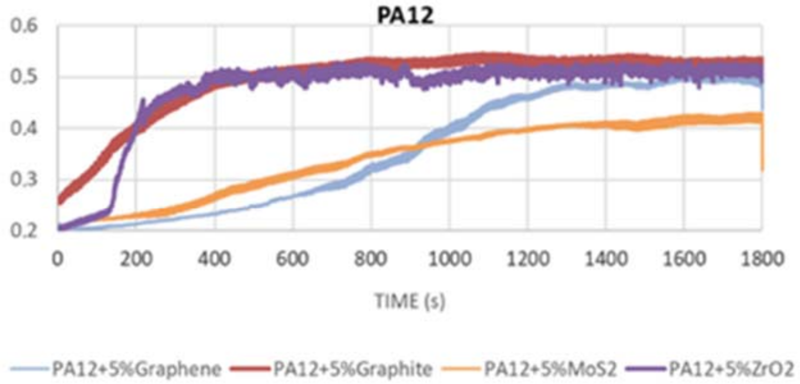

(c)

Figure 2. CoF evolution for composites based on (**a**) PA66, (**b**) PA46, and (**c**) PA12.

The results exhibit an increasing trend of the CoF during the running-in stage for all composites. Then, once the transfer film is created and remains intact, the curves reach a steady stage, exhibiting constant values [60,61].

Lower values of CoF are achieved with ZrO_2, graphene and MoS_2 in the case of the PA66 (Figure 2a) composites, obtaining values of 0.49, 0.52 and 0.53, respectively. PA66 samples doped with graphite have higher CoF values ($\mu = 0.59$). Regarding PA46 composites, lower values of CoF are achieved for samples doped with MoS_2 ($\mu = 0.45$). PA46 samples (Figure 2b) doped with graphene show a CoF value of 0.5, and those doped with graphite and ZrO_2 have higher friction coefficients ($\mu = 0.57$ and 0.58, respectively). In the case of PA12-based composites (Figure 2c), almost all the samples show lower CoF values than the rest of the composites for each additive. The low values of CoF achieved for samples doped with MoS_2 ($\mu = 0.41$) are remarkable.

Table 2 summarises the average values of the CoF, which were calculated by averaging the experimental values from the steady-state stage in Figure 2, as well as the specific wear rate w_s, calculated using Equation (1).

Table 2. Summary of wear test results for hybrid composites.

Material	μ		Δm (mg)	w_s 10^{-3} (mm^3/Nm)
	Average	Standard Deviation		
PA66GN	0.52	0.018	0.35	0.010
PA66GT	0.59	0.027	0.25	0.007
PA66M	0.53	0.051	0.24	0.006
PA66Z	0.49	0.011	0.000 *	-
PA46GN	0.51	0.063	0.11	0.003
PA46GT	0.57	0.030	0.02	0.001
PA46M	0.45	0.014	0.25	0.006
PA46Z	0.58	0.019	−0.06 *	-
PA12GN	0.48	0.010	0.07	0.002
PA12GT	0.52	0.011	0.10	0.003
PA12M	0.41	0.008	0.03	0.001
PA12Z	0.50	0.009	−0.09 *	-

* ZrO2 composites show odd weight results that will be further analysed in this manuscript.

According to Table 2, mass loss and, thus, its wear rate are reduced for the sample composites based on PA46 and PA12, achieving values under 0.003 for the wear rate in most of the samples. PA66 composites exhibit a worse behaviour with mass loss values over 0.24; 0.35 in the case of graphene, 0.25 in the case of graphite and 0.24 in the case of MoS_2. The role of ZrO_2 nanoparticles in all the composites is remarkable, leading to negative values of mass loss in the polymeric pin (zero mass loss in the case of PA66, −0.06mg in the case of PA46 and −0.09 mg in the case of PA12). That is the reason why w_s is not calculated for composites with ZrO2 nanoparticles in Table 2. This fact indicates that polymeric pins increase their mass instead of reducing it, and it will be further analysed. Again, the best results are achieved by the addition of 5% MoS_2 to PA12, reducing the wear rate up to 0.01.

It can be stated that composites with PA12 and PA46 matrices exhibit a better tribological behaviour than the rest of the composites, with lower CoF values and lower wear rates. Since polymers are viscoelastic materials, the material softens because of the relaxation of molecular chains as temperature increases during the friction process in the contact area. As a consequence, Young's modulus decreases, leading to a higher plastic deformation and a higher real contact area, making the adhesive wear mechanism dominant, reducing the wear resistance and increasing the CoF until a transfer layer is constituted [62]. On the other hand, the shear strength is also reduced by increasing the frictional heat, which contributes to the increment of the CoF. In the case of the PA46 matrix, its molecular structure is characterised by a higher number of functional groups in the polymeric chain, which form strong hydrogen bonds, as well as the highest amide group density of all commercial polyamides, resulting in a higher melting temperature [63]. Since the wear mechanism for polymers is mainly adhesive, and the wear is caused by frictional heat between the two contact surfaces, PA46 is capable of reducing damage thanks to the higher melting temperature and a less adhesive wear, due to a lower plastic deformation and a lower increase in contact area. On the other hand, both matrices, PA46 and PA12, have a higher crystallinity, near 70%, which keeps Young's modulus very high (3300 MPa for P46 [53] and 1700 MPa for PA12 [54]), even up to temperatures near their melting point, avoiding higher levels of plastic deformation [64] and thus reducing the wear. In the case of the PA66 matrix, a more severe wear is achieved corresponding to the generation of higher temperatures on the sample surfaces due to the increased frictional heating.

It seems that the transition point is associated with the softening temperature of the sample material. Provided that the surface temperatures with PA12 and PA46 matrices are below this level, mild wear occurs with very low rates of material loss for PA46 and PA12 composites. Above this level, a more severe wear is found for PA66 composites.

3.2. Influence of Nanoadditives

It has been demonstrated that incorporating nanoadditive contents into the polymer matrix modifies the wear mechanism [9]. This means that the particles incorporated in the polymer effectively act to restrain the direct contact between the polymer and the hard steel counterpart, owing to their good solid lubricating and easy shearing action [51]. Subsequently, the friction and the wear are seriously decreased regarding non-doped materials. The presence of nanoadditives plays two main roles in order to improve wear properties. Firstly, the thermal conductivity of some nanoadditives is much higher than the thermal conductivity of the polymeric matrix (0.1–0.4 W/mK for nylons, >3000 W/mK for graphene [65], 300 W/mK for graphite [66], 85 W/mK for MoS_2 [67] and ≈ 2 W/mK for ZrO_2 [68]). This fact and the large surface area of the nanofillers show that the heat between the contact surfaces can be easily dissipated during the wear process. Therefore, as a consequence of a weaker softening of the polymeric matrix, severe adhesive wear is reduced.

Secondly, the presence of nanoadditives in polymeric matrices prevents crack propagation generated during the sliding process, thanks to the efficient stress transfer from the polymer matrix to the nanoadditives, leading to a mild wear mechanism [69]. On the other hand, according to [44], a material can be worn in a chemical and/or mechanical way, and the heat generated during the wear process can contribute to it. In the case of MoS_2 particles, Mo atoms can become oxidised to MoO_3, and S atoms can become oxidised and react with the Fe substrate, turning into FeS. This enhances adhesion between the counterpart and the transfer film and prevents its loss, improving the wear properties of the MoS_2 composite [70].

These observations indicate that the proposed fillers, in small quantities, were helpful for a wear reduction, as has been supported in the literature [9].

3.3. Characterisation of the Worn Surface

Figure 3 shows worn surfaces of pins based on a PA66 matrix. A top layer disintegration is observed in Figure 3a,b for samples doped with graphene and graphite. Removed material appears in the form of blocks, indicating an adhesive wear mechanism. Figure 3a shows a smoother worn surface, which reveals that the graphene particles strongly protect the top of the composite material surface under dry sliding test conditions. There is not any significant crack formation, broken particles or wedge formation, which means good bonding between the graphene filler and the matrix material. Graphene particles become integrated in the PA66 composites and, consequently, the worn surface is protected from the wear and friction. This may be due to the excellent self-lubricity of graphene that reduced the friction and the wear of the polymer composites [9]. Figure 3b shows the back transfer of the material in a patchy form, indicating an adhesive wear, as well as some mild abrasive wear with shallow grinding marks. Nevertheless, the severity of the wear mechanism is reduced due to the presence of graphite. The bonding strength of graphite is appreciable on the surface of the composites, indicating the migration action and the layer formation of graphite with a polymeric matrix, although weak wear track formation is also visible [71,72].

Figure 3c shows a relatively rough worn surface of a sample doped with MoS_2, with some matrix damage and weak wear tracks, which also confirm the adhesive wear mechanism. In the same way, slight plastic deformation is observed in Figure 3d for PA66Z. Nevertheless, ZrO_2 particles could interrupt the material deformation during the wearing process and hinder the propagation of potential cracks, and thus reduce the wear rate and the coefficient of friction. Additionally, the formed smooth worn surface can facilitate the sliding movement by reducing the adhesion and abrasive wear, hence protecting the polymeric matrix.

In the case of samples based on a PA12 matrix, the distribution of graphene nanoplatelets results in a high surface mechanical strength. The high surface mechanical strength helps in preventing deep wear grooves during the sliding action that appear in non-doped PA12 [73].

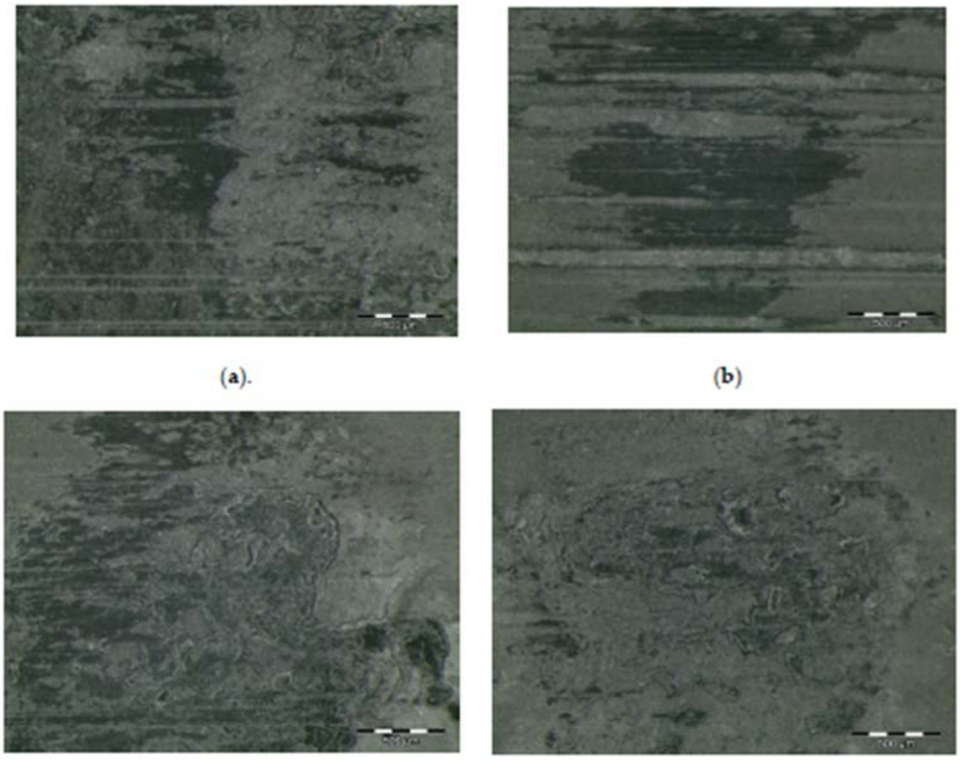

(a). (b)

(c). (d)

Figure 3. Worn surfaces of PA66 composites: (**a**) PA66 + 5% graphene; (**b**) PA66 + 5% graphite; (**c**) PA66 + 5% MoS2; (**d**) PA66 + 5% ZrO_2.

Besides the surface properties, the transfer films formed during sliding also play a significant role in controlling the wear behaviour of the materials [9]. During the sliding process, these graphene nanoplatelets were easily released from the PA12 nanocomposites and transferred between the PA12 nanocomposites contact zone and the abrasive counterface. Thus, graphene nanoplatelets could work as a solid lubricant material between the two contacted surfaces and prevent direct contact between them, thereby reducing the coefficient of friction and increasing the wear resistance. This resulted in a mild wear mechanism with fewer marks on a PA12GF pin surface, as shown in Figure 4a. Figure 4b shows that PA12GT abraded surfaces are less smooth than samples doped with graphene, as shown by the initiation of cracking on the worn surface. This phenomenon can be attributed to the presence of severe plastic deformation during the friction and wear tests. Accordingly, the wear mechanism can be defined as adhesive and slightly abrasive. Figure 4c shows some spiky marks indicating the presence of a tribofilm formed with the MoS_2. In the sample of PA12Z shown in Figure 4d, some crater grooves appear, indicating that some ZrO_2 particles detached and caused damage in the PA matrix. The dark colour can be attributed to steel material from the counterface.

Similar to samples of PA66 doped with graphene and graphite, an adhesive wear mechanism is activated for PA46 pin surfaces, as shown in Figure 5a,b, exhibiting removed material from the surface in the form of blocks. Regarding samples doped with MoS_2, in Figure 5c, transverse cracks, spaced unevenly, are seen across the wear surfaces of the PA46 + MoS_2 samples as well as the formation of polished surfaces and areas of melting, indicating a severe adhesive wear. Tensile stresses produced in the contact area and the high surface temperatures created play a significant role in the crack formation. These worn surfaces reflect some typical fatigue deformations with deep cracks and compact furrows.

Figure 5d shows local plastic deformation in the contact area for samples of PA46 doped with ZrO_2, confirming an adhesive wear mechanism.

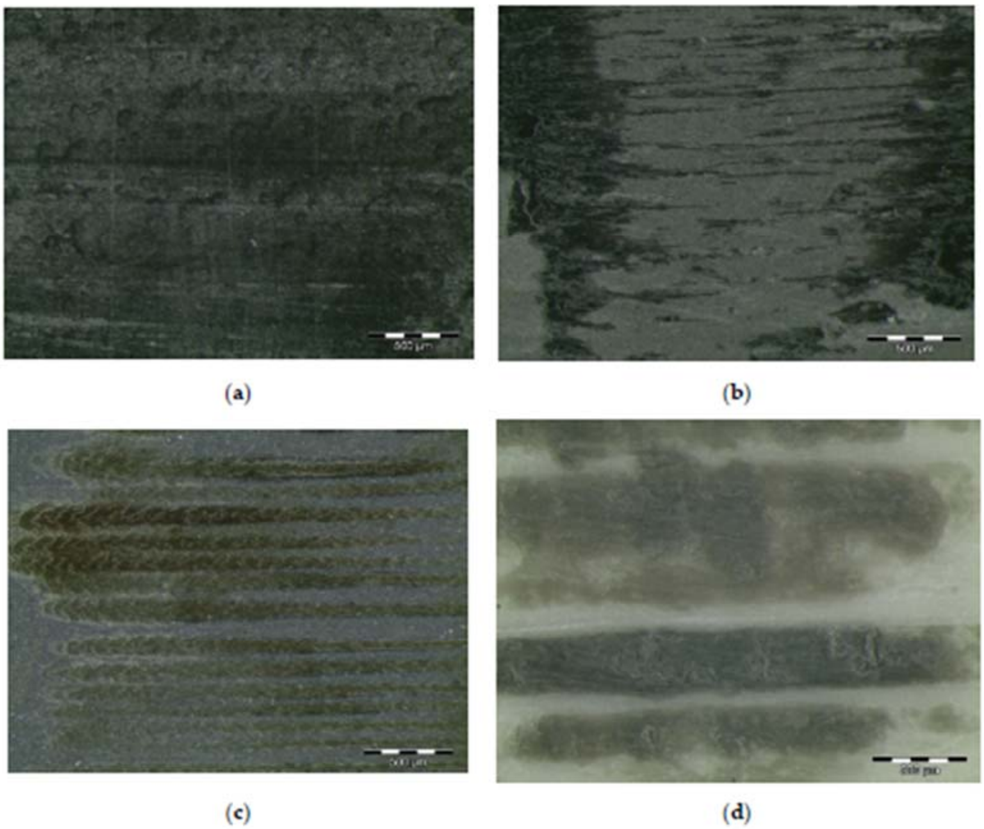

Figure 4. Worn surfaces of PA12 composites: (**a**) PA12 + 5% graphene; (**b**) PA12 + 5% graphite; (**c**) PA12 + 5% MoS_2; (**d**) PA12 + 5% ZrO_2.

Since PA46 has better mechanical properties than the rest of the matrix, which are required for global bearing cage design, we selected PA46 composites to perform a deeper analysis to better understand the influence of nanoadditives and transfer film generation after a pin-on-disc test. PA46 samples without nanoadditives were tested in the same conditions as the rest of the samples, obtaining a value of CoF of 0.62, which is coherent with previous literature [74,75]. The average coefficient of friction values reported for PA46 samples with nanoadditives are much lower than these values, demonstrating the positive effect of nanoadditives in reducing the CoF value significantly.

Given the results presented above, as previously stated, a deeper analysis of PA46 composites was performed in order to better understand transfer film generation. SEM images were obtained and EDS analysis was carried out on discs to check sample composition.

Based on the EDS spectrum results, summarised in Table 3, it can be concluded that, for non-doped PA46, transfer film is formed after the pin-on-disc test since the carbon quantity increases from 4.49, in Figure 6 for non tested disc, to 34.75% and oxygen appears with an amount of 5.82% in Figure 7. The same phenomena can be observed for PA46GT in Figure 8, where carbon weight changes from 4.49% to 10.56% and oxygen emerges with 32.88%. In PA46GN (Figure 9), tribofilm is also formed since the carbon quantity rises up to 7.12% and oxygen surfaces with a weight of 26.29%. When analysing PA46M in Figure 10, transfer film formation can be confirmed not only by a carbon quantity increase (from 4.49% to 10.72%) and oxygen presence (44.35%), but sulphur also arises with a content of 0.49%. Finally, concerning PA46Z samples in Figure 11, the rise of carbon weight grows from 4.49% to 38.79% and the emergence of oxygen by 13.68%, which leads to the conclusion of tribofilm formation.

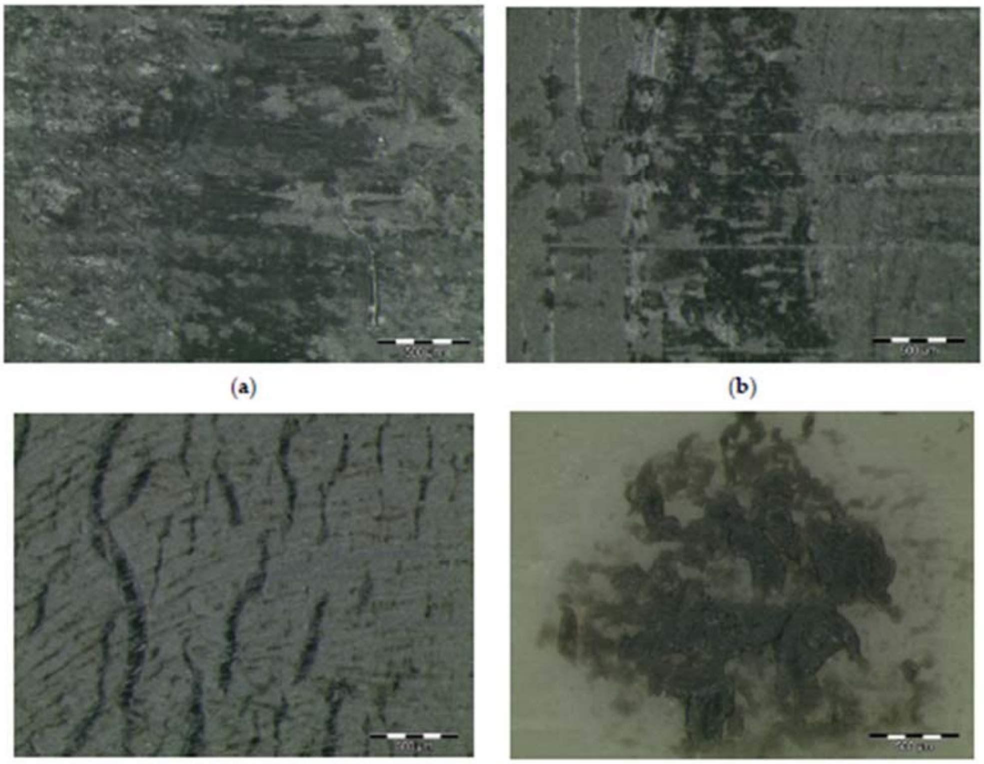

Figure 5. Worn surfaces of PA46 composites: (**a**) PA46 + 5% graphene; (**b**) PA46 + 5% graphite; (**c**) PA46 + 5% MoS_2; (**d**) PA46 + 5% ZrO_2.

Table 3. Summary of EDS spectra for PA46 samples.

Element	Weight (%)					
	Non-Tested Disc	**PA46**	**PA46GT**	**PA46GN**	**PA46M**	**PA46Z**
C K	4.49%	34.75%	10.56%	7.12%	10.72%	38.79%
Cr K	1.49%	0.73%	3.48%	1.76%	0.41%	0.34%
Fe K	93.24%	57.63%	50.67%	62.18%	43.65%	22.62%
Si K	0.77%	0.53%	2.02%	2.13%	0.38%	0.30%
O K		5.82%	32.88%	26.29%	44.35%	13.68%
Ca K		0.30%	0.38%			
S K					0.49%	0.30%
Al K		0.24%				
Cl K				0.53%		
Na K						0.86%
Cu K						14.62%
Zn K						8.49%

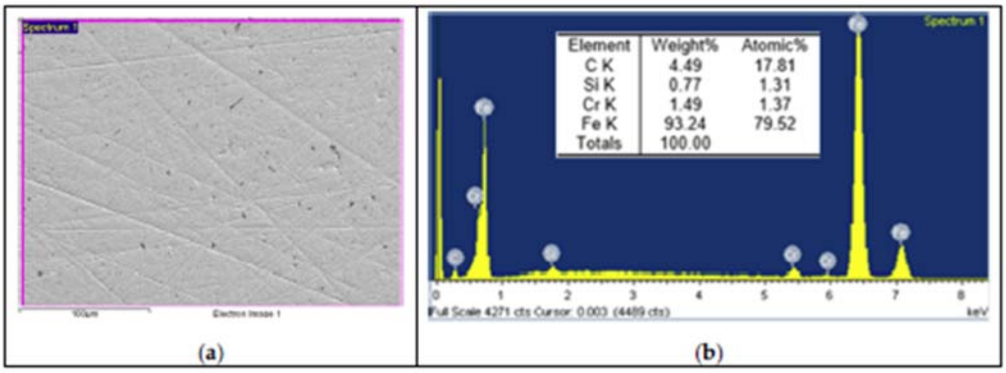

Figure 6. (**a**) SEM image and (**b**) EDS spectrum for non-tested discs.

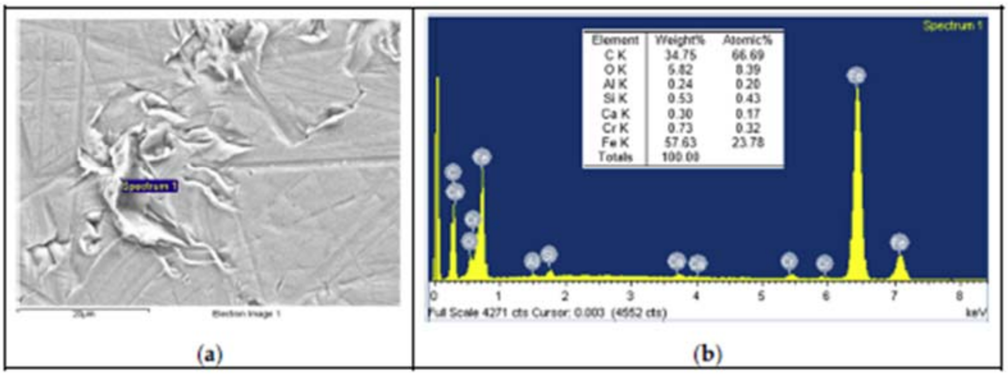

Figure 7. (**a**) SEM image and (**b**) EDS spectrum for discs tested against the non-doped PA46 sample.

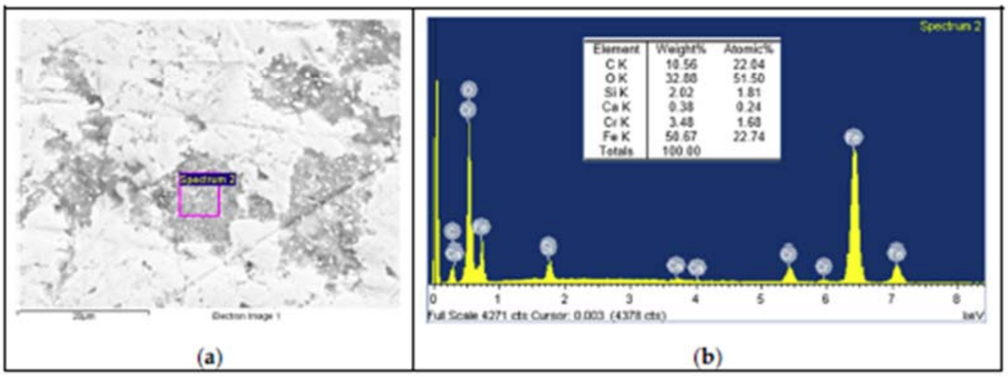

Figure 8. (**a**) SEM image and (**b**) EDS spectrum for discs tested against the PA46GT sample.

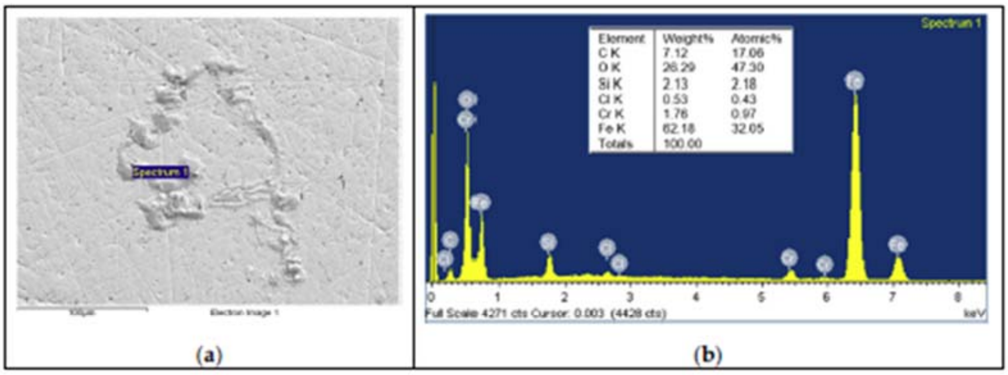

Figure 9. (**a**) SEM image and (**b**) EDS spectrum for discs tested against the PA46GN sample.

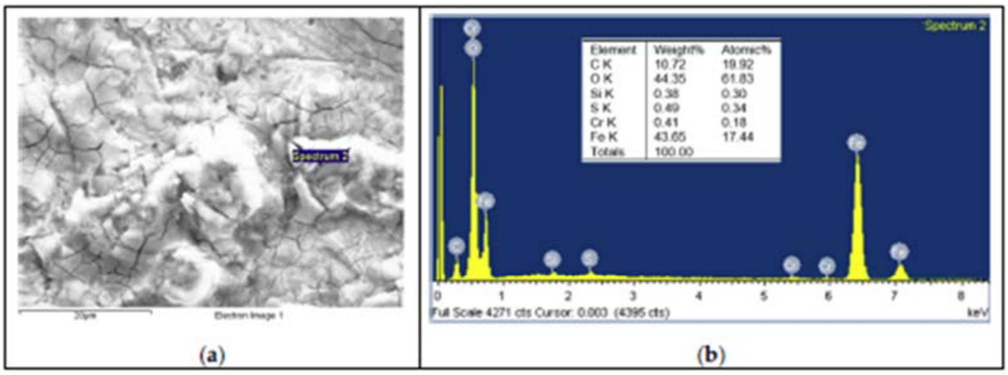

Figure 10. (**a**) SEM image and (**b**) EDS spectrum for discs tested against the PA46M sample.

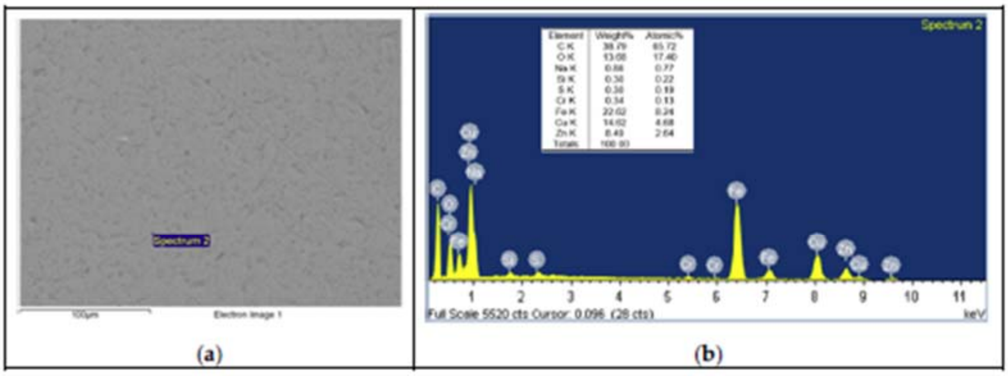

Figure 11. (**a**) SEM image and (**b**) EDS spectrum for discs tested against the PA46Z sample.

3.4. Analysis of Wear in ZrO_2 Composites

The negative wear values obtained in the tests and shown in Table 2 could be attributed to the transfer of metallic particles of the 100Cr6 disc to the polymeric pin. The dark colour in Figure 5d also could indicate the presence of steel material from the counterface. Since PA46Z samples show the highest negative mass loss, they were subjected to a further analysis of their surface and composition by means of SEM and EDS. Figure 12 shows the surface aspect of a pin on which two different zones, representative of the main wear mechanism produced in the pin surface, were analysed (zone 1 and zone 2). These two different zones are selected for further analysis because the contact of the pin against the counterface is not exactly the same at zone 1 and zone 2, as can be appreciated in Figure 12. Since the sample pin surfaces are not entirely flat and the pin could not be properly aligned during the test, zone 1 and 2 do not contact in the same way against the counterface, and they should both be studied.

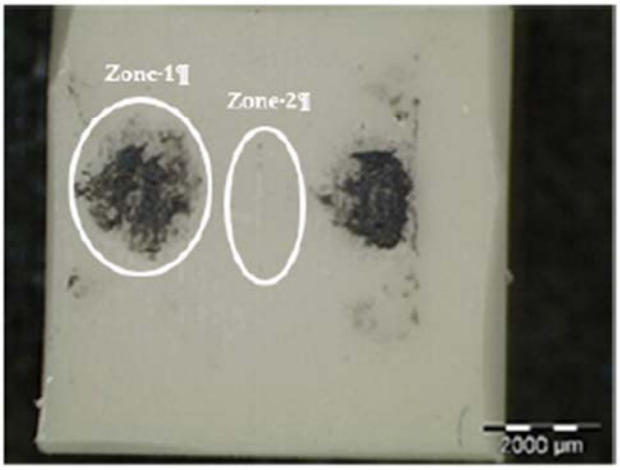

Figure 12. Surface of PA46Z after testing.

Figure 13 shows an SEM image of zone 1, where two EDS analyses were carried out. Figure 14 shows the EDS spectrum for the general area shown in Figure 13, and Figure 15 shows the EDS spectrum for the area marked with an arrow in Figure 13, where white spots of ZrO_2 appear. Figure 16 shows an SEM image of zone 2, where two EDS analyses were carried out as well. Figure 17 shows the EDS spectrum for the general area shown in Figures 16 and 18 shows the EDS spectrum for the area marked with an arrow in Figure 16, where white spots of ZrO_2 appear.

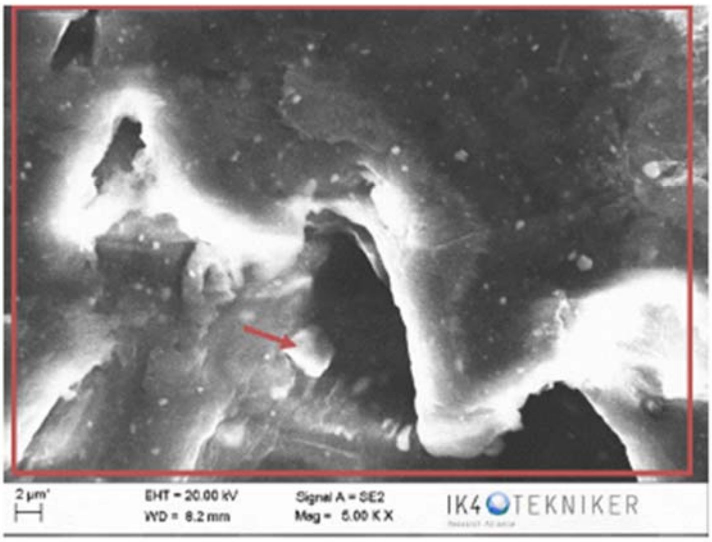

Figure 13. SEM image for zone 1 in the PA46Z sample.

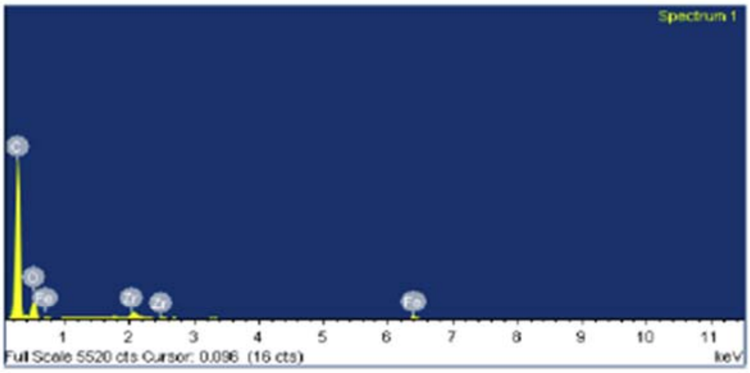

Figure 14. EDS spectrum for zone 1 in the PA46Z sample.

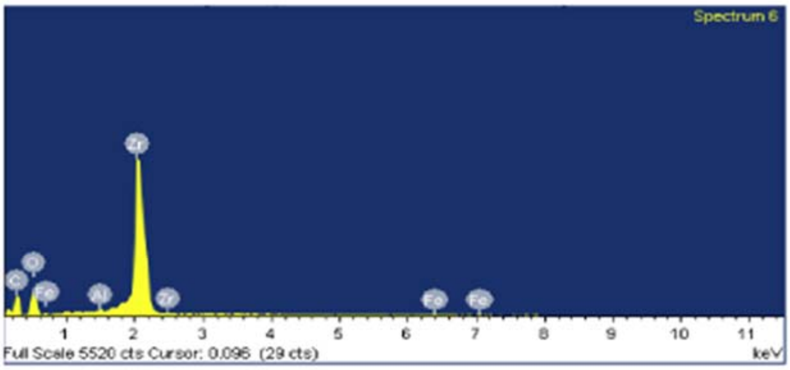

Figure 15. EDS spectrum for zone 1 in a local area marked with an arrow in Figure 13, where ZrO_2 is located.

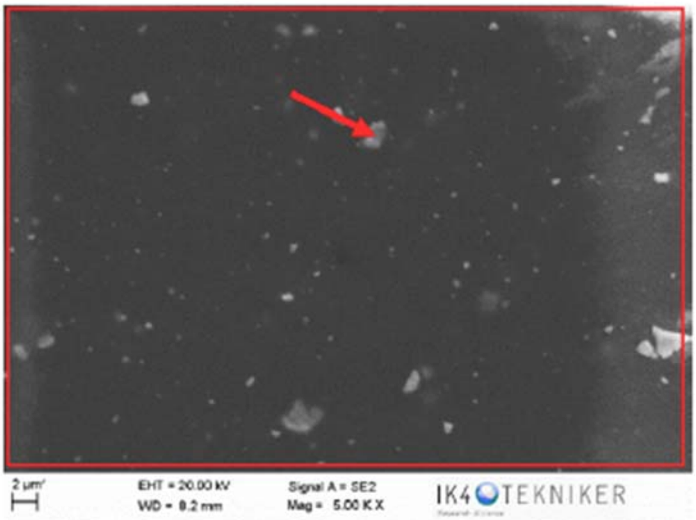

Figure 16. SEM image for zone 2 in the PA46Z sample.

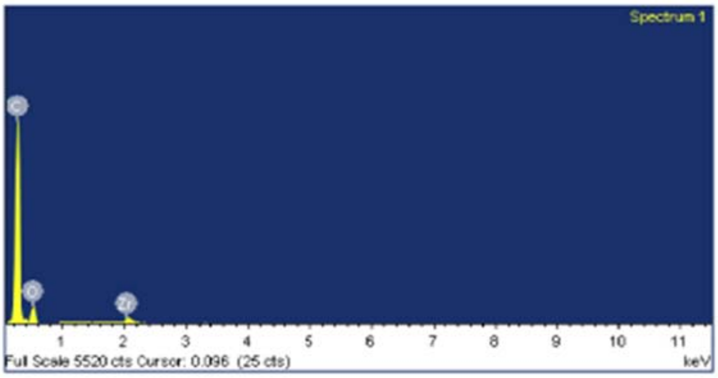

Figure 17. EDS spectrum for zone 2 in the PA46Z sample.

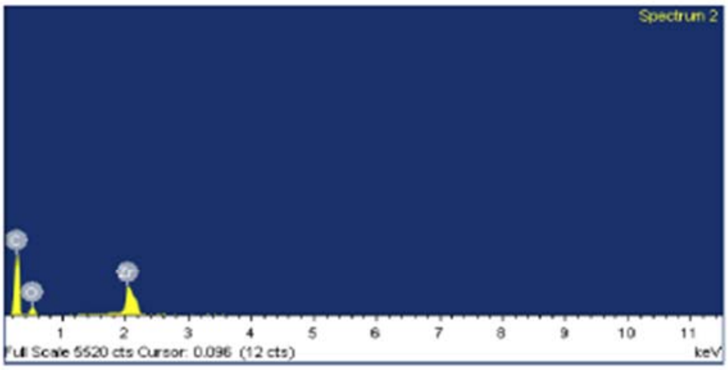

Figure 18. EDS spectrum for zone 2 in a local area marked with an arrow in Figure 16, where ZrO_2 is located.

In both zones 1 and 2 of the pin sample, white spots appear, indicating the presence of ZrO_2 particles dispersed into the polymer matrix (Figures 13 and 16). The presence of these particles in zone 1 is confirmed by the identification of Zr and O peaks of the spectra in Figures 14 and 15. Since the spectrum in Figure 15 is obtained directly from a particle of ZrO_2, the Zr peak intensity is higher than in Figure 14, where the spectrum is calculated for the whole area shown in Figure 13. Figures 17 and 18 also confirm the presence of these ZrO_2 particles in zone 2, with the appearance of Zr and O peaks in the spectra. These peaks are lower due to the poorer contact between the pin and counterface in zone 2.

EDS spectra in Figures 14 and 15 for zone 1 also show Fe peaks, indicating that the metallic wear particles of the 100Cr6 disc were transferred to the polymeric pin, which supports the hypothesis made from Figure 5d that metallic transfer to the pin had occurred.

The disc counterface area tested against the pin was also analysed by SEM and EDS. It can be observed in Figure 19 that abrasion marks appear, as well as some traces of ZrO_2 (marked with an arrow). A smoother surface is observed in Figure 20 for areas of the counterface that had not been tested against the pin. To confirm this hypothesis, an EDS analysis was carried out on the area in Figure 19. Figure 21 shows the EDS spectrum for the area marked with an arrow in Figure 19, where traces of ZrO_2 appear. The spectrum shows peaks of Zr and O, confirming that particles of ZrO_2 were transferred to the disc. Wear traces in Figure 19 could come from these detached particles of ZrO_2 transferred to the disc that, due to its high hardness (1200 HV), cause damage to the metallic disc. Figure 20 shows a SEM image of the disc of a non-tested area. It does not show any deep mark of abrasion nor any trace of ZrO_2.

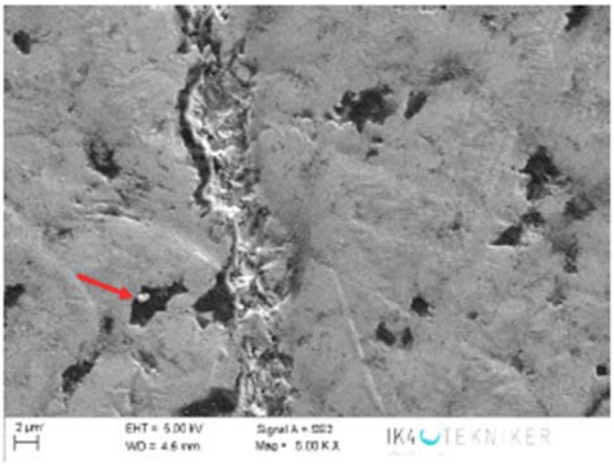

Figure 19. SEM image of a tested area of the disc against a PA46Z pin.

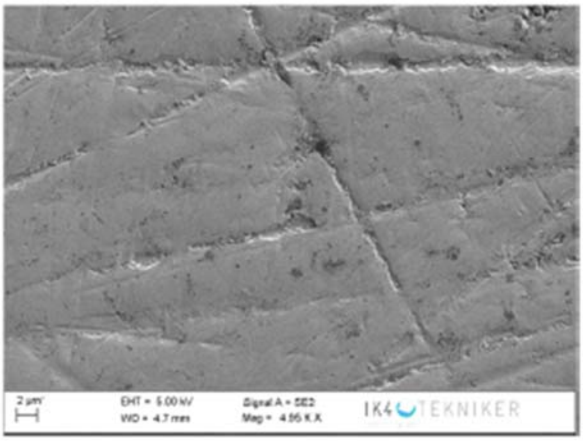

Figure 20. SEM image of a non-tested area of the disc.

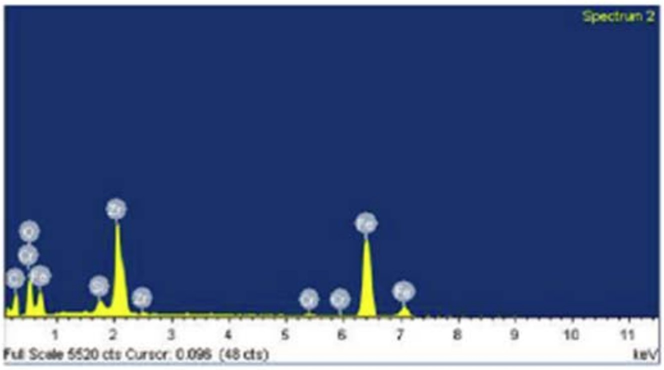

Figure 21. EDS spectrum of the marked area in Figure 19, where traces of ZrO_2 appear.

On the other hand, the presence of traces of tribofilm transferred to the disc can be confirmed from EDS analysis on tested and non-tested areas of the disc. Figure 22 shows the composition of a non-tested area of the disc, where low percentages of carbon appear. Figure 23 shows the composition of a tested area of the disc. In this case, the percentage of carbon is higher due to the presence of a polymer tribofilm on the disc surface. This presence of the tribofilm on the disc confirms the adhesive wear mechanism for this kind of tribopair.

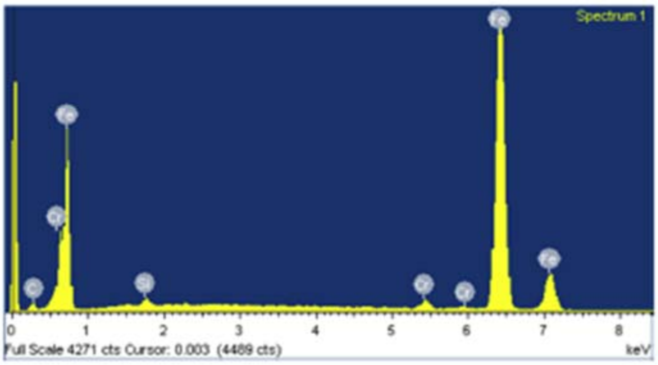

Figure 22. EDS spectrum of a non-tested area of the disc.

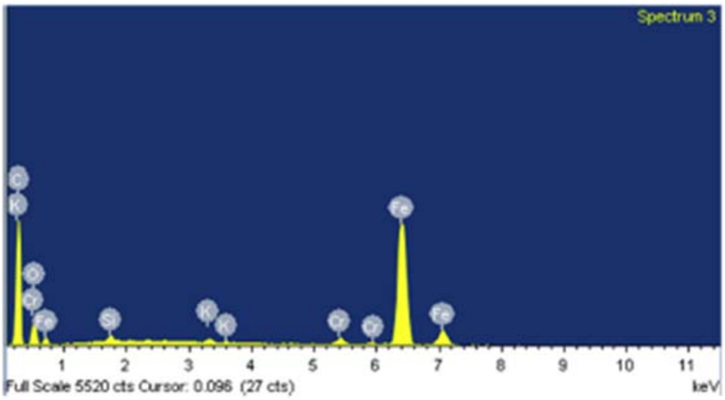

Figure 23. EDS spectrum of a tested area of the disc.

4. Conclusions

A systematic study comparing the tribological behaviour of different composites based on nylon matrices (PA66, PA46 and PA12) with nanoadditives and reinforcing additives (graphene, graphite, ZrO_2 and MoS_2) was carried out.

The results show that the polyamide matrix based on PA12 exhibits lower coefficients of friction for most of the additives tested, graphene, ZrO_2 and MoS_2, thanks to their better properties related to higher degrees of crystallinity. On the other hand, PA66 composites showed higher wear rate properties in comparison to PA46 and PA12 composites, mainly due to their poorer properties compared to PA46 and PA12.

The wear mechanism can be defined as adhesive. The presence of nanoadditives modifies the wear mechanism thanks to their higher thermal conductivity, larger surface area and prevention of cracking propagation in the polymer matrix. Graphene and MoS_2 exhibit better results than graphite for most of the matrices. Although composites doped with ZrO_2 achieve low coefficients of friction during tests, a transference of metallic particles from the disc to different areas of the polymeric pin is observed. ZrO_2 particles, detached from the pin, are deposited on the disc, causing abrasion damage and allowing metallic particles to be transferred to the polymeric sample, causing some mild abrasive wear.

Author Contributions: Conceptualisation, G.M., Á.F. and P.C.; Formal analysis, A.L., Á.F. and P.C.; Funding acquisition, S.G., I.M., Á.F. and P.C.; Investigation, G.M., A.L. and P.C.; Methodology, A.L., Á.F. and P.C.; Project administration, S.G. and I.M.; Resources, A.L. and D.E.; Supervision, S.G. and I.M.; Validation, S.G., I.M. and G.M.; Visualisation, I.C. and D.E.; Writing—original draft, I.C. and A.L.; Writing—review and editing, S.G., I.M. and G.M. All authors have read and agreed to the published version of the manuscript.

Funding: This research was funded by Fersa Bearings S.A, the Spanish Ministry of Industry, Economics and Competitivity (RTC-2016-5799-4), the Regional Government of Aragón, Spain (INNOVA-A1-008-15) and the University of Zaragoza (BOA 10-OTRI 2016/0172). The study was performed by members of the I+AITIIP (DGA-T08_17R) research group of the FEDER 2014-2020 "Building Europe from Aragón" programme recognised by the Regional Government of Aragón.

Acknowledgments: Authors wish to thank Cristina Zubizarreta and Bihotz Pinedo for the role they played during tests performed at TEKNIKER facilities.

Conflicts of Interest: The authors declare no conflict of interest.

References

1. Holmberg, K.; Andersson, P.; Nylund, N.-O.; Mäkelä, K.; Erdemir, A. Global energy consumption due to friction in trucks and buses. *Tribol. Int.* **2014**, *78*, 94–114. [CrossRef]
2. Jost, H.P. Tribology: Origin and future. *Wear* **1990**, *136*, 1–17. [CrossRef]
3. Morita, T.; Andatsu, K.; Hirota, S.; Kumakiri, T.; Ikenaga, M.; Kagaya, C. Effect of Hybrid Surface Treatment Composed of Plasma Nitriding and DLC Coating on Friction Coefficient and Fatigue Strength of Stainless Steel. *Mater. Trans.* **2013**, *54*, 732–735. [CrossRef]
4. Ceschini, L.; Chiavari, C.; Marconi, A.; Martini, C. Influence of the countermaterial on the dry sliding friction and wear behaviour of low temperature carburised AISI316L Steel. *Tribol. Int.* **2013**, *67*, 36–37. [CrossRef]
5. Claveria, I.; Lostalé, A.; Fernández, A.; Castell, P.; Elduque, D.; Mendoza, G.; Zubizarreta, C. Enhancement of tribological behaviour of rolling bearings by applying a multilayer ZrN/ZrCN coating. *Coatings* **2019**, *9*, 434. [CrossRef]
6. Lin, Z.; Sun, F.; Shen, B. Friction properties of polished CVD diamond films sliding against different metals. *Surf. Rev. Lett.* **2016**, *23*, 1550096. [CrossRef]
7. Zhang, X.; Xu, H.; Dong, J. Tribological Properties of Magnesium Ion-exchanged α-Zirconium Phosphate as a Solid Lubricant Additive in Lithium Grease. *J. Wuhan Univ. Tech. Mater. Sci.* **2019**, *34*, 47–54. [CrossRef]
8. Holmberg, K.; Ronkainen, H.; Matthews, A. Tribology of thin coatings. *Ceram. Int.* **2000**, *26*, 787–795. [CrossRef]
9. Claveria, I.; Elduque, D.; Lostalé, A.; Fernández, A.; Castell, P. Analysis of self-lubrication enhancement via PA66 strategies: Texturing and nano-reinforcement with ZrO_2 and graphene. *Tribol. Int.* **2019**, *131*, 332–342. [CrossRef]
10. Ai, S.; Wang, W.; Wang, Y.; Zhao, Z. Temperature rise of double-row tapered roller bearings analysed with thermal network method. *Tribol. Int.* **2015**, *87*, 11–22. [CrossRef]
11. Zhao, X.; Liang, L.; Liu, Z. Tapered Roller Bearings Cage to Improvement Design. *Indones. J. Electr. Eng.* **2014**, *12*, 1855–1859.
12. Neis, P.D.; Ferreira, N.F.; Poletto, J.C.; Sukumaran, J.; Ando, M.; Zhang, Y. Tribological behavior of polyamide-6 plastics and their potential use in industrial applications. *Wear* **2017**, *376*, 1391–1398. [CrossRef]
13. Kastan, A.; Unal, H. Abrasive wear behaviour of polyamide 6/polypropylene/nanoclay composites. *Rom. J. Mater.* **2018**, *48*, 185–190.
14. Blanchet, T.A.; Kennedy, F.E. Sliding wear mechanism of polytetrafluoroethylene (PTFE) and PTFE composites. *Wear* **1992**, *153*, 229–243. [CrossRef]
15. Seo, W.S.; Choe, B.; Lee, Y.; Lee, J.K. Wear of Polymer Composite Solid Lubricants for Cryogenic Ball Bearing Cages. In Proceedings of the Asia International Conference on Tribology 2018, Kuching, Sarawak, 17–20 September 2018; pp. 271–272.

16. Gu, D.; Zhang, L.; Chen, S.; Song, K.; Liu, S. Significant Reduction of the Friction and Wear of PMMA Based Composite by Filling with PTFE. *Polymers* **2018**, *10*, 966. [CrossRef] [PubMed]
17. Li, J. The effect of PTFE on the mechanical and friction and wear properties of GF/PA6 composites. *Adv. Mater. Res.* **2011**, *284–286*, 2370–2373. [CrossRef]
18. Moder, J.; Grun, F.; Summer, F.; Kohlhauser, M.; Wohlfahrt, M. Application of high performance composite polymers with steel counterparts in dry rolling/sliding contacts. *Polym. Test.* **2018**, *66*, 371–382. [CrossRef]
19. Song, J.F.; Zhao, G.; Ding, Q.J.; Qiu, J.H. Reciprocating friction and wear of polyimide composites filled with solid lubricants. *J. Polym. Eng.* **2018**, *38*, 363–370. [CrossRef]
20. Xibata, K.; Fukuda, M.; Yamaguchi, T. Relationship between sliding induced wear and severity of sliding contact for polyamide66 filled with hard filler. *Proc. Inst. Mech. Eng. Part J J. Eng. Tribol.* **2017**, *231*, 783–790. [CrossRef]
21. Pogacnik, A.; Kupec, A.; Kalin, M. Tribological properties of polyamide (PA6) in self-mated contacts and against steel as a stationary and moving body. *Wear* **2017**, *378–379*, 17–26. [CrossRef]
22. Lenfeld, P.; Běhálek, L.; Boruvka, M.; Prusek, J. Dynamic-Mechanical Properties of Polymer Composites with the Short and Long Glass Fibers. *Mater. Sci. Forum* **2016**, *862*, 166–173. [CrossRef]
23. Huynh, D.S.T.; Le, H.G.; Nguyen, T.N.H.; Pham, S.M. Enhancing the Fatigue Property of Nylon 6 by Using Glass-Fiber Reinforcement and Injection Molding. *Mater. Sci. Forum* **2019**, *971*, 85–90. [CrossRef]
24. Gordon, D.H.; Kukureka, S.N. The wear and friction of polyamide 46 and polyamide 46/aramid-fibre Kumar, S.S.; Kanagaraj, J. Investigation on Mechanical and Tribological Behaviours of PA6 and Graphite-Reinforced PA6 Polymer Composites. *Arab. J. Sci. Eng.* **2016**, *41*, 4347–4357.
25. Rajamani, G.; Paulraj, J.; Krishnan, K. Analysis of wear behaviour of graphene oxide—Polyamide gears for engineering applications. *Surf. Rev. Lett.* **2019**, *24*, 1850018. [CrossRef]
26. Hassan, A.E.M.; Eid, A.I.; El-Sheikh, M.; Ali, W.Y. Mechanical and tribological performance of polyamide 12 reinforced with graphene nanoplatelets and paraffin oil nanocomposites. *Mater. Werkst.* **2019**, *50*, 74–85. [CrossRef]
27. Karami, P.; Shojaei, A. Improvement of dry sliding tribological properties of polyamide 6 using diamond nanoparticles. *Tribol. Int.* **2017**, *115*, 370–377. [CrossRef]
28. Khandanur, S.S.; Rafiee, M.A.; Yavari, F.; Schrameyer, M.; Yu, Z.; Blanchet, T.A.; Koratkar, N. Suppression of wear in graphene polymer composites. *Carbon* **2012**, *50*, 3178–3183. [CrossRef]
29. Kalin, M.; Zalaznik, M.; Novak, S. Wear and friction behaviour of poly-ether-ether-ketone (PEEK) filled with graphene, WS2 and CNT nanoparticles. *Wear* **2015**, *332–333*, 855–863. [CrossRef]
30. Yan, S.; Yang, Y.; Song, L.; Qi, X.; Xue, Y.; Duan, C. Tribological Behaviour of Graphite Oxide Reinforced Polyethersulfone Composite Under Drying Sliding Condition. *Polym. Compos.* **2018**, *39*, 2320–2335. [CrossRef]
31. Quiang, L.; Xu, F.; Voisey, K.T.; Nekouie, W.; Zhou, Z.; Silberschmidt, V.V.; Hou, X. Incorporation and evolution of ZrO_2 nanoparticles in Pt-modified aluminide coating for high-temperature applications. *Surf. Coat. Technol.* **2017**, *31*, 238–247. [CrossRef]
32. Ma, J.; Xu, C.H.; Yi, M.D.; Xiao, G.C.; Wang, X.H. Friction and wear property of Ti(C, N)/ ZrO_2/WC nano-composite cermet die material. *Adv. Mater. Res.* **2013**, *834–836*, 23–28. [CrossRef]
33. Song, J.; Liu, Y.; Liao, Z.; Wang, S.; Tyagi, R.; Liu, W. Wear studies on ZrO_2-filled PEEK as coating bearing materials for artificial cervical discs of Ti6Al4V. *Mater. Sci. Eng. C* **2016**, *69*, 985–994. [CrossRef] [PubMed]
34. Mordina, B.; Tiwari, R.K. A comparative study of mechanical and tribological properties of poly (ether ether ketone) composites filled by micro- and nano-Ni and ZrO_2 fillers. *J. Compos. Mater.* **2013**, *47*, 2835–2845. [CrossRef]
35. Cao, W.; Gong, J.; Qi, Y.; Yang, D.; Gao, G.; Wang, H.; Ren, J.; Chen, S. Tribological Behaviour of Nano-ZrO_2 Reinforced PTFE-PPS Composites. *J. Wuhan Univ. Technol. Mater. Sci. Ed.* **2019**, *34*, 527–533. [CrossRef]
36. Vazirisereshk, M.R.; Martini, A.; Strubbe, D.A.; Mehmet, Z.; Baykara, M.Z. Solid Lubrication with MoS_2: A Review. *Lubricants* **2019**, *7*, 57. [CrossRef]
37. Zalaznik, M.; Novak, S.; Huskic, M.; Kalin, M. Tribological behaviour of a PEEK polymer-containing solid MoS_2 lubricants. *Lubr. Sci.* **2016**, *28*, 27–42. [CrossRef]
38. Theiler, G.; Gradt, T. Friction and wear of PEEK composites in vacuum environment. *Wear* **2010**, *269*, 278–284. [CrossRef]

39. Wang, L.; Shi, B.; Hu, E.; Hu, K.; Hu, X. Reuse of spent bleaching clay for supporting MoS_2 nanoparticles as a lubricating filler in ABS plastics. *Tribol. Int.* **2019**, *131*, 415–423. [CrossRef]
40. Xin, Y.; Li, T.; Gong, D.; Xu, F.; Wang, M. Preparation and tribological properties of graphene oxide/nano-MoS_2 hybrid as multidimensional assembly used in the polyimide nanocomposites. *RSC Adv.* **2017**, *7*, 6323–6335. [CrossRef]
41. You, Y.; Li, D.; Si, G.; Deng, X. Investigation of the influence of solid lubricants on the tribological properties of polyamide 6 composite. *Wear* **2014**, *311*, 57–64. [CrossRef]
42. Basavaraj, E.; Ramaraj, B.; Lee, J.; Siddaramaiah. Microstructure, Thermal, Physico–Mechanical and Tribological Characteristics of Molybdenum Disulphide-Filled Polyamide 66/Carbon Black Composites. *Polym. Eng. Sci.* **2013**, *53*, 1676–1686. [CrossRef]
43. Horovistiz, A.; Laranjeira, S.; Davim, J.P. Influence of sliding velocity on the tribological behaviour of PA66GF30 and PA66 + MoS_2: An analysis of morphology of sliding surface by digital image processing. *Polym. Bull.* **2018**, *75*, 5113–5131. [CrossRef]
44. Bai, J.; Song, J.; Wei, J. Tribological and mechanical properties of MoS_2 enhanced polyamide 12 for selective laser sintering. *J. Mater. Process. Technol.* **2019**, *264*, 382–388. [CrossRef]
45. Sahoo, R.R.; Biswas, S.K. Deformation and friction of MoS2 particles in liquid suspensions used to lubricate sliding contact. *Thin Solid Films* **2010**, *518*, 5995–6005. [CrossRef]
46. Zhu, G.P.; Sun, J.L.; Wang, B.; Wang, Y.Z. Study on Tribological Properties of the Rolling Fluid Containing Nano-MoS2 for Cold Rolling of Steel Strip. *China Pet. Process. Petrochem. Technol.* **2011**, *13*, 64–69.
47. Singh, K.K.; Prabhu, B.R.; Choudhary, S.; Pramanik, C. Effect of Graphene and MoS_2 Flakes in Industrial Oils to Enhance Lubrication. *ACS Omega* **2019**, *4*, 14569–14578. [CrossRef]
48. Sahoo, R.R.; Biswas, S.K. Microtribology and Friction-Induced Material Transfer in Layered MoS_2 Nanoparticles Sprayed on a Steel Surface. *Tribol. Lett.* **2010**, *37*, 313–326. [CrossRef]
49. Han, H.L.; Qian, Z.Y. Tribological performances of graphite-MoS_2 coating at various high temperatures. *Proc. Inst. Mech. Eng. Part J J. Eng. Tribol.* **2019**, *233*, 1888–1902. [CrossRef]
50. Mutyala, K.C.; Wu, Y.M.A.; Erdemir, A.; Sumant, A.V. Graphene—MoS_2 ensembles to reduce friction and wear in DLC-Steel contacts. *Carbon* **2019**, *146*, 524–527. [CrossRef]
51. Zhang, X.; Liao, G.; Jin, Q.; Feng, X.; Jian, X. On dry sliding friction and wear behaviour of PPESK filled with PTFE and graphite. *Tribol. Int.* **2008**, *41*, 195–201. [CrossRef]
52. BADAMID A70 S Technical Datasheet. 2008. Available online: http://www.performance-plastics.co.uk/wp-content/uploads/TD_Badamid_A70_S.pdf (accessed on 17 January 2020).
53. Stanyl® TW341 Technical Datasheet. 2018. Available online: https://plasticsfinder.com/en/datasheet/Stanyl%C2%AE+TW341/V67x4 (accessed on 17 January 2020).
54. BADAMID® PA12H Technical Datasheet. 2011. Available online: http://www.performance-plastics.co.uk/wp-content/uploads/PA12-TDS.pdf (accessed on 17 January 2020).
55. MICROZIR® ULTRAFINE Technical DATA SHEET. 2018. Available online: http://www.chilchesmaterials.com/producto/microzir-ultrafine-2/ (accessed on 17 January 2020).
56. Brugarolas, S.L. 2020. Available online: https://brugarolas.com (accessed on 17 January 2020).
57. Graphene Tech S.L. 2016. Available online: http://www.graphene-tech.net/ (accessed on 17 January 2020).
58. Blanco, M.; Sarasua, J.A.; López, M.; Gonzalo, O.; Marcaide, A.; Muniesa, M.; Fernández, A. Ultrasound Assisted Extrusion of Polyamide 6 Nanocomposites Based on Carbon Nanotubes. *Macromol. Symp.* **2012**, *321–322*, 80–83. [CrossRef]
59. Muniesa, M.; Fernández, A.; Claveria, I.; Javierre, C.; Sarasua, J.A.; Blanco, M. A new extrusion head with integrated ultrasonic device and online process parameters measurements system—Design and testing. *Polimery* **2015**, *60*, 209–216. [CrossRef]
60. Bahadur, S. The development of transfer layers and their role in polymer tribology. *Wear* **2000**, *245*, 92–99. [CrossRef]
61. Quaglini, V.; Dubini, P.; Ferroni, D.; Poggi, C. Influence of counterface roughness on friction properties of engineering plastics for bearing applications. *Mater. Des.* **2009**, *30*, 1650–1658. [CrossRef]
62. Meng, H.; Sui, G.X.; Sie, G.Y.; Yang, R. Friction and wear behaviour of carbon nanotubes reinforced polyamide 6 composites under dry sliding and water-lubricated condition. *Compos. Sci. Technol.* **2009**, *69*, 606–611. [CrossRef]

63. PA46 Technical Data. 2020. Available online: https://www.designerdata.nl/kunststoffen/thermoplasten/PA46?cookie=YES (accessed on 17 January 2020).
64. Boric, A.; Kalendová, A.; Urbanek, M.; Pepelnjak, T. Characterisation of Polyamide (PA) 12 Nanocomposites with Montmorillonite (MMT) Filler Clay Used for the Incremental Forming of Sheets. *Polymers* **2019**, *11*, 1248. [CrossRef]
65. Balandin, A.A.; Ghosh, S.; Bao, W.; Calizo, I.; Teweldebrhan, D.; Miao, F.; Lau, C.N. Superior Thermal Conductivity of Single-Layer Graphene. *Nano Lett.* **2008**, *8*, 902–907. [CrossRef]
66. Li, Z.; Sun, W.G.; Wang, G.; Wu, Z.G. Experimental and numerical study on the effective thermal conductivity of paraffin/expanded graphite composite. *Sol. Energy Mater. Solar Cells* **2014**, *128*, 447–455. [CrossRef]
67. Aiyiti, A.; Bai, X.; Wu, J.; Xu, X.; Li, B. Measuring the thermal conductivity and interfacial thermal resistance of suspended MoS_2 using electron beam self-heating technique. *Sci. Bull.* **2018**, *63*, 452–458. [CrossRef]
68. Orain, S.; Scudeller, Y.; Brousse, T. Thermal conductivity of ZrO_2 thin films. *Int. J. Therm. Sci.* **2000**, *39*, 537–543. [CrossRef]
69. Yan, S.; Yan, Y.; Song, L.; Qi, X.; Zuo, Z.; Xue, Y. Tribological property of 3-aminopropyltriethoxysilane-graphite oxide nanosheets reinforced polyethersulfone composite under drying sliding condition. *Tribol. Int.* **2016**, *103*, 316–330. [CrossRef]
70. Yu, L.; Yang, S.; Liu, W.; Xue, Q. An investigation of the friction and wear behaviours of polyphenylene sulfide filled with solid lubricants. *Polym. Eng. Sci.* **2010**, *40*, 1825–1832. [CrossRef]
71. Wang, Q.; Zhang, X.; Pei, X. Study on the synergistic effect of carbon fibre and graphite and nanoparticle on the friction and wear behaviour of polyimide composites. *Mater. Des.* **2010**, *31*, 3761–3768. [CrossRef]
72. Suresha, B.; Chandramohan, G.; Renukappa, M.N.; Siddaramaiah. Mechanical and Tribological Properties of Glass–Epoxy Composites with and Without Graphite Particulate Filler. *J. Appl. Polym. Sci.* **2007**, *103*, 2472–2480. [CrossRef]
73. Kim, S.S.; Shin, M.W.; Jang, H. Tribological properties of short glass fibre reinforced polyamide 12 sliding on medium carbon steel. *Wear* **2012**, *274–275*, 34–42. [CrossRef]
74. Yamada, Y.; Kurobe, T.; Toyooka, Y. XPS study of transfer films of MoS_2 filled nylon-46 composites sliding against steel counterfaces. *J. Mater. Sci. Lett.* **2001**, *20*, 577–579. [CrossRef]
75. Cong, P.; Xiang, F.; Liu, X.; Li, T. Morphology and microstructure of polyamide 46 wear debris and transfer film: In relation to wear mechanisms. *Wear* **2008**, *265*, 1100–1105. [CrossRef]

6.4. EMSS2017: VALIDATION OF DESIGN SOLUTIONS AND MATERIALS FOR A HIGH PERFORMANCE BEARING CAGE

El artículo "*Validation of design solutions and materials for a high performance bearing cage*" se centra en uno de los elementos que conforman los rodamientos de rodillos cónicos, la jaula. En este trabajo se analiza la viabilidad de su moldeo por inyección y la influencia, tanto en el propio proceso como en las propiedades del componente obtenido, de usar diferentes matrices poliméricas o materiales compuestos. También se analiza un diseño geométrico alternativo optimizado para su comportamiento frente a la lubricación, con el fin de asegurar la viabilidad de su fabricación. Los resultados concluyen que la poliamida, mejorada mecánicamente con fibra de vidrio, es la mejor opción de matriz polimérica para el proceso de moldeo por inyección. Por otro lado, la nueva geometría de la jaula requiere algunas modificaciones en los parámetros de moldeo por inyección para cumplir con los requisitos del proceso.

Contribución del doctorando: Revisión del estado del arte. Realización de simulación mediante software Moldflow. Análisis e interpretación de resultados. Redacción y revisión del artículo.

VALIDATION OF DESIGN SOLUTIONS AND MATERIALS FOR A HIGH PERFORMANCE BEARING CAGE

Aleida Lostalé[(a)], Isabel Clavería[(a)], Ángel Fernández[(a)], Manuel Muniesa[(a)], Carlos Javierre[(a)], Daniel Elduque[(a)], Sergio Santodomingo[(a)]

[(a)]University of Zaragoza I+

[(a)]isabel.claveria@unizar.es,

ABSTRACT

Bearings are one of the most used components in mechanical engineering. One element in the bearing assembly having a great influence in its performance is the cage. Cages work mainly under friction and inertia loads, so the selection of a proper material with low density and good mechanical and friction properties is essential. This paper analyzes the injection molding feasibility of different polymeric matrix to be used in composite materials for cage design. Alternative geometrical design of the cage optimized for lubrication purposes will be also analyzed in order to make sure its manufacturing feasibility. Results conclude that polyamide, mechanically improved with glass fiber, is the best option for polymeric matrix regarding injection molding process. On the other hand new cage geometry requires some modifications in injection molding parameters to meet process requirements.

Keywords: bearing, cage, mechanical design, injection molding.

1. INTRODUCTION

Bearings are the most used components in mechanical engineering to allow relative rotational motion between two concentric elements. Conical bearings are one of the most widespread bearings because of their stiffness, load capacity, rotation speed and equilibrium between radial and axial load. One of the components of the conical bearing assembly is the cage, which have a great influence on the suitability of the bearing for a specific purpose. Cages on bearings are required for keeping the rolling elements separated, for achieving a uniform distribution of the rolling elements, for guiding rolling elements to avoid sliding, and for retaining the rolling elements during assembly.

Cages usually have a passive role during bearing performance, and this study pretends them to become an active role thanks to the usage of new materials and new geometries.

Cages usually work under loads derived from friction and inertia (Kohar and Hreck 2016), as well as deformation due to pressure. Besides, the usage of lubricants and greases can affect chemically the cage material reducing its properties. That is why a proper selection of matrix materials for the cage and additives are strongly relevant to make sure the functionality of the bearing and improve its performance (Gunst Zabel Valle 2010).

New trends in cage design are focused on solid cages that are the most used for conical bearings and the most suitable for innovation. These cages combine in a very profitable way flexibility and resistance (Fang, Pugh, and Themudo 2007). If polymeric materials are used, the advantages of a serial manufacturing process like injection molding process can be combined with the good friction properties of some polymers. Injection molding process also allows to achieve an excellent surface quality to get in touch with the rollers. Another advantage of using polymers is their low density, minimizing the effect of inertia loads on the cage, which make them optimum for high speed and long term performances.

The most important limitations that solid cages have are two: high temperatures reached due to low conductivity of polymers under continuous work conditions, and ageing caused by some kind of lubricants on the polymer matrix.

New trends for high performance bearings are focused on new materials (Foster, Rosado, Brown et al. 2002), with low friction and high mechanical properties and high working temperature, new methods of lubrication for high temperatures and higher limits of speed-pressure (Ettefaghi 2013; Liu 2011; Huang 2011), new surface treatments for the rolling roads (Ciarsolo Fernández Ruiz de Gopegui Zubizarreta Abad Mariscal caretti Jiménez sánchez-López, 2014; Manier Ziegele Barriga, Goikoetxea Woydt, 2010) and new design of the components.

The goal of this research is to optimize cage geometry and material in order to obtain a more effective design for high performance purposes. Different cage geometries and materials will be analyzed from the point of view of mechanical and rheological behavior to meet the optimum design according to mechanical and manufacturing process requirements.

Regarding to geometry, the goal of this paper is validate new shape of the cage from the point of view of injection molding process, establishing strong and weak points regarding the original geometry. On the other hand, regarding to material, another aim of the paper is to analyze the mechanical and rheological behavior of

Proceedings of the European Modeling and Simulation Symposium, 2017
ISBN 978-88-97999-85-0; Affenzeller, Bruzzone, Jiménez, Longo and Piera Eds.

different potential materials for the polymeric matrix of the cage.

2. METHODOLOGY

Two different geometrical models are going to be analyzed varying some geometrical features that could be relevant to get a better tribological performance as well as different materials. Figure 1 shows a basic geometry that is now being used in some applications. From this geometry, a modification in the size of rolling elements cells will be carried out to create an alternative model that could be tested from tribological point of view. Anyway, a rheological and mechanical analysis is before required to guarantee the feasibility of the component.

Figure 1: Basic model to analyze

Regarding to materials, different polymeric matrix have been analyzed. A first group of technical polymers including Polyamide 66 (PA66), Polyamide 46 (PA46), Polyacetal (POM) and Polytetrafluoethylene (PTFE) will be tested. On the other hand a set of high purpose polymers including Polieteretercetone (PEEK) and Polyeterimide (PEI) will be also tested in order to validate mechanical and rheological behavior.

A matrix of tests has been designed to compare rheological and mechanical behavior according to Table 1.

Table 1: Study cases

	Material	Geometry
M1	PA66	Basic
M2	PA46	Basic
M3	POM	Basic
M4	PEEK	Basic
M5	PTFE	Basic
M6	PEI	Basic
G1	PA66	Alternative
G2	PEEK	Alternative

For each of the study cases a rheological analysis evaluating their manufacturing feasibility by injection molding process will be carried out by means of software MOLDFLOW PLASTICS INSIGHT®. The methodology follows a flow+warp analysis including filling, packing and cooling stages of injection molding process as well a warpage calculation. Results related to both process feasibility such as melt front advancement, injection pressure and shear stress, and related to mechanical behavior such as deflection of the part will be discussed. These results are essential to determine the suitability of the material or design for bearing performance because the rolling elements must fit perfectly between the cage spaces to minimize friction between components.

3. RESULTS

3.1. Rheological analysis

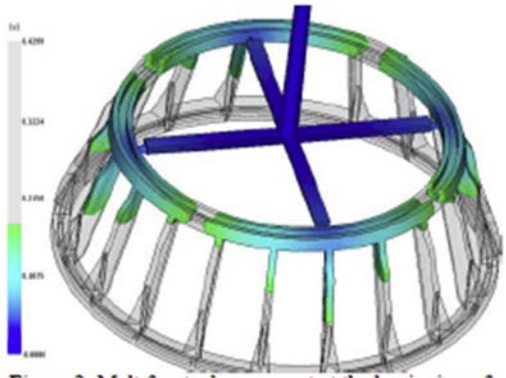

Figure 2: Melt front advancement at the beginning of injection time

Figure 2 shows melt front advancement result for M1 study case. It provides information about the proper flow pattern along part during injection time. This pattern is required to be both as uniform as possible and finishing filling at the same time all around the part contour. This fact can be seen on figure 3 for a total injection time of 0.5 seconds. It can be observed that flow near part entrance points goes further and this area of the part completes its filling slightly before. That is the reason why short filling times are considered in order not to let the first material freeze while the part completes the filling. Melt front advancement depends strongly on the injection point. As the feeding system remains the same for all the study cases this result is similar for all the materials and geometries tested.

Proceedings of the European Modeling and Simulation Symposium, 2017
ISBN 978-88-97999-85-0; Affenzeller, Bruzzone, Jiménez, Longo and Piera Eds.

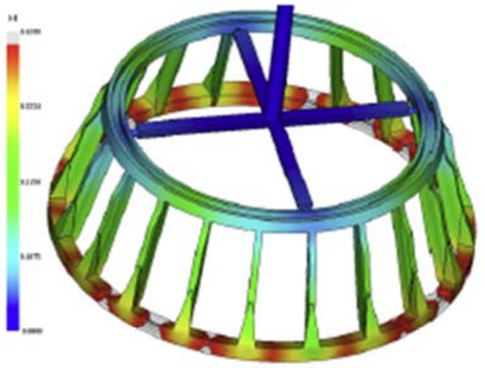

Figure 3: Melt front advancement at the end of injection time

One of the most important results to validate the feasibility of an injected part is maximum injection pressure reached at the end of filling stage when the whole cavity of the mold part is 99% completely filled. This pressure value has to do with part thickness, part flow length, material viscosity and flow rate. For this kind of geometry with short flow length values under 60 MPa are recommended. For the base cases analyzed M1 a maximum value of 25 MPa is obtained in figure 4. Pressure distribution at the end of filling is another parameter related to injection pressure to be taken into account. It should homogenous around the outer contour of the part, which indicates that the part has completed its filling at the same practically at the same time as described in Figure 4.

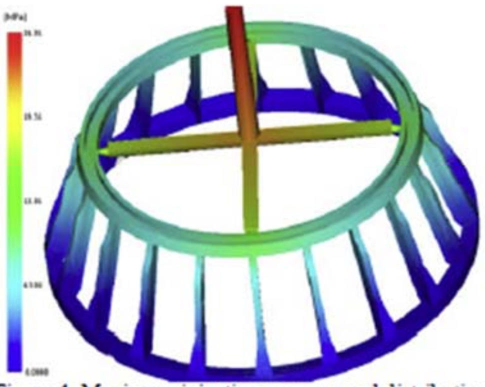

Figure 4: Maximum injection pressure and distribution for study case M1

Table 2 shows pressure results of different material cases M1 to M6 analyzed. It can be observed that PEI, PTFE and POM require higher injection pressures above 60 MPa even over 100 MPa for PEI. It is mainly due to high viscosity values of theses material for the shear rates reached during injection molding. PEEK and PA46 reach medium values around 50 MPa that would be an adequate limit pressure for this kind of geometry, and finally PA66 reaches low pressure values under 30 MPa due to mainly its lower viscosity. Maximum injection pressures for alternative geometry are around 10% lower due to the higher thickness of the rolling elements cells walls that makes easier the flow.

Table 2: Maximum injection pressure

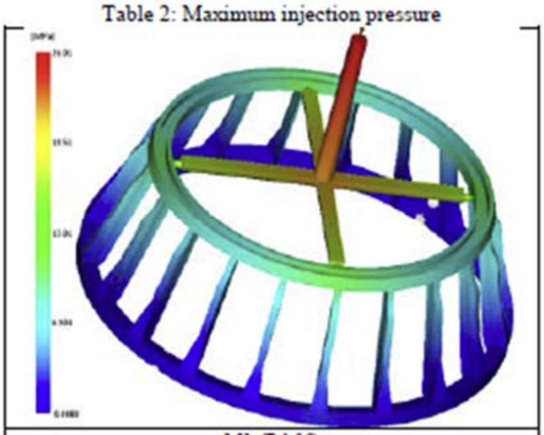

M1-(PA66)
Max. Pressure: 26.8 MPa

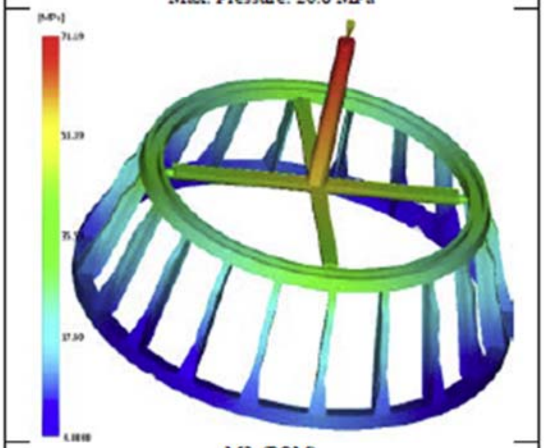

M3-(POM)
Max. Pressure: 71.1 MPa

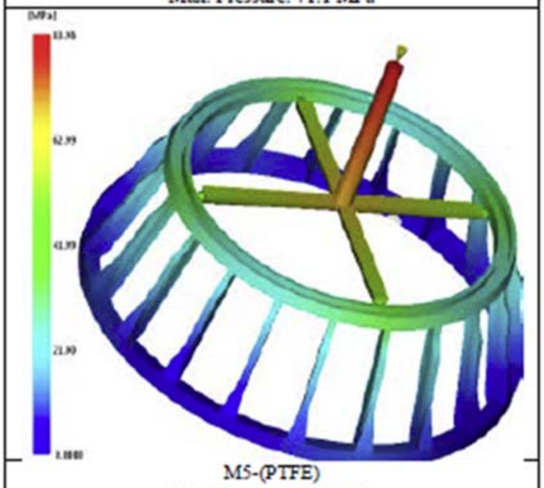

M5-(PTFE)
Max. Pressure: 83.9 MPa

Proceedings of the European Modeling and Simulation Symposium, 2017
ISBN 978-88-97999-85-0; Affenzeller, Bruzzone, Jiménez, Longo and Piera Eds.

Shear stress is another result to be taken into account for this kind of components subjected during its working life to mechanical loads. Shear stress provides information about the residual stress that remains into the injected part due to manufacturing injection process. This residual stress will be added to the stresses generated by the external loads applied to the component. It is advisable to reduce to a minimum this stress, and, on the other hand to be confident about not to overpass maximum allowable shear stress values for different materials. Shear stress generated has to do mainly with maximum injection pressures reached and part thickness.

Figure 5 shows shear stress results for base geometry (M1, M4) and alternative geometry (G1, G2). All the results have been scaled to 0.1 MPa, therefore red areas indicate higher shear stress values. Study cases with base geometry (M1, M4) shows red areas with top stress values. These areas correspond to a change in the cross section thickness of the part, where it is more likely to appear shear stress problems. For alternative geometry (G1, G2), these areas have been softened with transition thickness areas to avoid abrupt changes in cross section of the part, which leads to lower shear stress values.

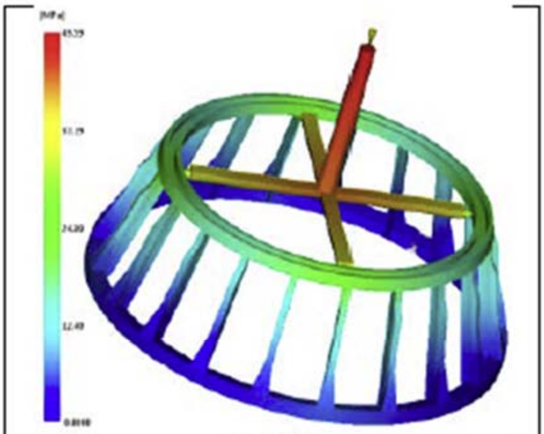

M2-(PA46)
Max.Pressure: 49.5 MPa

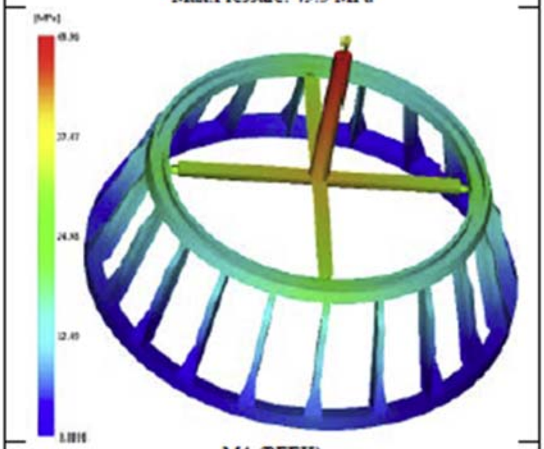

M4-(PEEK)
Max.Pressure:49.9 MPa

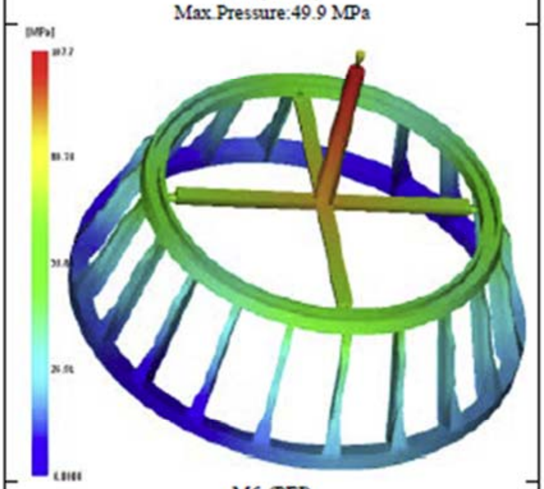

M6-(PEI)
Max. Pressure: 107.7 MPa

G2 (PEEK)
Max. Pressure: 37.9 MPa

G1 (PA66)
Max. Pressure: 23.2 MPa

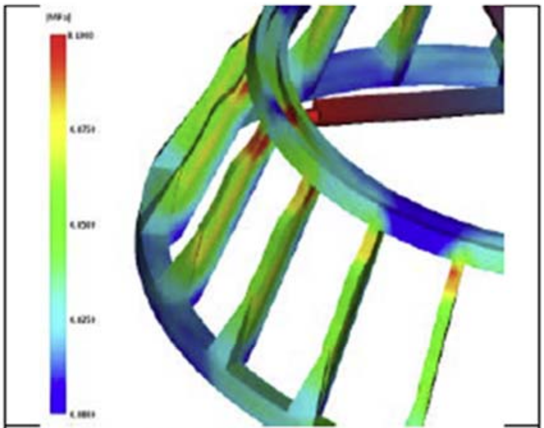

M1-(PA66)-Max. Shear Stress

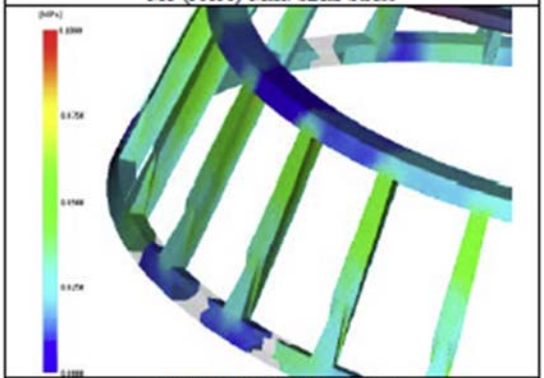

G1-(PA66)-Max. Shear Stress

Proceedings of the European Modeling and Simulation Symposium, 2017 74
ISBN 978-88-97999-85-0; Affenzeller, Bruzzone, Jiménez, Longo and Piera Eds.

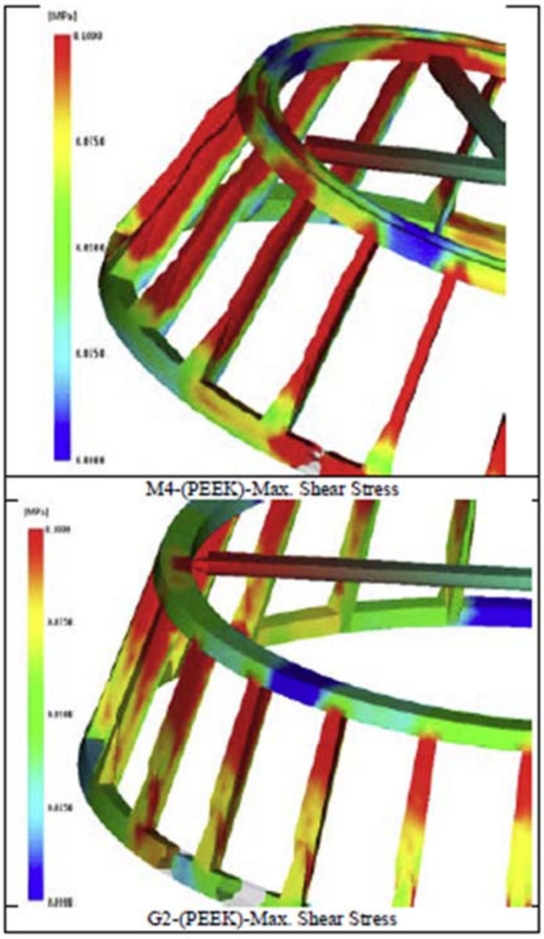

Figure 5: Shear stress for base geometry (M1, M4) and alternative geometry (G1, G2)

3.2. Mechanical analysis

Main purpose of the bearing cages is housing the rolling elements. To achieve an optimum performance of the bearing friction between rolling elements and the cage must be reduced at minimum. The way how injection process contributes to meet this requirement is finding the material, geometry and process conditions to obtain a post-molding deflection as low as possible to avoid undesirable additional friction between components.

Figure 6 shows qualitative results for cage deflection due to injection manufacturing process. From the graphical result can be observed that part tends to close radial and tangentially by reducing both outer and inner diameters and leaving less space for the rolling elements. Because of the same filling pattern obtained for all the study cases the deflection mechanism is the same for all the materials and geometries. In spite of it, different mechanical and shrinkage properties of the different materials maximum deflection values change according to values shown in table 3.

Higher deflections values are reached for PEEK and POM near 1 mm. Lower values are achieved for PTFE and PEI and medium values are obtained for PA66 and PA46. According to functionality tests, deflection values under 0.5 millimeters are allowed for the cage performance, so POM and PEEK would be discarded by this reason. Both PA66 and PA46 reach values next to the limit, however these values could be reduced by optimizing process parameters, especially at cooling stage.

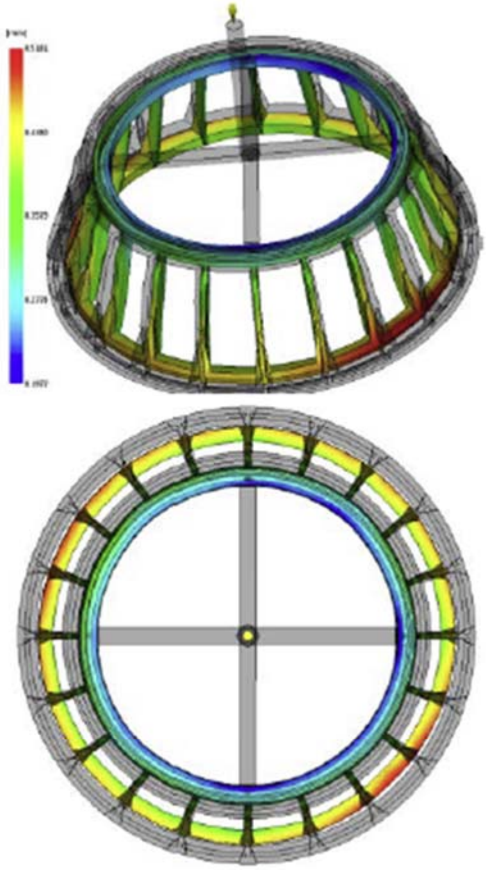

Figure 6: Qualitative post molding deflection for the analyzed study cases

For all different materials the deflection results are shown in Table 3:

Table 3: Results of maximum deflection

CASE	Max. Deflection (mm)
M1-(PA66)	0.5
M2-(PA46)	0.43
M3-(POM)	0.78
M4-(PEEK)	0.97
M5-(PTFE)	0.32
M6-(PEI)	0.35

Proceedings of the European Modeling and Simulation Symposium, 2017
ISBN 978-88-97999-85-0; Affenzeller, Bruzzone, Jiménez, Longo and Piera Eds.

4. CONCLUSIONS

A FEM analysis has been carried out to determine the most suitable material for a polymeric matrix in a composite focused to a bearing cage component from the point of view of process feasibility and induced mechanics induced by the injection process.

Melt front advancement is adequate for both proposed geometries with an uniform flow and an homogenous end of filling along the part contour. Maximum injection pressure is more adequate for PA46 and PEEK offering values under 60 MPa, and specially PA66 with values under 30 MPa. Regarding to mechanical analysis, better results are achieved by PTFE and PEI, followed by PA66 and PA46 that are also under performance specifications. It can be conclude that polyamide 66, mechanically improved with glass fiber, is the best option for polymeric matrix regarding injection molding process.

On the other hand, a new cage geometry has been tested. The change of geometry, especially cross section thickness, has a direct impact on maximum injection pressure and shear stress induced into the part. Results show that a new geometry with a slightly higher thickness at rolling element cells walls provides lower injection pressures and lower shear stress.

ACKNOWLEDGMENTS

This research has been carried out with the aid of project INNOVA-A1-008/15 granted by Aragon Regional Government in Spain.

REFERENCES

Ciarsolo I., Fernández X., Ruiz de Gopegui U., Zubizarreta C., Abad MD., Mariscal A., Caretti I., Jiménez I., Sánchez-López JC., 2014. Tribological comparison of different C-based coatings in lubricated and unlubricated conditions. Surface & Coatings Technology 257, 278–285.

Ettefaghi, 2013. Preparation and thermal properties of oil-based nanofluid from multi-walled carbon nanotubes and engine oil as nano-lubricant. International. Communications. in Heat and Mass Transfer 46, 142–147.

Fang N., Pugh D., Themudo R. 2007. On stress concentration factors of rolling elements bearing cages. Tribology Transactions 50(4), 445-452.

Forster NH, Rosado L., Brown JR., et al. 2002. The development of carbon-carbon composite cages for rolling element bearings. Tribology Trransactions 45 (1), 127-131.

Gunst U., Zabel W., Valle N. et al, 2010. Investigation of laminated fabric cages used in rolling bearings by ToF-SIMS. Tribology International 43 (5-6), 1005-1011.

Hwang, (2011). Effect of the size and morphology of particles dispersed in nano-oil on friction performance between rotating discs. Journal of Mechanical Science and Technology 25 (11), 2853–2857.

Kohar R., Hrcek S., 2016. Dynamic analysis of Rolling bearings with Elastic Cage. Modern Methods of Construction Design, Lecture notes in Mechanical Engineering 249-254.

Liu, 2011. Lubrication Effect of the Paraffin Oil Filled with Functionalized Multiwalled Carbon Nanotubes for Bismaleimide Resin. Tribology Letters 42, 59–65.

Manier CA, Ziegele H., Barriga J., Goikoetxea J., Woydt M, 2010. Zirconium-based coatings in highly stressed rolling contacts as alternative solution to DLC and ta-C coatings. Wear 269, 770–781.